Development of a Novel Air Hybrid Engine

by

Amir Fazeli

A thesis
presented to the University of Waterloo
in fulfillment of the
thesis requirement for the degree of
Doctor of Philosophy
in
Mechanical Engineering

Waterloo, Ontario, Canada, 2011

AUTHOR'S DECLARATION

I hereby declare that I am the sole author of this thesis. This is a true copy of the thesis, including any required final revisions, as accepted by my examiners.

I understand that my thesis may be made electronically available to the public.

Abstract

An air hybrid vehicle is an alternative to the electric hybrid vehicle that stores the kinetic energy of the vehicle during braking in the form of pressurized air. In this thesis, a novel compression strategy for an air hybrid engine is developed that increases the efficiency of conventional air hybrid engines significantly. The new air hybrid engine utilizes a new compression process in which two air tanks are used to increase the air pressure during the engine compressor mode. To develop the new engine, its mathematical model is derived and validated using GT-Power software. An experimental setup has also been designed to test the performance of the proposed system. The experimental results show the superiority of the new configuration over conventional single-tank system in storing energy.

In addition, a new switchable cam-based valvetrain and cylinder head is proposed to eliminate the need for a fully flexible valve system in air hybrid engines. The cam-based valvetrain can be used both for the conventional and the proposed double-tank air hybrid engines. To control the engine braking torque using this valvetrain, the same throttle that controls the traction torque is used. Model-based and model-free control methods are adopted to develop a controller for the engine braking torque. The new throttle-based air hybrid engine torque control is modeled and validated by simulation and experiments. The fuel economy obtained in a drive cycle by a double-tank air hybrid vehicle is evaluated and compared to that of a single-tank air hybrid vehicle.

Acknowledgments

I would like to express my deepest gratitude to my supervisors Professor Amir Khajepour and Professor Cécile Devaud for their guidance and continuous support throughout my graduate studies at University of Waterloo. I cannot thank them enough for all they have done for me.

I am also grateful to my committee members, Prof. Roydon Fraser, Prof. Bill Epling, Prof. Behrad Khamesee and Prof. Lino Guzzella, for their insightful comments and valuable suggestions.

I am grateful for Mahsa, my beloved wife, for her patience and support. She stood by me through all the successes and setbacks during the last four years. I want to thank my parents, Maryam Ghavidel Tehrani and Mohammad Javad Fazeli for their unconditional support and continuous encouragement. I also wish to thank my sisters, Torfeh and Elham Fazeli for their love and support.

My special thanks to all my friends who helped me over the years: Ali Nabi, Mohammad Pournazeri, Dr. Hamid Bolandhemmat, Negar Rasti, Dr. Meisam Amiri, Omid Aminfar, Soroosh Hassanpour, Dr. Vahid Fallah, Dr. Meysar Zeinali, Dr. Nasser Lashgarian and Saman Mohammadi.

I would like to thank all the staff at the University of Waterloo who gave me this opportunity to learn and grow.

The financial support from Ontario Centres of Excellence (OCE) and Natural Sciences and Engineering Research Council of Canada (NSERC) is also appreciated.

Table of Contents

List of Figures

List of Tables

Nomenclature

a	Piston stroke
$A(\theta)$	Throttle effective area
A_{valve}	Valve area
A	Vehicle frontal area
A_{cyl}	Cylinder instantaneous area
B	Cylinder bore
C_d	Discharge/Drag coefficient
C_r	Compression ratio
C_v	Air specific heat
C_0	Sound speed
C	Engine heat capacity
C_p	Specific heat capacity
d	External disturbance
e	Tracking error
E	Estimation error
f	Final state
F	Discrete function
f_r	Rolling resistance coefficient
$F_{Trrac/Braking}$	Traction/Braking force
g	Gravitational acceleration
$\hat{g}_1$	Knowledge of g_1
$\hat{g}_2$	Knowledge of g_2
$\tilde{g}$	Lumped model uncertainties
$\tilde{g}_{est}$	Online estimate of $\tilde{g}$
h	Enthalpy per unit mass
K	Controller proportional gain
k	Time step
l	Length of connecting rod
$\dot{m}_{throttle}$	Mass flow rate through the throttle
$\dot{m}_{engine}$	Mass flow rate to the engine [kg/s]
m_{cyl}	Cylinder air mass

m_{tank}	Tank air mass
m_{i}	Mass at point ‘i’
$\dot{m}_{\text{intake}}$	Cylinder inlet mass flow rate from intake manifold
$\dot{m}_{\text{LP}}$	Cylinder inlet mass flow rate from LP tank
$\dot{m}_{\text{HP}}$	Cylinder inlet mass flow rate from HP tank
M_{air}	Air average molecular mass
$M_{vehicle}$	Vehicle mass
n	System order
P_0	Ambient pressure
P_i	Pressure at point ‘i’
P_{tank}	Tank pressure
P_{atm}	Atmospheric pressure
P_{LP}	LP tank pressure
P_{HP}	HP tank pressure
P_{cyl}	Cylinder pressure
P_{in}	Downstream pressure
P_{out}	Upstream pressure
P_r	Ratio of manifold pressure to ambient pressure
P_m	Manifold pressure
P_{cyl}^{k}	Cylinder pressure after feeding k^{th} storage
$\dot{Q}$	Heat flux
r	Tire radius
R	Ideal gas constant
S	Sliding surface
t	Time
T_{engine}	Engine brake torque
T_f	Engine friction torque
T_d	Desired torque
U_0	Environment internal energy
U	System internal energy
u_{cyl}	Internal energy per unit mass of the gas inside the cylinder
u_{tank}	Internal energy per unit mass of the gas inside the tank
V_d	Engine displacement volume

V_0	System volume at equilibrium with environment
V	System volume
V_{tank}	Tank volume
V_{LP}	LP tank volume
V_{HP}	HP tank volume
V_{cyl}	Cylinder volume
V^*	Variable volume
v_1	Vehicle initial velocity
v_2	Vehicle final velocity
$\bar{v}$	Mean piston speed
W_{ad}	Adiabatic work
W_{ij}	Work from point ‘i’ to ‘j’
$\dot{W}_{ad}$	Adiabatic power
$\dot{W}_{iso}$	Isentropic power
$\dot{W}_{act}$	Actual power
$\dot{W}_{shaft}$	Shaft power
x_k	System state
x	Independent variable
ν_{man}	Manifold temperature
ν_{atm}	Atmospheric temperature
ν_0	Ambient temperature
ν_{wall}	Cylinder wall temperature
ν_{LP}	LP temperature
ν_{HP}	HP temperature
ρ	Air density
δ	Bound of Lumped uncertainty variation
λ	Positive constant
ω	Engine speed
θ	Crank angle
$\theta_{throttle}$	Throttle angle [deg]
$\theta_{throttle,com}$	Commanded throttle angle [deg]
φ	Exergy
φ_1	Initial exergy of the system

φ_2	Final exergy of the system
$\hbar$	Heat transfer coefficient
η_{ad}	Adiabatic efficiency
η_{iso}	Isentropic efficiency
η_{mech}	Mechanical efficiency
η_{Reg}	Efficiency of Regeneration
η_{vol}	Engine volumetric efficiency
ε	Boundary layer thickness
γ	Adiabatic index
Γ	Controller adaptation gain
Y	Lyapanov function
ζ_0	Environment entropy
ζ	System entropy
Φ	Neural network
FTP75	American driving cycle
SoC	State of Charge
NEDC	New European Driving Cycle
CVO	Charging valve opening
CVC	Charging valve closing
IVO	Intake valve opening
IVC	Intake valve closing
TDC	Top dead centre
BDC	Bottom dead centre
LP	Low pressure
HP	High pressure
FMEP	Friction mean effective pressure
CAD	Crank Angle Degree
AM	Air motor
CB	Compression braking

Chapter 1
Introduction

The automotive industry has been in a marathon of advancement over the past decade. This is partly due to global environmental concerns about increasing air pollution and decreasing fossil fuel resources. In 2006, the transportation sector comprised more than 135 million passenger cars in the United States representing the largest consumption of energy [1]. Also, the sector has accounted for 28% of the green house emissions in the United States [1]. Internal Combustion Engines (ICEs), the primary power source of conventional vehicles, have a maximum efficiency of 30-40%. However, ICEs work at a low efficiency level most of the time and, furthermore, the vehicle's kinetic energy cannot be recovered during braking and it is wasted.

1.1 Air Hybrid Vehicles

Air hybrid vehicles are founded on the same principle as hybrid electric ones. They employ two energy sources, fuel and pressurized air, to propel the vehicle. During braking, the kinetic energy of an air hybrid vehicle is converted into pressurized air by running the same ICE in the compressor mode. Air hybrid engines can have four modes of operation: Compression Braking (CB), Air Motor (AM), supercharged, and conventional internal combustion. The energy flow in the CB mode is illustrated in Figure 1-1. This mode is activated when the driver applies the brake pedal. At this mode, fuel is shut off and the engine operates as a two-stroke air compressor, storing the vehicle's kinetic energy in the form of pressurized air in the reservoir tank.

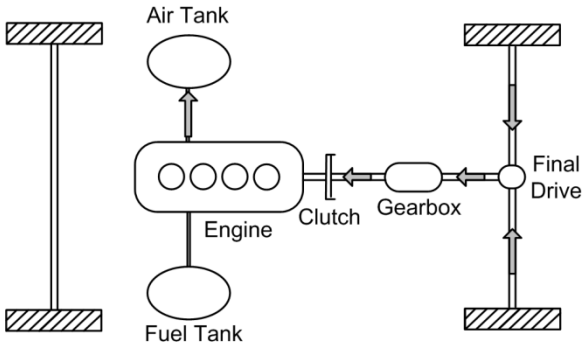

Figure 1-1: Energy flow in the CB mode

The energy stored in the tank can be used in various ways. The first option is to run the internal combustion engine as an air motor in long-term cruising. In the air motor mode, the charging valve between the air tank and engine opens and the pressurized air runs the engine as a two-stroke air motor. Usually, this mode is triggered during low load engine conditions to avoid a high fuel consumption. The energy flow at this mode is illustrated in Figure 1-2.

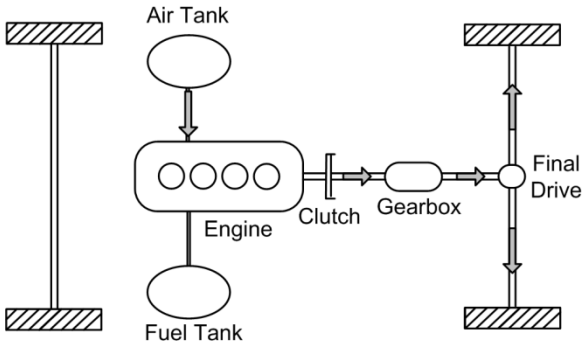

Figure 1-2: Energy flow in the AM mode

The second option for using the stored braking energy is to run the engine in air motor mode to start up the engine. The startup mode can be activated after a long stop to avoid a cold start or after a short stop to avoid the engine idling resulting in a lower engine fuel consumption and emission. After a long stop, the powertrain clutch can be disengaged at the beginning of the startup mode allowing the engine to run freely; however, after a short stop, the powertrain clutch remains engaged. In this case, the pressurized air in the tank is not only used to run the engine, but also to propel the vehicle for a relatively short period of time. Then, the conventional mode is triggered by fueling the engine. The advantage of such a case is that the engine can be turned off during short stops, and generate the required torque immediately by using the stored pressurized air.

In addition, stored energy can be used to run the engine accessories. There are some efforts, described in the literature to remove all or some of the engine accessories from the engine to avoid excessive power losses, particularly at high engine speeds [2], [3]. In an air hybrid engine, some or all of the engine accessories can be removed from the engine, and run by an auxiliary air motor which is fed by the air stored in the tank through one of the following configurations:

Series configuration:

In this configuration (Figure 1-3), the shaft that runs the engine accessories is connected to the engine through a clutch. This shaft also passes through an air motor. If the tank pressure is high enough to run the engine accessories, the clutch is disengaged and air motor runs all or some of the engine accessories. If the tank pressure is not high enough, the clutch is engaged, the air motor works in the idle mode and the engine runs the accessories.

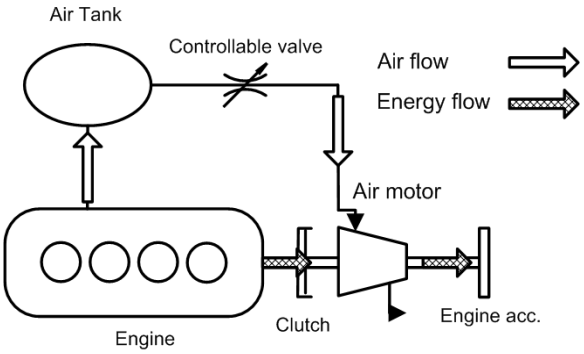

Figure 1-3: Series configuration for running the engine accessories

Parallel configuration:

In this configuration (Figure 1-4), air motor and engine output shafts are connected to the accessories' main shaft through a planetary gear. If the tank pressure is high enough, the air motor clutch is engaged and the engine clutch is disengaged. This way, the air motor runs all or some of the accessories. If the air tank pressure is not high enough, the air motor clutch is disengaged, the engine clutch is engaged and the engine runs all the accessories.

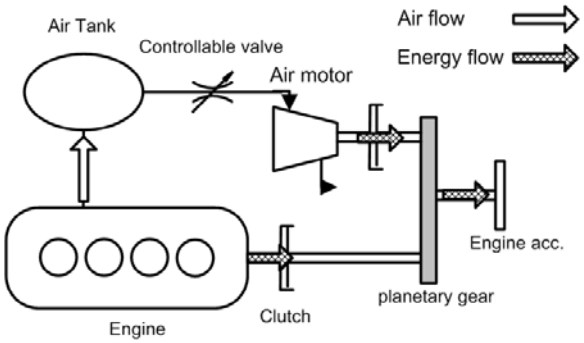

Figure 1-4: Parallel configuration for running the engine accessories

The supercharged mode is depicted in Figure 1-5. This mode is activated when the desired torque is high. In this mode, the engine is supercharged by the pressurized air from the tank and the mass of fuel and air entering the engine cylinders is increased, resulting in a high engine torque and power. In contrast to typical supercharged engines, which exhibit a low efficiency at low speeds and loads, air hybrid engines can be supercharged at any operating point thanks to the air stored in the tank [4]. Conventional mode is also activated when the desired load is moderate or the tank pressure is relatively low or empty.

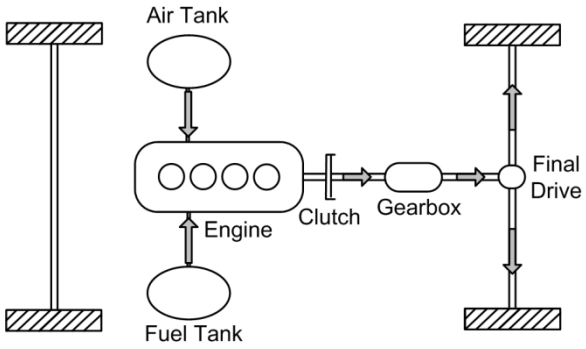

Figure 1-5: Energy flow in supercharged mode

1.2 Implementation of Air Hybrid Engines

In contrast to other alternatives such as electric hybrid or hydraulic hybrid engines which require a secondary powertrain system, air hybrid engines use the same engine as the secondary powertrain which reduces the extra mass. Although the air hybrid concept seems to be simple, there are some practical issues which need to be resolved before the concept is accepted as a hybrid powertrain solution.

One of the most important challenges of air hybrid engines is the poor energy storing capacity of the system due to the low energy and power density of air. To increase the efficiency of regenerative braking, storing pressure should be increased, but the maximum storing pressure is a function of the tank volume and engine compression ratio. In other words, to increase the energy storing capacity of the system, either the engine compression ratio or the tank volume should be increased; however, tank volume and compression ratio are restricted by the space available in the vehicle and engine performance related issues.

The other challenge in the implementation of an air hybrid engine is the inevitability of using flexible valvetrains. Since an air hybrid engine has different operational modes, a flexible valvetrain is needed for the implementation of the concept. Although conventional valvetrains limit the engine's performance and cannot practically be used in an air hybrid engine, they have operational advantages, because the valve motion is governed by a cam profile, designed to confine the valve seating velocity and lift [5]. In contrast, a flexible camless valvetrain with no direct mechanical connection with the engine introduces control complexities, a high power consumption, and an increased cost into the system. Several ongoing studies address the technical challenges of using fully flexible valvetrains [6], [7] [8].

In addition, the implementation of torque control in an air hybrid engine during the AM, CB, and supercharged modes has not been addressed by any researcher so far. To implement an air hybrid engine, the engine configuration should be further modified to control the engine torque in the AM and CB modes. Furthermore, a robust controller for adjusting the torque should be developed.

1.3 Research Objectives and Thesis Layout

Although there are many challenges there are also many advantages in the implementation and commercialization of air hybrid engines. This research is intended to address some of these challenges by focusing on improving the overall efficiency and reducing the complexity in the valve system and torque control of air hybrid engines.

The objectives of this thesis, in general, are:

1. Development and testing a novel compression strategy to increase the energy storing capacity of regenerative braking system in air hybrid engines.
2. Development and testing a cam-based valvetrain and cylinder head structure to relax the need for a fully flexible valvetrain.
3. Design and implementation of an engine torque controller for regenerative braking mode.
4. Evaluation of the overall efficiency of the proposed air hybrid engine in various standard drive cycles.

This thesis is organized in eight chapters and nine appendixes. Chapter 1 provides an introduction to air hybrid engines and the objectives of this thesis. Ongoing studies in different aspects of air hybrid engines are addressed in Chapter 2. Chapter 3 introduces a new compression process using two air tanks for the regenerative braking system, and presents a comparison between the conventional and developed compression processes. Chapter 4 describes experimental studies and results of the proposed compression strategy. A novel cam-based valvetrain for conventional and proposed air hybrid configurations is developed and assessed using simulation and experimental studies in Chapter 5. Chapter 6 is devoted to the design and implementation of model-based and model-free regenerative braking torque controllers. Chapter 7 presents the drive cycle simulation and provides a comparison between the conventional and proposed air hybrid engines based on their optimized mode scheduling. Chapter 8 summarizes the contributions and provides some suggestions for future work.

Chapter 2
Literature Review

Powertrains can be divided into two groups, according to the number of their energy sources: single-source vehicles such as gas, diesel, pure electric and compressed air vehicles, and double-source vehicles such as electric and air hybrid vehicles. In this chapter, the investigations on air hybrid vehicles are discussed in detail.

2.1 Air Hybrid Vehicles

Hybrid Electric Vehicles (HEVs) have overcome production limits and are regarded as one of the most effective and feasible solutions to current environmental concerns. HEVs use two sources of energy: fossil fuel and electrochemical energy stored in batteries. They are usually comprised of an ICE and an electric motor. HEVs are able to store the vehicle's kinetic energy in the shape of electrochemical energy in a battery by running the electric motor as a generator. Despite the beneficiary improvements that this kind of vehicle provides, there are some serious concerns about HEVs performance. The HEV powertrain system is complex, which introduces a very complicated control problem and increases the maintenance cost of the vehicle. Using a battery in the powertrain is also a drawback for HEVs because battery-charging efficiency is highly dependent to the charging strategy [9], the state of charge of the battery (which forms the basis of vehicle control strategy) cannot be precisely defined [10]. In addition, HEVs are 10% to 30% heavier than ICE-based vehicles [11].

Compared with a hybrid electric vehicle, an air hybrid-based vehicle could provide a better efficiency with less complexity, weight and cost. In 1999, Schechter [12] proposed the idea of an air hybrid engine for the first time. The idea evolved from the fact that the internal combustion engine can be run as a compressor and an air motor by changing the valve timing. Schechter [12] has introduced a new cylinder head configuration in which there is an extra valve connecting the cylinder to an air tank, called the charging valve. This extra valve is active only when the engine works as a compressor or air motor. The valve sends the pressurized air from the cylinder to the air tank, and vice versa. The

author also studied the thermodynamic cycle of each mode. He reported more than a 50% reduction in fuel consumption by using the air hybrid engine in a 45 second driving cycle.

In 2000, Schechter published his second paper [13]. He used the same cylinder head configuration, but showed that by changing the valve timings, different engine loads can be achieved. He suggested that approximately 30 [litre] air-tank volume per 1000 [kg] of the vehicle mass is needed for a gasoline engine, and suggested a new definition for regenerative efficiency. Efficiency is defined as a fraction of the energy absorbed during braking that can be used in the subsequent acceleration. Based on a rough calculation, Schechter reported an efficiency of 74% for the regenerative braking system during the braking of a typical vehicle from an initial speed of 48 [km/hr]. In 2007, Schechter patented the two-stage air hybrid configuration in which, some of the engine cylinders receive atmospheric air and after compression, transfer it to an intermediate air tank. Other cylinders receive compressed air from the intermediate tank and compress it further [14].

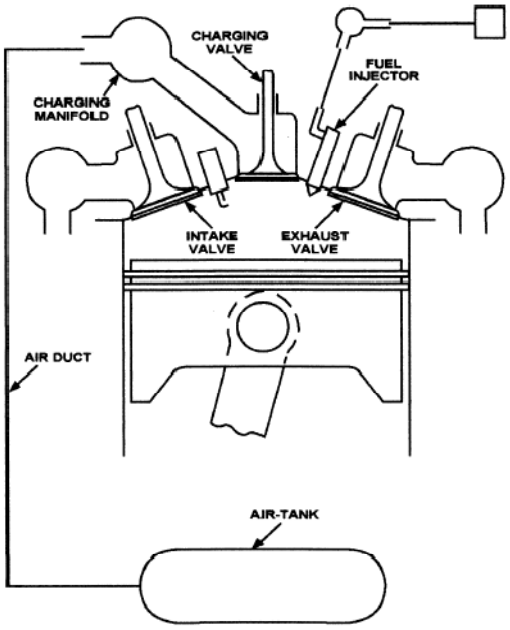

Figure 2-1: Schechter's proposed configuration [12]

After these initial investigations on the air hybrid engine concept, six research groups at different universities and research centres started investigating this new concept:

1. UCLA in collaboration with Ford Motor Company.
2. Lund Institute of Technology.
3. Brunel University.
4. Institute PRISME/ EMP Université d'Orléans.
5. ETH University.
6. National Taipei University of Technology.

In the next section the work of each research group is reviewed.

2.1.1 UCLA Research Group

In 2003, Chun Tai et al., in collaboration with Ford Motor Company [15], proposed a new cylinder head configuration which enabled different modes of operation without adding an extra valve to the head. The group utilized four fully flexible camless valves for each cylinder, two intakes, and two exhausts. In this configuration, one of the intake valves is switchable, and connects either the intake manifold or air tank to the cylinder by a three-way valve. The group also optimized the valve timings according to the desired load, the tank pressure, and speed. The researchers claimed a 64% and 12% fuel economy improvement in city and highway driving, respectively. This improvement is reported to be partly due to using the camless valvetrain which permitted the engine to run unthrottled. The authors have provided no experimental results, but did use GT-POWER to simulate the proposed air hybrid engine configuration.

In 2008, Kang et al. [16] published their first experimental work on an air hybrid engine in collaboration with Volvo and Sturman Industries. They converted a six-cylinder diesel engine to an air hybrid engine utilizing a Sturman hydraulic camless valvetrain. They optimized the valve timings of the AM and CB modes at two engine speeds and three tank pressures, and implemented the obtained valve timings experimentally. They also reported the transient performance of the engine in switching from the CB to the AM mode.

In a dissertation submitted by one of the group members [17], the concept of using a double-stage regenerative braking, initially introduced by Schechter in 2007, was compared to a single-stage system in simulations

2.1.2 Lund Institute of Technology

In 2005, Andersson et al. from the Lund Institute of Technology proposed a regenerative braking system with two tanks for a typical city bus [18]. The authors concluded that the regenerative braking system with only one tank was not capable of producing high enough torque in the CB or AM modes. Thus, the idea was to use a pressure tank as a substitute for the atmosphere as the supplier of the low-pressure air. The proposed configuration is shown in Figure 2-2.

In this configuration, the engine works between a 600 [litre] low-pressure and a 145 [litre] high-pressure tank at different modes of operation. The engine cylinders are charged with the air from the low-pressure tank, which has a higher pressure compared to the ambient during braking. In the proposed configuration, the low-pressure tank must be replenished by an onboard compressor on a regular basis. The authors reported an average efficiency of 55% for the regenerative braking system and a 22% fuel consumption saving in a typical urban driving cycle obtained through simulations.

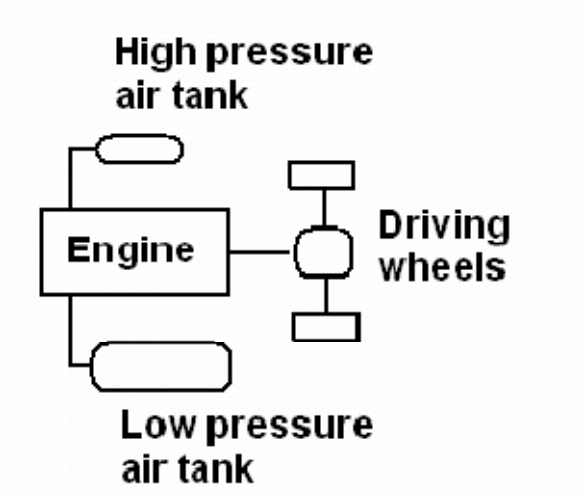

Figure 2-2: Air hybrid concept using two tanks [18]

Later, in 2007, Trajkovic et al. [19] from the same research group published the experimental results of an air hybrid engine. They converted a single-cylinder diesel

engine to an air hybrid engine. Pneumatic valve actuators were used to make the air hybrid configuration possible. Two modes, CB and AM, were tested and studied in this work. The Engine's Indicated Mean Effective Pressure (IMEP) and tank pressure were reported for different valve timings and engine speeds at the AM and CB modes. A new definition for efficiency was also presented, based on the negative and positive IMEP at the CB and consequent AM modes. An efficiency of 33% for the regenerative braking system was reported.

Trajkovic et al. [20] published their second investigation on the same air hybrid engine in 2008. They optimized the valve timings for the CB and AM modes at various tank pressures. Additionally, they modified the tank valve diameter to increase the system efficiency. They showed that, by using a larger charging valve, the efficiency of the regenerative system, based on their definition of efficiency, could be increased to approximately 44%. They also compared the experimental results with GT-POWER results and found them to be in agreement.

In their next study, the authors validated an engine model in GT-Power by the experimental results and used the GT-Power model to study the effect of different parameters such as tank valve diameter and valve timings on pneumatic hybrid performance [20]. In 2010, they published the driving cycle simulation results of their single-cylinder air hybrid engine. They chose a lower limit of 8 [bar] for the tank pressure and reported a reduction in the fuel consumption up to 30% in the Braunschweig driving cycle [21].

2.1.3 Brunel University

In 2009, Hua Zhao's group from Brunel University proposed four stroke air modes for an air hybrid engine. To implement the concept without using a camless valvetrain, a new valve configuration was proposed utilizing a Cam Profile Switching (CPS) system for the operational mode switching, a controllable solenoid valve for managing the amount of air entering or exiting the air tank, and a variable valve timing system to shift the valve events without changing the valve duration. They reported a regenerative braking efficiency of 15% from the simulations, but the need for a high speed solenoid valve was a substantial drawback of the proposed design. Later in 2010, the team tackled the

problem by introducing two new designs for air hybrid engines. In one of their designs, the researchers introduced and extra check valve between the tank and one of the intake valves, and a butterfly valve in the intake manifold to eliminate the need for a high speed solenoid valve. In their other design, they proposed a valvetrain with the intake opening duration of 360 degrees and a check valve between the intake manifold and the intake valves. Their proposed configurations will be discussed in more detail in Chapter 5.

2.1.4 Institute PRISME/ EMP Université d'Orléans

P. Higelin et al. [6] published their work on the air hybrid concept in 2003. They presented a thermodynamic model of each operational mode, and also adopted a set of operating mode selection rules, based on the tank pressure and vehicle speed. The optimized values for the tank volume and maximum allowable tank pressure were defined based on NEDC cycle simulation results. The author reported a 15% fuel saving in NEDC driving cycle. They proposed and compared different energy management strategies in their work in 2009 [22].

2.1.5 ETH University

Guzzella et al. [4], [23] proposed and conducted experiments on the four-stroke air hybrid engine to eliminate the need for a complete set of fully camless valves. In their proposed configuration, the intake and exhaust valves remained camshaft-driven but an extra camless valve connecting the cylinder to the tank was added. They classified the air tank as an ultra short-term storage device due to the low energy density of pressurized air. They concluded that the best way to use the tank-pressurized air was to supercharge the engine. Since the engine could be supercharged even at low torques and speeds, a larger engine can be downsized in an air hybrid vehicle and there is no need to design the engine turbocharger for an optimal dynamic performance. Thus, the supercharged mode is activated whenever a sudden increase in the engine torque is required until the supercharger reaches the steady state condition and as a result, the turbo lag is eliminated. This was reported to be the most important advantage of air hybrid engines, leading to 25-35% reduction in fuel consumption, compared with that of a typical engine. They proposed the concept of a cold air tank in contrast to an insulated, hot tank proposed in

[12] to reduce the knock probability. The team was successful in running the air hybrid engine in all operational modes, including conventional mode.

They employed the Dynamic Programming (DP) algorithm to find the optimum mode scheduling for the air hybrid vehicle in a drive cycle and also conduct a comparison between different hybrid structures in [24].

2.1.6 National Taipei University of Technology

In addition to the aforementioned air hybrid structures, there is also a totally different configuration of an air hybrid, proposed by Huang [25] in 2004. In this configuration, a typical ICE was connected to a screw compressor and operates at the engine's most efficient point. Then, a pneumatic motor is driven by the compressed air to generate power. Thus, the main difference between the proposed air hybrid configuration and a series hybrid electric vehicle is that an air compressor replaces the generator, a pneumatic motor replaces the electric motor, and a high-pressure air tank replaces the battery. Huang achieved an 18% improvement in efficiency, compared with that of an ICE-based powertrain. However, the author has not considered the effect of the vehicle weight increase (due to adding extra components such as pneumatic motor and compressor) on the overall efficiency of the vehicle. The author reported his proposed system's experimental results in [26] and [27].

2.2 Summary

In this chapter, a literature survey on the concept of air hybrid engines was presented. The concept is not new; however, the practical challenges in implementing the concept have prevented researchers from exploiting its potential to increase the powertrain efficiency. Except for the ETH research group who was successful in running the engine in various modes, most of the experimental work has been limited to testing regenerative or air motor modes of an air hybrid engine. Although some substitute valvetrain configurations have been suggested to avoid a camless valvetrain in theory, all experimental work is based on camless valvetrain in the literature.

Chapter 3
Double-tank Compression Strategy

A significant fraction of energy is wasted in braking in a typical city driving cycle, where stop-and-go driving patterns are common. For instance, in the FTP75 urban driving cycle approximately 40% of the energy is wasted while braking [28]. Thus, if the braking energy can be recovered, the vehicle energy consumption can be significantly reduced [28]. The main motivation to hybridize a vehicle's powertrain is to capture and reuse the energy wasted during braking. Air hybrid vehicles can capture and store braking energy in the form of pressurized air for further use.

3.1 Efficiency of Energy Storing

As mentioned, an internal combustion engine works as a simple compressor during regenerative braking. Although there are several efficiency definitions for compressors, such as volumetric, adiabatic, isothermal, isentropic and mechanical efficiency (Appendix A), none of them represents the ratio of the stored energy in the tank to the consumed energy. The efficiency of regenerative braking should be represented in terms of energy stored in the tank to the change in the kinetic energy of the decelerating vehicle. While stored energy in the tank cannot be expressed by internal energy of the stored air (as it does not represent the ability of stored gas to perform work), it can be expressed by the exergy of the stored gas. Exergy, or availability of a system, is defined as the maximum useful work of a process which brings the system to equilibrium with the environment, and can be expressed by the following relation [29]:

$$\varphi = (U - U_0) + P_{atm}(V - V_0) - \upsilon_{atm}(\zeta - \zeta_0). \qquad 3\text{-}1$$

Based on the definition for exergy in Eq.(3-1), the second law efficiency of the regenerative braking process can be defined as:

$$\eta_{\text{Reg,stored}} = \frac{\varphi_2 - \varphi_1}{\frac{1}{2} M_{vehicle}\left(v_1^2 - v_2^2\right)}. \qquad 3\text{-}2$$

Exergy represents the maximum potential of a system to perform useful work and is only achievable through a reversible process which brings the system to the dead state.

The dead state is a condition at which the system has the same pressure and temperature as those of the surroundings. However, in the case of a regenerative braking system, the stored energy in the tank is used later through an adiabatic expansion which brings the system only to pressure equilibrium with the environment, not thermal equilibrium. This means that the maximum amount of work that can be performed by the system is the isentropic work ($W_{isen.}$), which is defined by the following relation:

$$W_{isen.} = \frac{P_{\text{tank}} V_{\text{tank}} - P_{atm} V_{\text{tank}} \sqrt[k]{P_{\text{tank}} / P_{atm}}}{\gamma - 1}. \qquad 3\text{-}3$$

Now the efficiency of the regenerative braking with respect to the subsequent isentropic process, can be defined as:

$$\eta_{\text{Reg,achievable}} = \frac{W_{isen.,2} - W_{isen.,1}}{\frac{1}{2} M_{vehicle} \left(v_1^2 - v_2^2 \right)}. \qquad 3\text{-}4$$

In the present study, both definitions are used. The first expression, Eq.(3-3), helps to determine how much useful energy is stored, and the second definition, Eq.(3-4), represents the maximum achievable energy from the system.

3.2 Single-tank (conventional) Regenerative Braking

The ideal air cycle of the two stroke compression braking mode is shown in Figure 3-1 with solid lines. When the piston is at the Bottom Dead Centre (BDC), the intake valve closes. The piston starts going up to the Top Dead Centre (TDC) and compresses the air adiabatically (assuming that there is no heat transfer through the cylinder walls).

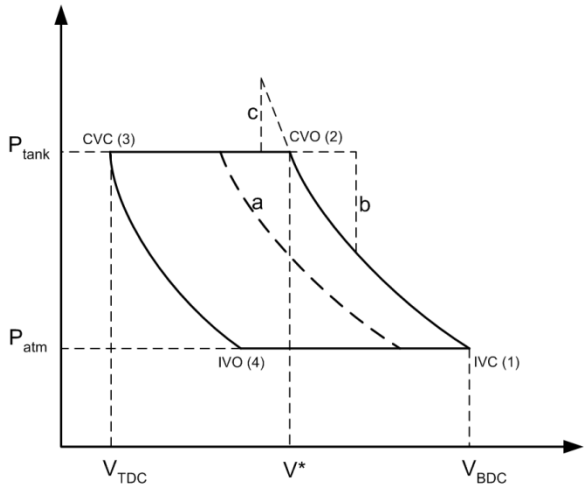

Figure 3-1: Regenerative braking ideal air cycle

The charging valve opens (CVO) when the air pressure in the cylinder equals the tank pressure (assuming all the valves are fully flexible). At this time, air enters the tank in a reversible constant pressure process, assuming that the air tank is large enough and its pressure does not change while charging. The charging valve closes (CVC) when the piston is at TDC. The piston goes down and the intake valve opens (IVO) when the pressure in the cylinder equals the atmospheric pressure. The afore-mentioned cycle in which all the process are reversible, is called the ideal braking cycle hereafter and is shown in the figure with solid lines. With reference to Figure 3-1, braking torque can be regulated by advancing the intake valve closing time, which reduces the amount of air entering the cylinder (cycle ‘a’), and by advancing or retarding charging valve opening (cycles ‘b’ and ‘c’). Cycle ‘a’ produces lower braking torque while cycles ‘b’ and ‘c’ produce higher braking torque than that of the ideal cycle as proposed in [13]. Although cycles ‘b’ and ‘c’ produce higher braking torque, they store the same amount of energy in the storage tank as the ideal cycle, which can be shown to have the maximum efficiency of energy storing (Appendix B). Thus, to increase the efficiency of regenerative braking, the ideal braking cycle in which the tank and cylinder charging happen during constant pressure processes, should be followed at each tank pressure.

The enclosed area of the ideal braking cycle not only represents the braking torque, but it also represents the amount of energy stored in the air tank. Figure 3-2, shows the cylinder P-V cycle for different tank pressures following the ideal braking cycle.

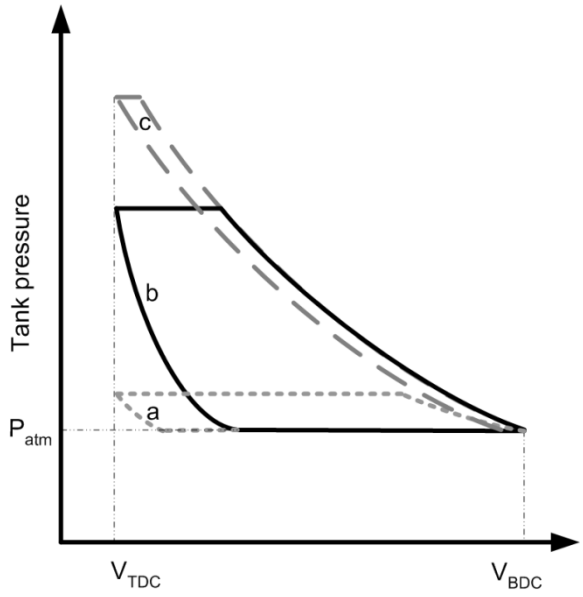

Figure 3-2: Cylinder P-V cycle at various tank pressures

As can be seen, the enclosed area of the P-V cycle changes with the tank pressure and decreases rapidly at high tank pressures (cycle 'c' on Figure 3-2). Thus, following the conventional compression strategy, the system is neither able to produce enough torque nor capable of storing energy at high pressures, which significantly challenges the performance of the air hybrid engines. This is mainly due to the fact that the maximum amount of air mass that could be stored in the tank is limited as (following ideal regenerative cycle):

$$m_{\text{tank,max}} = C_r \frac{P_{atm}}{\upsilon_{atm} R} V_{\text{tank}} M_{air}. \qquad 3\text{-}5$$

To obtain the above equation, suppose that the storage tank is already full and its pressure and temperature are P_{tank} and υ_{tank}. The valve and gas exchange dynamics through the valves are also neglected, assuming that the valves' opening, closing and gas mixing happen instantaneously, since the tank is full, its pressure and temperature are related based on Eq.(3-5) and ideal gas law, by:

$$P_{\text{tank}} = \frac{P_{atm} \upsilon_{\text{tank}}}{\upsilon_{atm}} C_r. \qquad 3\text{-}6$$

At point '1' (Figure 3-1), the air mass in the cylinder is:

$$m_1 = \frac{P_{atm} V_{cyl}}{R \upsilon_{atm}} M_{air}. \tag{3-7}$$

Considering adiabatic compression and ideal mixing of gases when the charging valve is opened, cylinder pressure at arbitrary point '2' where the cylinder volume is V^*, (this point may not be necessarily the point where the cylinder pressure equals the tank pressure), is:

$$P_2 = \frac{P_{atm}\left(\frac{V_{cyl}}{V^*}\right)^{\gamma} V^* + \frac{P_{atm}\upsilon_{\text{tank}}}{\upsilon_{atm}} V_{\text{tank}} C_r}{V^* + V_{\text{tank}}}, \tag{3-8}$$

and the temperature at point '2' is:

$$\upsilon_2 = \frac{P_{atm}\left(\frac{V_{cyl}}{V^*}\right)^{\gamma} V^* + \frac{P_{atm}\upsilon_{\text{tank}}}{\upsilon_{atm}} V_{\text{tank}} C_r}{\frac{P_{atm}\left(\frac{V_{cyl}}{V^*}\right)^{\gamma} V^*}{\upsilon_{atm}\left(\frac{V_{cyl}}{V^*}\right)^{\gamma-1}} + \frac{P_{atm}}{\upsilon_{atm}} V_{\text{tank}} C_r}. \tag{3-9}$$

Air pressure and temperature at point '3' are defined by:

$$P_3 = P_2\left(\frac{V_{\text{tank}} + V^*}{V_{\text{tank}} + \frac{V_{cyl}}{C_r}}\right)^{\gamma}, \tag{3-10}$$

$$\upsilon_3 = \upsilon_2\left(\frac{V_{\text{tank}} + V^*}{V_{\text{tank}} + \frac{V_{cyl}}{C_r}}\right)^{\gamma-1}. \tag{3-11}$$

The charging valve closes at point '3' so the amount of air mass trapped in the cylinder dead volume can be found as follows:

$$m_{cyl} = \frac{P_3 \frac{V_{cyl}}{C_r}}{R \upsilon_3} M_{air}. \tag{3-12}$$

Now if we plug Eqs.(3-10) and (3-11) into Eq.(3-12), the trapped mass in the cylinder after closing the charging valve will be:

$$m_{cyl} = \frac{P_{atm} V_{cyl}}{R \upsilon_{atm}} M_{air}\,, \qquad 3\text{-}13$$

which equals the amount of air mass entered into the cylinder at point '1' (Eq. (3-7)). This means that no air can be stored in the tank if the amount of the air mass in the tank equals to what is shown by Eq.(3-5). Since the maximum amount of air mass in the air tank is limited, to increase the energy storing ability of the system, tank temperature should be kept as high as possible. Although higher tank temperature increases the storing pressure and, consequently, increases the energy storing capacity of the system, tank temperature should be bounded because it increases the engine body temperature and causes pre-ignition in the cylinder. Thus, the storing pressure and energy storing capacity of the regenerative system are also bounded. For an air hybrid engine with the compression ratio of 10 and maximum tank temperature of 450[K], the maximum achievable tank pressure is about 15[bar]. Considering these results, the maximum energy storing capacity of a pneumatic regenerative braking system is about 1.57[kJ/litre]. Compared to the energy density of Lithium-ion batteries which is about 700-1000[kJ/Litre] [28,30,31], the pneumatic regenerative braking system's ability to store energy is insignificant. Based on Eq.(3-5), there are two options to increase the capacity of energy storing of the air tank – either using a larger tank or increasing the compression ratio. Increasing the volume of the tank is not a viable solution due to space limitation in the vehicle. Likewise, increasing the compression ratio of the cylinder is not achievable because of engine performance limitations. However, the system overall compression ratio can be increased indirectly if a multi-tank compression technique is employed.

3.3 Double-tank Regenerative Braking

The double-tank regenerative system is comprised of two storage tanks, one small in size, low pressure tank (LP) and one large in size, high pressure tank (HP), as shown in Figure 3-3. With reference to this figure, the four steps of a cycle are defined as follows:

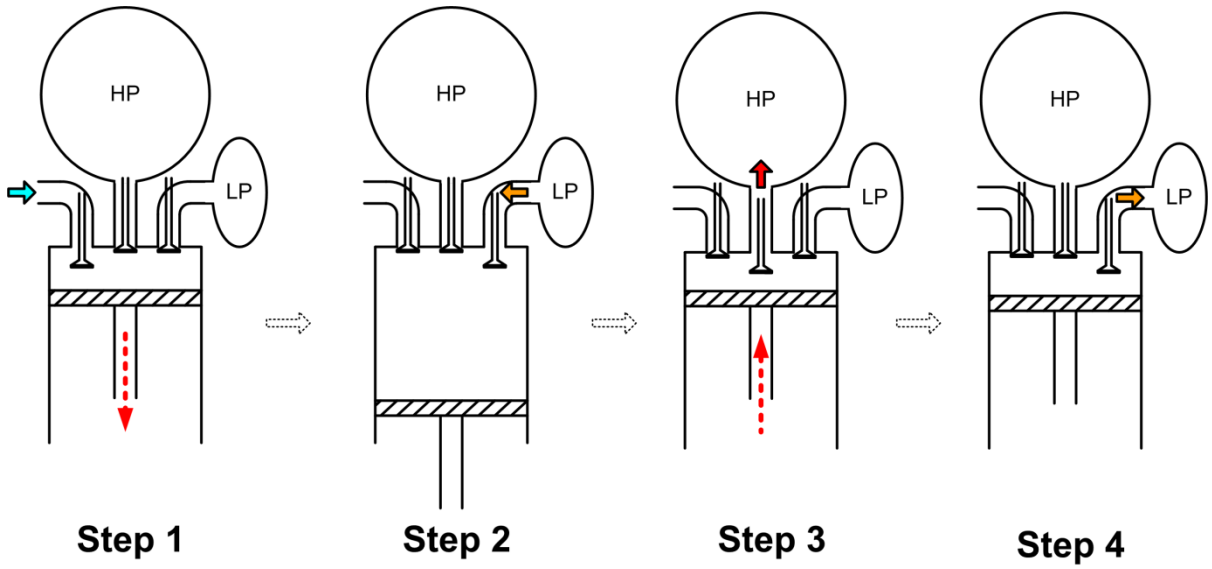

Figure 3-3: Proposed compression strategy

Step 1: In this step, the intake valve opens and the cylinder is filled with atmospheric pressure.

Step 2: While the piston is still in the vicinity of the BDC, the intake valve closes and the charging valve between the low pressure tank and the cylinder opens and, consequently, the cylinder is charged with the pressurized air from the LP tank. Thus, the cylinder pressure increases to higher than atmospheric pressure. The charging valve closes after the cylinder pressure equals the LP tank pressure to avoid sending the pressurized air back to the LP tank.

Step 3: In this step, gas in the cylinder is compressed adiabatically and the charging valve between the cylinder and high pressure tank opens allowing the HP tank to be charged adiabatically. It closes when the piston is in the vicinity of the TDC.

Step 4: While the piston is still in the vicinity of the TDC and the pressure in the cylinder is still high enough, the charging valve between the cylinder and low pressure tank opens to charge the LP tank with the remaining of the pressurized air in the cylinder. The charging valve closes when the piston starts going down and the cylinder pressure starts to drop.

Following the above charging procedure, higher air mass in the main tank (HP tank) can be stored because the cylinder pressure is supercharged by the LP tank in step 2. It is

important to note that this strategy is different from a multi-stage compression strategy since it only needs one cylinder and the compression cycle is completed in only one revolution of the crank shaft. This results in doubling the flow rate to the air tank compared to the double-stage strategy proposed by Schechter [14]. It has to be mentioned that as the case of double-stage compression strategy in which air is cooled down between the stages to increase the overall efficiency of the system, in double-tank compression strategy the LP tank should be cooled down to increase the mass flow rate from the LP to the cylinder and, consequently, to increase the energy storing efficiency of the system.

Figure 3-4 shows the thermodynamic cycle of the double-tank compression strategy. As can be seen, the double-tank regenerative cycle produces higher braking torque compared to the single-tank cycle as the cylinder P-V cycle has bigger enclosed area for the double-tank case. LPVC and LPVO in the figure indicate low pressure valve opening and closing, respectively.

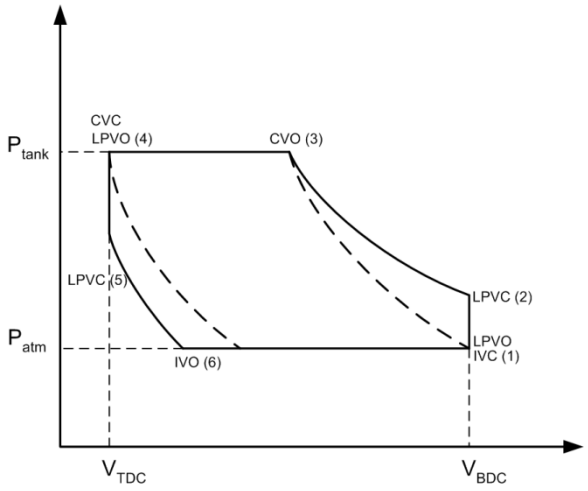

Figure 3-4: Double-tank regenerative ideal braking cycle

Theoretically, based on the above compression algorithm, the maximum amount of air mass that can be stored in a double-tank regenerative system considering adiabatic compression and expression in the cylinder is:

$$m_{\text{tank,max}} = \frac{P_{atm} V_{\text{tank}}}{\upsilon_{atm} R} C_r \left(\frac{1 + C_r \frac{V_{LP}}{V_{cyl}}}{1 + \frac{V_{LP}}{V_{cyl}}} \right) M_{air}. \qquad 3\text{-}14$$

To prove the above equation we consider Figure 3-4 again. It is assumed that the LP tank is cooled down to the environment temperature. The maximum LP pressure when both of the tanks are completely full, is defined by the following relation (For more details see Appendix C):

$$P_{LP} = P_{atm} C_r. \qquad 3\text{-}15$$

Assuming an ideal mixing process, the cylinder pressure at point '2', after supercharging the engine with the LP tank pressurized air, is:

$$P_2 = \frac{P_{atm} V_{cyl} + P_{LP} V_{LP}}{V_{cyl} + V_{LP}}. \qquad 3\text{-}16$$

Since HP tank is already full, we can assume that the charging valve opens and closes precisely at TDC. Thus, pressure and temperature at point '4' will be defined by:

$$P_{3,4} = \frac{P_{atm} V_{cyl} + P_{LP} V_{LP}}{V_{cyl} + V_{LP}} C_r{}^{\gamma}, \qquad 3\text{-}17$$

$$\upsilon_{3,4} = \upsilon_{atm} C_r{}^{\gamma - 1}. \qquad 3\text{-}18$$

Since the HP tank is full, $P_{HP} = P_{3,4}$, thus, the maximum amount of mass stored in the HP tank becomes:

$$m_{\text{tank,max}} = \frac{P_4 V_{\text{tank}}}{R \upsilon_4} M_{air} = \frac{P_{atm} V_{\text{tank}}}{R \upsilon_{atm}} C_r \left(\frac{1 + C_r \frac{V_{LP}}{V_{cyl}}}{1 + \frac{V_{LP}}{V_{cyl}}} \right) M_{air}. \qquad 3\text{-}19$$

Considering $\upsilon_{HP,\max} = 450$[K], $V_{LP} = V_{cyl}$ and $C_r = 10$, the maximum pressure could go up to 82.5[bar], which is a considerable improvement compared to 15[bar]. Consequently, the aforementioned double-tank compression technique can increase the energy density of the main storage by a factor of 8.5 (based on the definition for efficiency given in Eq. (3-4)).

3.4 Simulations

The above-mentioned compression processes are used to simulate and compare the single-tank and the double-tank regenerative braking of a quarter vehicle model with the specifications shown in Table 3-1. It is assumed that the vehicle decelerates from 60[km/hr] only by using regenerative braking and no energy is lost due to engine friction, vehicle resistance or any other source of energy losses. The LP tank in the double-tank system is assumed to be cooled down to the environment temperature. In these simulations, the valve and gas exchange dynamics through the valves are neglected.

Table 3-1 Simulated vehicle specifications

Vehicle Mass	450 [kg]
Engine Type	Single Cylinder
Cylinder Volume	500 [cc]
Storage Tank Volume	7.5 [l]
Compression Ratio	10
Storage Tank Initial Pressure	1 [bar]
Maximum Tank Temperature	450 [k]
LP Tank Volume	0.5 [l]

Figure 3-5.a charts the vehicle velocity versus time for the single-tank regenerative system. It shows that by using only regenerative braking, the vehicle stops in about 25 [s]. Figure 6.b shows the pressure in the storage tank. As can be seen, there is a limit for pressure increase in the air tank. The tank pressure builds up to 15 [bar], but cannot increase further. Based on the definition for efficiency (Eq.(3-2)), the regenerative braking system is able to store only 21% of the vehicle's kinetic energy.

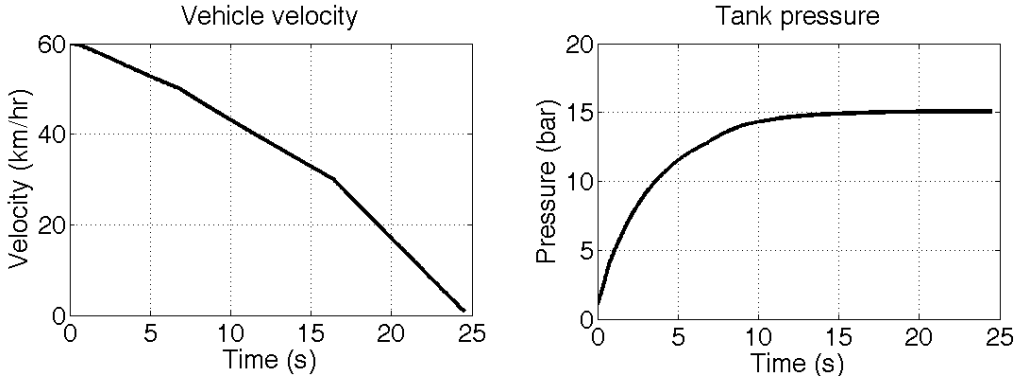

Figure 3-5: Vehicle velocity (a) and Tank pressure (b)

Figure 3-6 shows the simulation results for the double tank system. As shown in this figure, the pressure in the main storage tank increases to more than 26 [bar]. This increases the system energy-storing efficiency to about 43% (based on Eq.(3-2)), which is a sizeable improvement compared to the case of single-tank regenerative cycle. The results also show that the double-tank regenerative system slows down the vehicle much faster, which implies that it produces higher braking torques.

The effect of adding more tanks to the compression strategy is studied in Appendix D. It is shown that the maximum pressure is achieved mostly when a double-tank system is used.

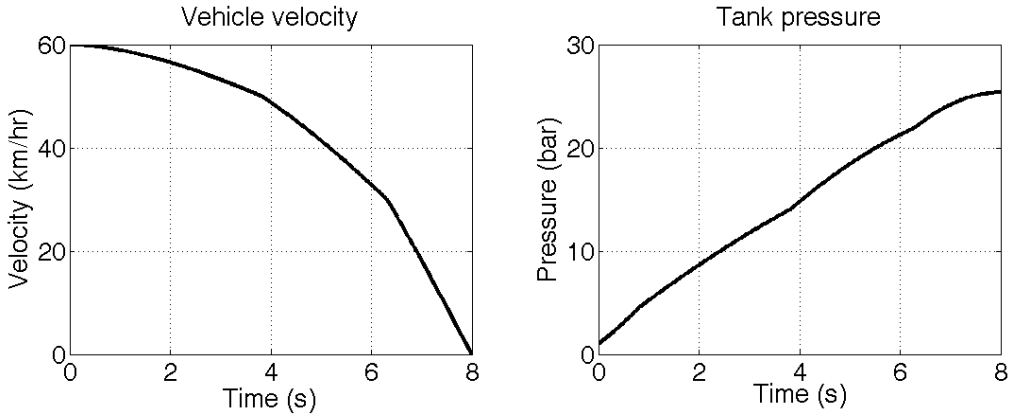

Figure 3-6: Vehicle velocity (a) and Tank pressure (b)

3.5 Detailed System Modeling Based on the First Law of Thermodynamics

In this section, a detailed model for the regenerative braking system is derived. Figure 3-7 shows the cylinder geometrical parameters.

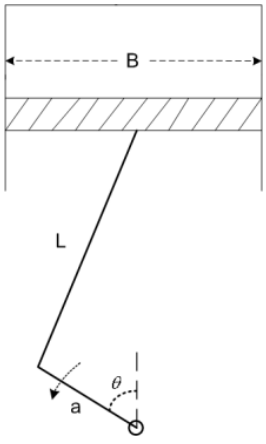

Figure 3-7: Cylinder geometrical parameters

Based on these parameters, the rate of change of cylinder volume can be expressed as a function of engine speed, as:

$$\frac{dV_{cyl}}{dt} = \frac{\pi B^2}{4}\left[a\sin(\theta) + \frac{a^2 \sin(\theta)\cos(\theta)}{\sqrt{l^2 - a^2 \sin^2(\theta)}} \right]\omega . \tag{3.14}$$

Figure 3-8 displays the cylinder inlet flows from intake manifold, low-pressure and high-pressure tanks.

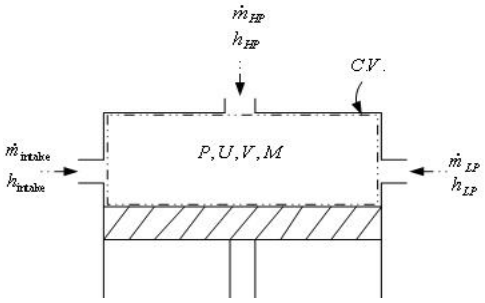

Figure 3-8: Inlet flows to the cylinder

Applying the first law of thermodynamics for the control volume shown in the Figure 3-8 leads to the following relation:

$$m_{cyl}\dot{u}_{cyl} + \dot{m}_{cyl}u_{cyl} + P_{cyl}\dot{V}_{cyl} = \dot{Q} + \dot{m}_{\text{intake}}h_{\text{intake}} + \dot{m}_{\text{HP}}h_{\text{HP}} + \dot{m}_{\text{LP}}h_{\text{LP}}. \tag{3-20}$$

Assuming that the gas follows the ideal gas rule, the following relation for the cylinder can be derived:

$$\frac{\dot{P}_{cyl}}{P_{cyl}} - \frac{\dot{m}_{cyl}}{m_{cyl}} - \frac{\dot{\upsilon}_{cyl}}{\upsilon_{cyl}} + \frac{\dot{V}_{cyl}}{V_{cyl}} = 0. \tag{3-21}$$

The rate of change of internal energy is also related to rate of change of temperature by the following relation:

$$\dot{u}_{cyl} = c_v \dot{\upsilon}_{cyl} . \tag{3-22}$$

The mass flow rate through the engine valves can be expressed by [32]:

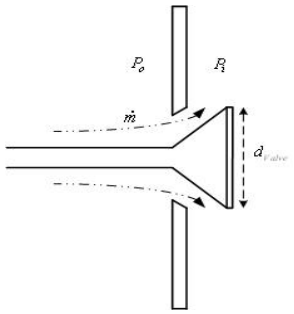

Figure 3-9: Flow through engine valves

$$\dot{m}_{valve} = \rho_{air} A_{valve} C_d C_o \sqrt{\frac{2}{\gamma - 1}\left[\left(\frac{P_{in}}{P_{out}}\right)^{2/\gamma} - \left(\frac{P_{in}}{P_{out}}\right)^{1+\gamma/\gamma}\right]}. \quad 3\text{-}23$$

In the case of choked flow, where $\frac{P_{out}}{P_{in}} > \left(\frac{\gamma+1}{2}\right)^{\gamma/\gamma-1}$, the above equation will be modified as follows [32]:

$$\dot{m} = \rho_{air} A_{valve} C_d C_o \sqrt{\frac{2}{\gamma - 1}\left[\left(\frac{2}{\gamma+1}\right)^{2/\gamma-1} - \left(\frac{2}{\gamma+1}\right)^{1+\gamma/\gamma-1}\right]}. \quad 3\text{-}24$$

The first law formulation for HP and LP tanks is written as follows:

$$m_{\text{tank}}\dot{u}_{\text{tank}} + \dot{m}_{\text{tank}} u_{\text{tank}} = \dot{Q}_{\text{tank}} + \dot{m}_{\text{i}} h_i, \quad 3\text{-}25$$

Assuming ideal behavior of the gas, the following relation can also be derived for the tanks set:

$$\frac{\dot{P}_{\text{tank}}}{P_{\text{tank}}} - \frac{\dot{m}_{\text{tank}}}{m_{\text{tank}}} - \frac{\dot{\upsilon}_{\text{tank}}}{\upsilon_{\text{tank}}} = 0. \quad 3\text{-}26$$

The friction of the cylinder is also an important issue. There are several models in the literature for estimating the cylinder friction. The following model expresses the Friction Mean Effective Pressure (FMEP) as a function of engine speed [33].

$$FMEP = 0.97 + 0.15\left(\frac{\omega}{1000}\right) + 0.05\left(\frac{\omega}{1000}\right)^2. \quad 3\text{-}27$$

The heat transfer from the cylinder is calculated using the Woschni correlative model for convective heat transfer. This model assumes simple heat transfer from a confined volume surrounded on all sides by walls representing the cylinder head, and piston face

areas exposed to the combustion chamber [33]. The heat transfer coefficient of Woschni model is:

$$\hbar = 3.26 B^{-0.2} P_{cyl}^{0.8} \upsilon_{cyl}^{-0.55} v_{gas}^{0.8}. \quad 3\text{-}28$$

In the above equation, v_{gas} is the gas mean speed and is estimated by the following relation [34]:

$$v_{gas} = 2.28 \bar{v}_p, \quad 3\text{-}29$$

where $\bar{v}_p = 4a\omega$. Based on the Woschni model, heat transfer to the cylinder is expressed as:

$$\dot{Q}_{cyl} = \hbar A_{cyl} \left(\upsilon_c - \upsilon_{cyl} \right), \quad 3\text{-}30$$

where υ_c is coolant temperature and A_{cyl} is the cylinder exposed area which is a function of the crank angle based on:

$$A_{cyl} = \frac{\pi}{2} B^2 + \pi B a \left(\left(l/a \right) + 1 - \cos(\theta) + \left(\left(l/a \right)^2 - \sin(\theta) \right)^{0.5} \right). \quad 3\text{-}31$$

For the sake of simplicity, heat flux from the tanks surfaces is modeled by the following relations:

$$\dot{Q}_{LP} = \hbar_{LP} \left(\upsilon_0 - \upsilon_{LP} \right), \quad 3\text{-}32$$

$$\dot{Q}_{HP} = \hbar_{HP} \left(\upsilon_0 - \upsilon_{HP} \right), \quad 3\text{-}33$$

where υ_o is environment temperature. As discussed previously, to increase the efficiency of compression braking LP tank should be cooled down but the HP tank should be insulated. Since there is no specific design for both of the tanks, $\hbar_{LP}$ is considered to be much larger than $\hbar_{HP}$.

The above differential equations could be coupled with vehicle dynamic equations through the following relation:

$$\left(P_{cyl} - P_{atm} + FMEP \operatorname{sgn}\left(\dot{V}_{cyl} \right) \right) \dot{V}_{cyl} = F_{Trac.,Braking} \, v. \quad 3\text{-}34$$

Vehicle velocity, which is related to the engine speed by:

$$v = \frac{1}{rG} \omega. \quad 3\text{-}35$$

The vehicle dynamic equation is also written as follows:

$$F_{trac,braking} - \frac{1}{2}\rho_{air} C_d A v^2 - M_{vehicle}\, g \sin(\theta) - M_{vehicle}\, g\, f_r = M_{vehicle}\, \dot{v}. \qquad 3\text{-}36$$

Equations (3-14) to (3-36) comprise a system of nonlinear differential equations which should be solved together.

3.6 Simulation of Mathematical and GT-POWER Models

GT-POWER is a simulation program which is widely used by major vehicle manufacturers and engine developers. It can be used for engine and powertrain analysis. This software is based on 1-D simulation of gas dynamics and has the ability to model and analyze heat transfer, combustion, and vibration. In this section, the simulation results of the mathematical model described in Section 3.5 and GT-POWER model for both single-tank and double-tank regenerative braking system are presented and compared. A vehicle quarter model with the specifications shown in Table 3-2 decelerated from 80 [km/hr] to a complete stop utilizing a single-storage regenerative braking system.

Table 3-2: Vehicle quarter model specifications [1]

Vehicle Mass	1800/4 [kg]
Initial Velocity	80 [km/hr]
Final Velocity	0 [km/hr]
Engine Displacement	450 [cc]
Compression Ratio	8.5
HP Tank Volume	10 [l]
LP Tank Volume	1 [l]

Table 3-3 lists intake and charging fixed valve timing with respect to TDC used in both GT-POWER and mathematical model.

Table 3-3: Single tank system valve timing

	Opening Degree	Closing Degree
Intake Valve	20	160
Charging Valve	270	350

[1] More simulation parameters may be found in Appendix E

GT-Power and mathematical model simulation results for tank pressure are shown and compared in Figure 3-10 This figure indicates that GT-POWER and the mathematical model results are consistent. As can be seen, the tank pressure increases to about 17[bar] but it is bounded below 20[bar] using single-tank regenerative braking. Figure 3-11 shows the vehicle velocity versus time. As can be seen, the vehicle stops in less than 10 seconds. Although the obtained results from GT-Power and mathematical model are consistent, the difference between GT-POWER and mathematical results are due to following factors:

1. different engine friction models,
2. different heat transfer coefficients.

Figure 3-11 also shows that the deceleration rate increases by the increase in the tank pressure. This means that in spite of considering fixed valve timing, the produced braking torque by regenerative braking system changes with tank pressure.

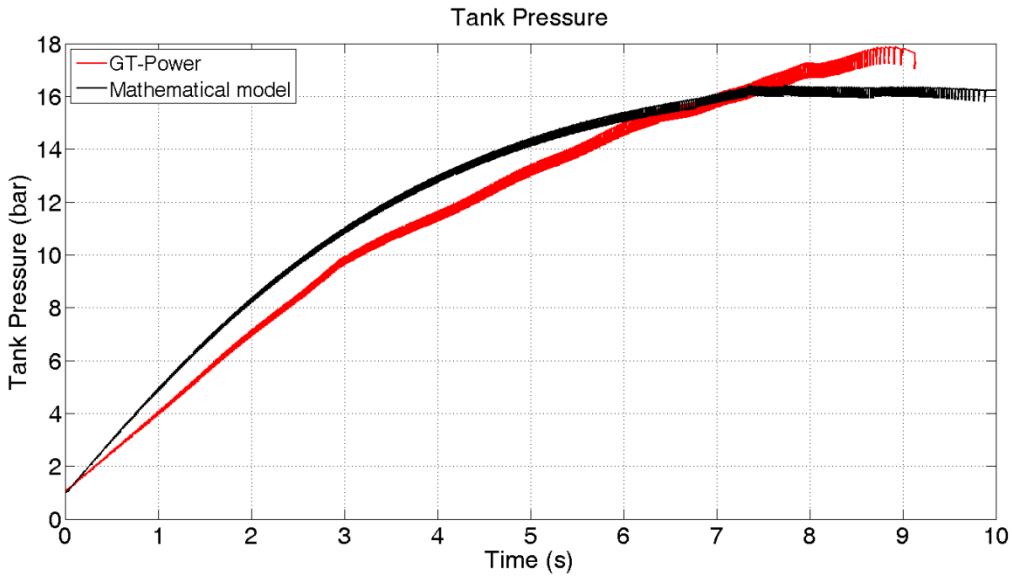

Figure 3-10: Tank pressure vs. time

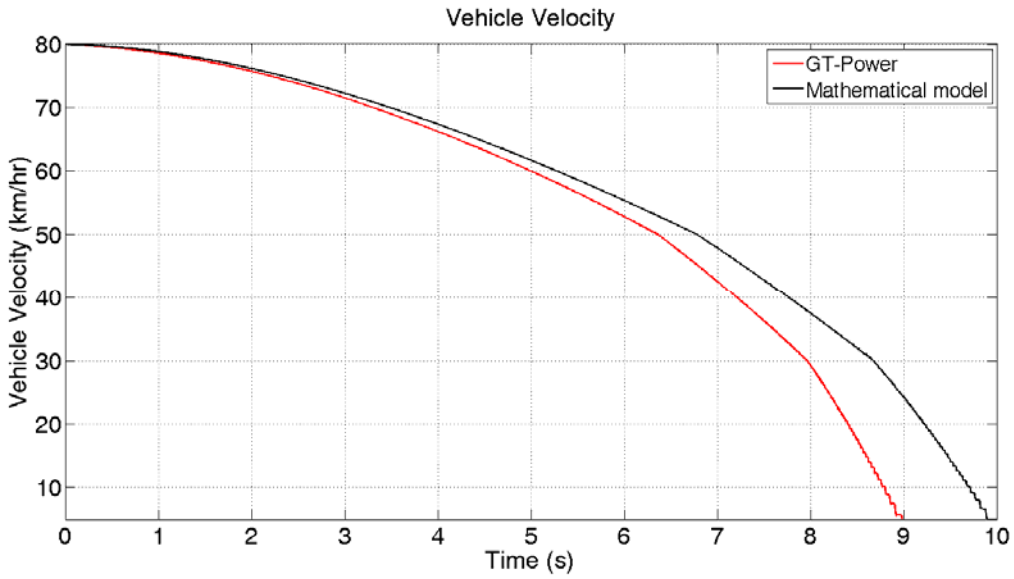

Figure 3-11: Vehicle velocity vs. time

Table 3-4 lists intake, HP and LP fixed valve timing with respect to TDC for the case of double-tank regenerative system. As can be seen, the LP valve opens and closes two times per cycle.

Table 3-4: Double tank system valve timing

	Opening Degree	Closing Degree
Intake Valve	20	160
Charging Valve	270	350
LP Valve	180	200
	355	15

Figure 3-12 shows HP tank pressure versus time. Pressure in the HP tank increases to about 28[bar], which is a sizeable improvement compared with the single-tank system result. The rate of change of pressure is also positive at the end of deceleration which means that the system is still able to store more energy. The inflections seen in this figure are due to the gear change. Figure 3-13 and Figure 3-14 illustrate LP tank pressure and vehicle velocity versus time. As can be seen in Figure 3-14, double-tank system stops the vehicle faster than single-tank system. This implies that the average braking torque of the double-tank system is higher than single-tank system. The difference between mathematical and GT-POWER model results could be explained as mentioned before.

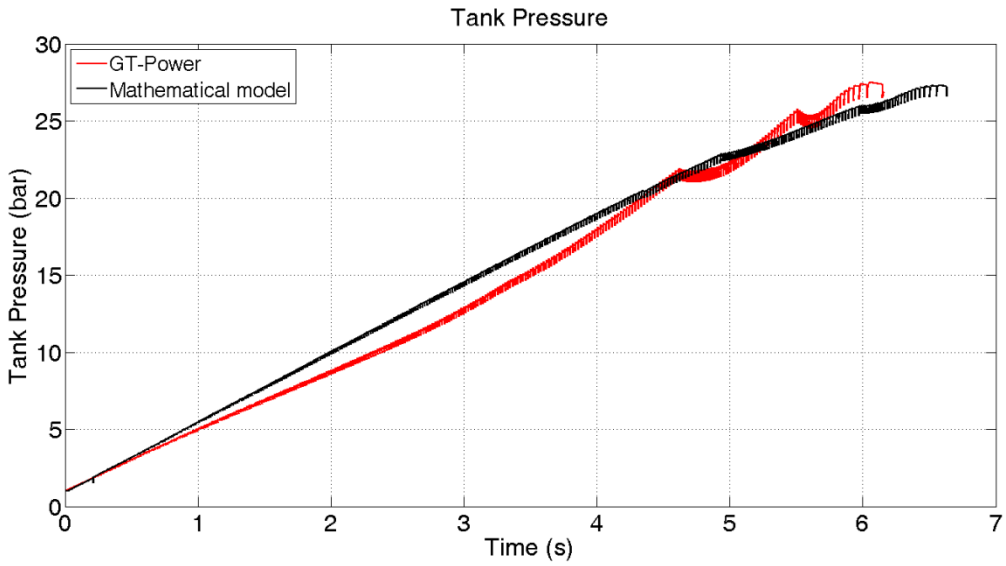

Figure 3-12: HP tank pressure vs. time

The simulation results are summarized in Table 3-5. The maximum temperature using both approaches is in the same range but the final pressures are significantly different. The obtained results show that by using the multi-tank regenerative braking system, the stored energy is twice as much energy as could be stored in a single-tank system. The maximum efficiency of 28% might seem to be low at first glance, but it should be taken into consideration that these results are obtained based on fixed valve timing. In other words, using a multi-tank system, the efficiency of energy storing could be enhanced by optimizing valve timing based on tank pressure, and desired load, by following the ideal braking cycle but the efficiency of a single-tank system is limited due to the limitation on the maximum mass of air stored in the tank.

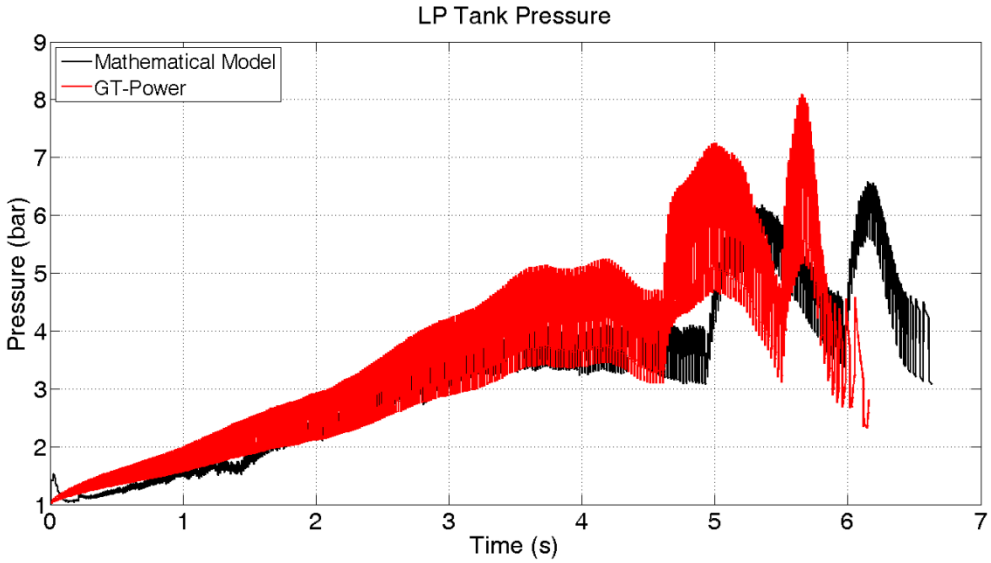

Figure 3-13: LP tank pressure vs. time

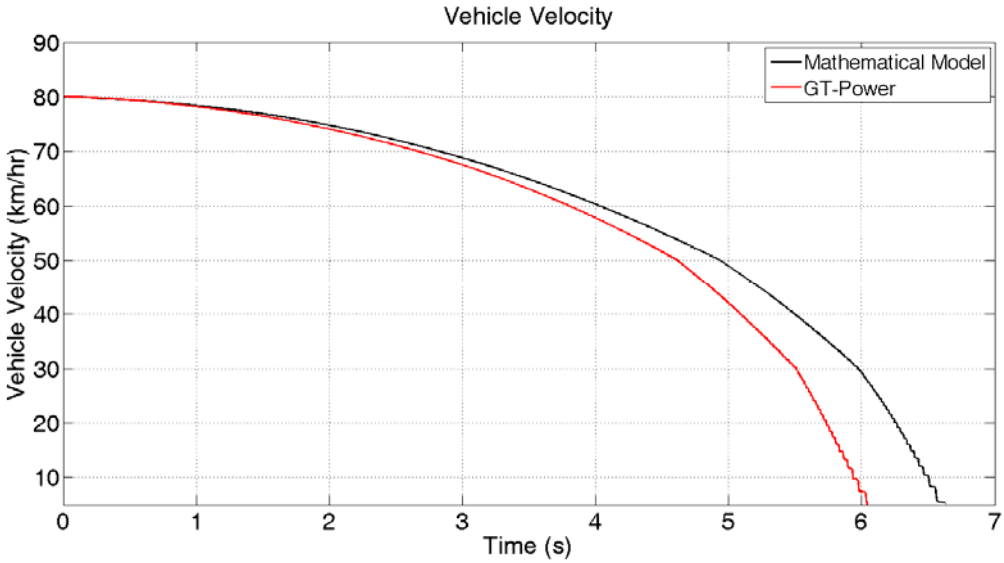

Figure 3-14: Vehicle velocity vs. time

The obtained results show a good consistency between GT-POWER model and mathematical model and confirm the derived mathematical model.

Table 3-5 Simulation results

	Single Tank	Double Tank
Maximum Pressure	20 [bar]	35 [bar]
Maximum Temperature	800 [k]	800 [k]
Efficiency	14 %	28 %

3.7 Summary

In this chapter a new compression strategy was introduced for air hybrid engines. The theoretical results showed the advantage of the proposed strategy over the conventional single-tank system. The proposed compression algorithm can be utilized in an air hybrid vehicle to increase the efficiency of energy recovery by the compression braking system. Compared to the double-stage regenerative braking, the double-tank system doubles the air flow rate because only one cylinder is needed to implement the proposed concept and thus, all the cylinders can be connected directly to the main tank. The proposed compression algorithm can be applied not only in air hybrid vehicle compression braking system, but also in any other applications where higher pressure with higher air mass flow rate is demanded such as typical reciprocating compressors. Double-tank compressors are expected to have the same working pressure and outlet flow rate as double-stage compressors, but with a weight of almost half of a double-stage one. The following chapter presents the experimental results of implementing the double-tank regenerative system.

Chapter 4
Experimental Analysis

To test the proposed double-tank compression technique and compare it with the single-tank technique in practice, an experimental setup has been designed and built as shown in Figure 4-1 and Figure 4-2. This setup enables the testing of two modes of operation: AM and CB. In the setup, a single cylinder engine has been turned into an air hybrid engine by replacing the cylinder head with a new one that connects the engine to two air tanks. Figure 4-1 shows the schematic of the system layout. A servo DC motor is connected to a large flywheel through an electromagnetic clutch and an electromagnetic brake. The motor shaft is connected to the engine shaft by a timing pulleys set with the ratio of 60/28. The engine angular rotation is measured by an incremental encoder mounted on the engine shaft. The encoder's signal defines the accurate angular position of the crank shaft w.r.t. TDC. The experimental set-up is comprised of the following components:

1. A single cylinder engine
2. Electromagnetic clutch and brake
3. Flywheel
4. Servo motor and drive
5. Timing pulleys
6. Pressure sensors
7. Thermocouples
8. Small and large tanks
9. Solenoid valves
10. Beckhoff PLC controller
11. Encoder
12. Couplings and universal joint

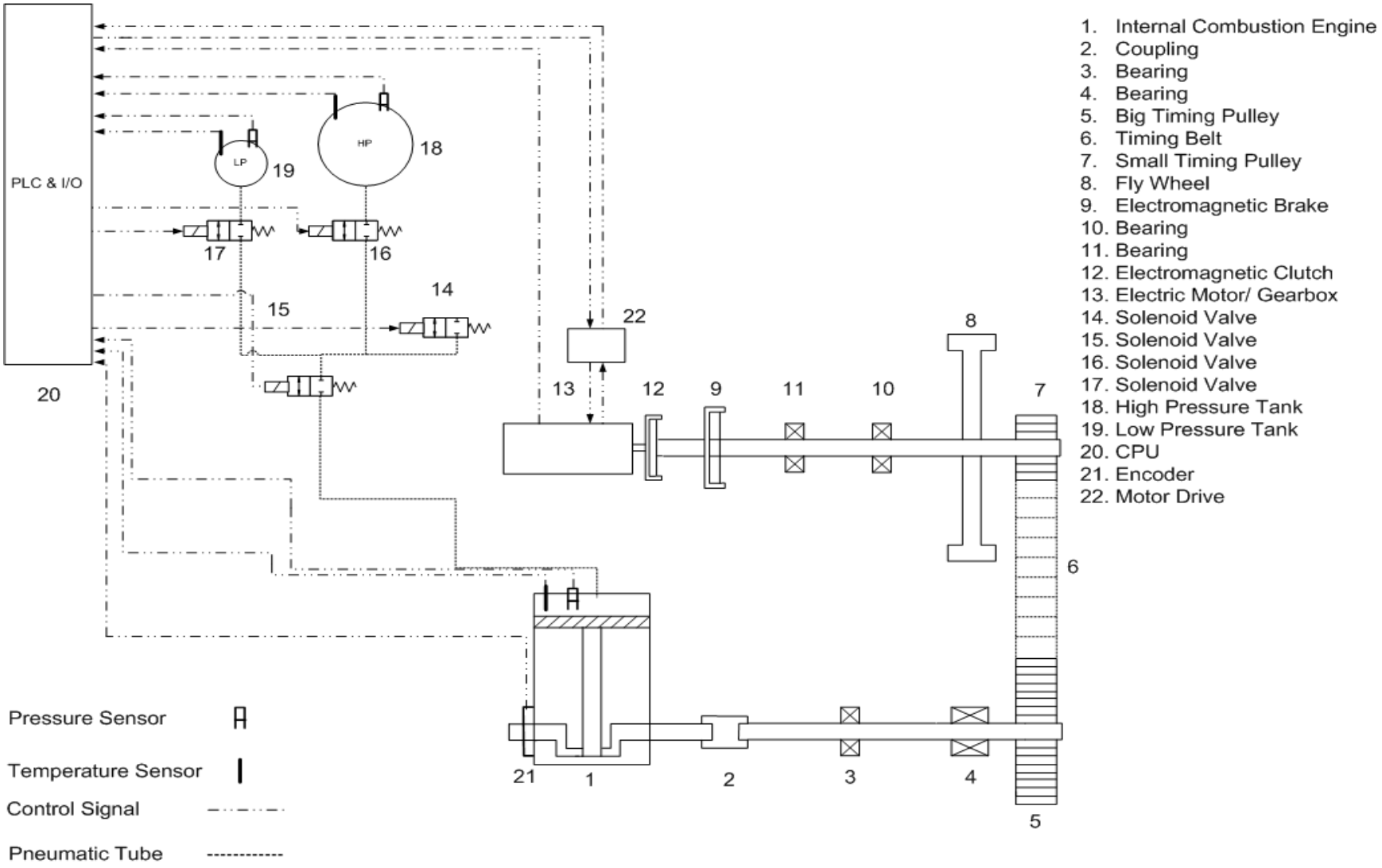

Figure 4-1: Experimental set-up layout

The specifications of some of the components of the setup are listed in Table 4-1. In the present study a 2-litre air tank is used. However, for practical applications the storage volume of the system should be optimized to increase the efficiency of the regenerative braking in the vehicle driving cycles.

Table 4-1: Engine and tanks' characteristics

Bore	90 [mm]
Stroke	67 [mm]
Compression ratio	8.5
LP tank volume	450 [cc]
HP tank volume	2 [l]

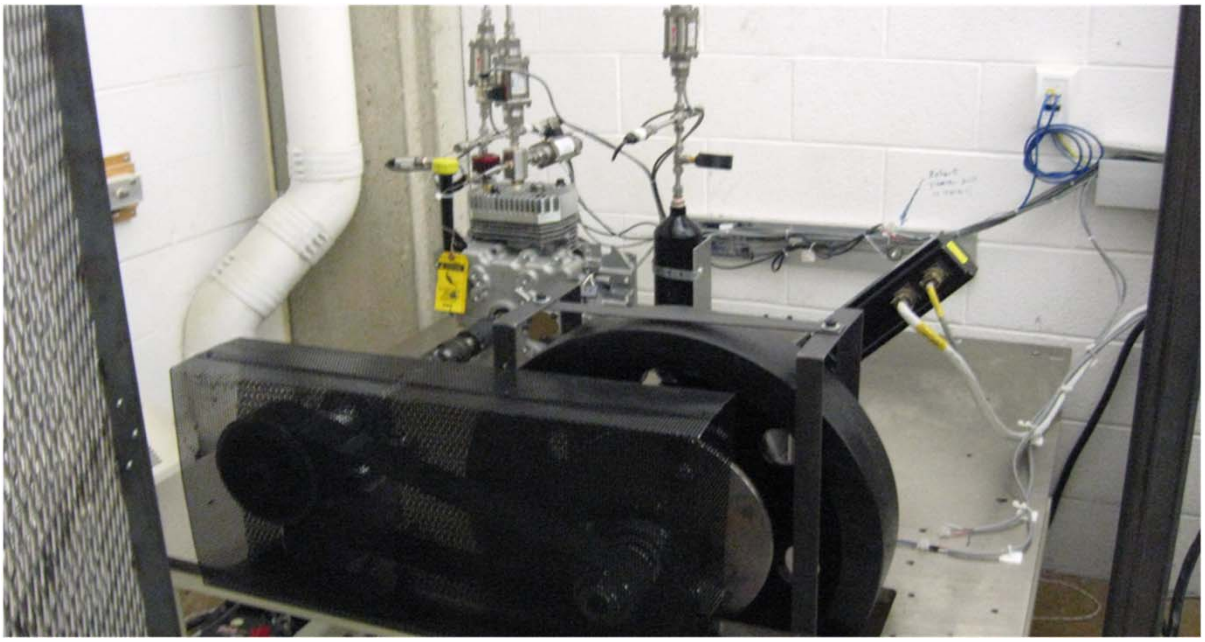

Figure 4-2: Experimental setup

The conventional cylinder head was replaced with a new cylinder head that was designed and fabricated. The cylinder head configuration is shown in Figure 4-3. In the new cylinder head configuration, a check valve with relatively low breaking pressure is directly mounted on the cylinder head to let the fresh air flow into the cylinder when the piston goes down. A manifold was also designed and manufactured to connect the cylinder to other parts of the setup. Two solenoids ('1' and '2') were mounted directly on this manifold. The first solenoid

connects the cylinder to the environment and is only activated during startup. The second one connects the cylinder to the tank set. Solenoids ‘3’ and ‘4’ are LP and HP valves, respectively. The solenoid valves have the characteristics listed in Table 4-2.

Table 4-2: Solenoid valves characteristics

Flow capacity	2.5 [m3/h]
Maximum allowable temperature	100 [c]

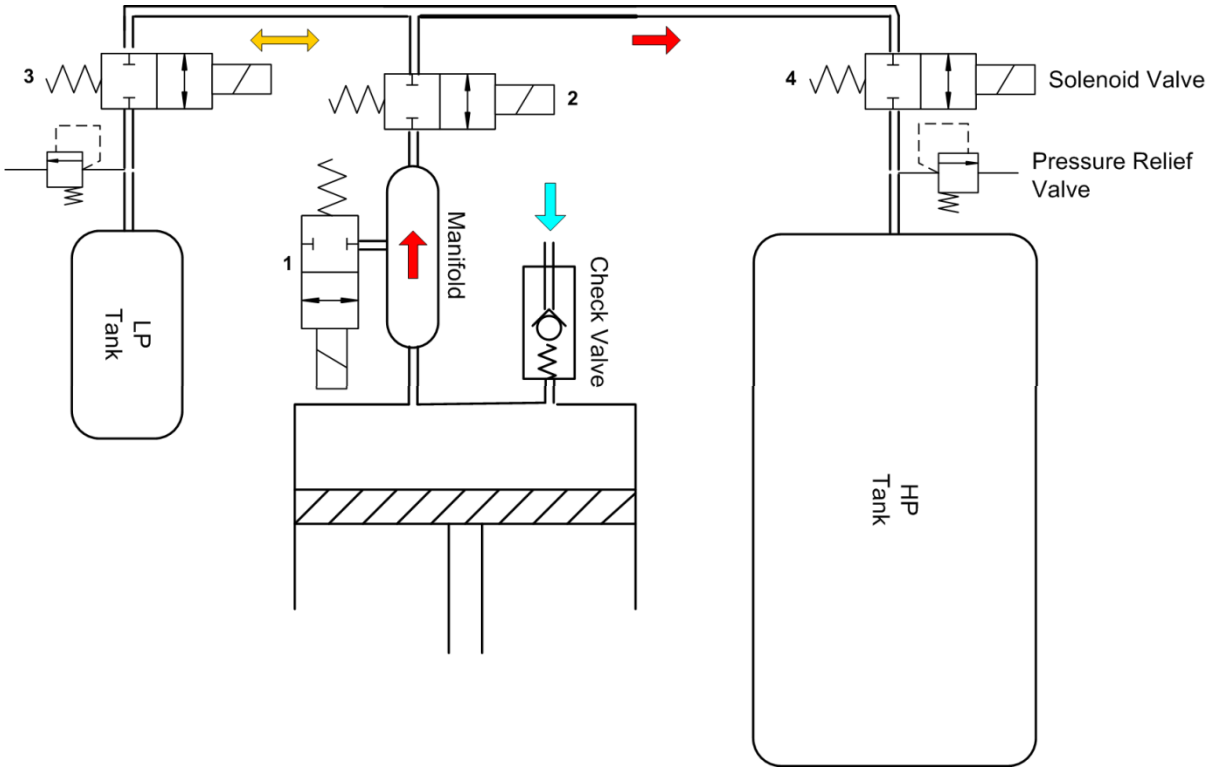

Figure 4-3: Cylinder head configuration

Figure 4-4.a and 4-4.b indicate approximate valve timings of the single-tank and double-tank regenerative braking systems respectively with respect to the crank shaft angle. As Figure 4-4 shows, valve ‘1’ is always closed, valve ‘2’ is always open, and valve ‘4’ opens after BDC and closes in the vicinity of TDC during CB mode. Valve ‘3’, which is only activated in the double-tank system, opens and closes twice in each engine revolution – once in the vicinity of TDC and once in the vicinity of BDC.

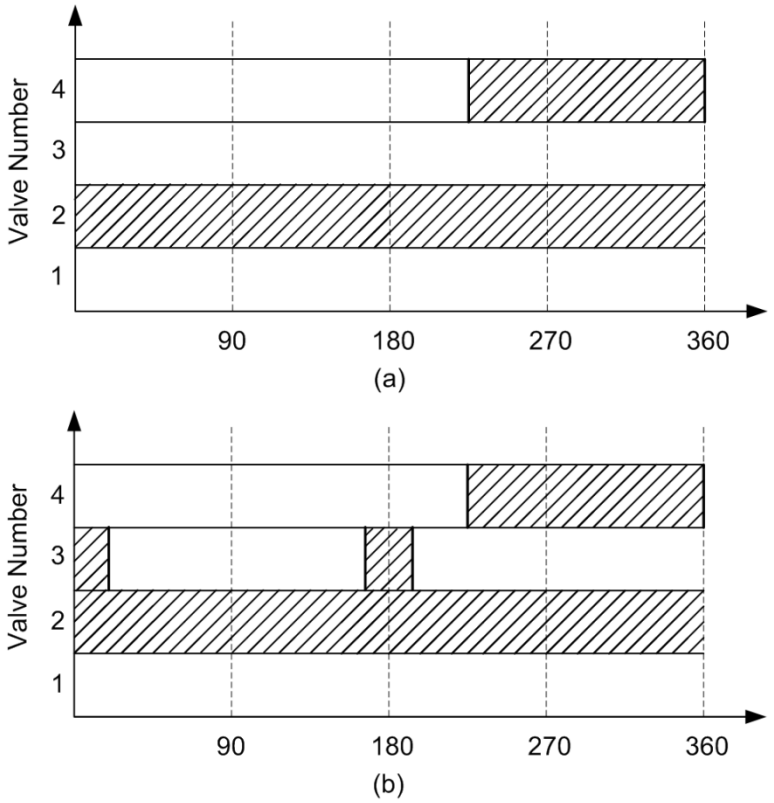

Figure 4-4: Valve timing (a) Single-tank system, (b) Double-tank system

Following the valves timing depicted on Figure 4-4, the single-tank and double-tank compression strategies can be implemented and compared experimentally.

4.1 Test Procedure

A test was designed to simulate the full throttle braking of a 1400 [kg] vehicle from 30 [km/hr] down to zero equipped with a four-cylinder engine. Since a single-cylinder engine was used for this test, the flywheel speed was set at 1500 [rpm], where it has a quarter of the vehicle kinetic energy. At this speed, the engine rotates at 700[rpm]. However, the solenoid valves response time is found to be much slower than what was expected, and in fact, to implement the required timings, they do not act at the ICE speeds of higher than 50[rpm]. Consequently, the test procedure was changed to compensate for the valves' limitations. In the revised procedure, the ICE speed is set to 42[rpm] by removing the electromagnetic clutch and using a 1 to 12 transmission at the electric motor output to ensure that all the solenoid valves have enough time to switch on and off. Although the test is performed at

42[rpm] due to valves' speed limitations, the same results are expected for higher engine speeds. Valve '2' is opened initially to let the ICE rotate freely. Then, the PLC activates the regenerative cycle by closing the second valve and controlling other valves, based on the timings shown in Figure 4-4. This procedure is done for the single-tank regenerative system and then for the double-tank system by activating and deactivating valve '3'.

4.2 Experimental Results

In this section, the experimental results are presented. The single-tank regenerative braking is considered first. Table 4-3 shows solenoid valve timing for the single-tank case. As can be seen, solenoids '1' and '3' are closed, solenoid '2' is always open, and solenoid '4' is activated based on the crank angle.

Table 4-3: Solenoid valves activation

Solenoid '1'	Always closed
Solenoid '2'	Always open
Solenoid '3'	Always closed
Solenoid '4'	Opens from 290 to 355 CAD

The experimental results for the HP tank pressure are shown in Figure 4-5. As Figure 4-5 illustrates, the tank pressure increases to more than 3 [bar] after 60 seconds, but the rate of pressure build up decreases rapidly with time. It is worth mentioning that since the cylinder head is completely replaced with a new one, the compression ratio of the system decreases from 8.5 (Table 4-1) to less than 4 because the volume of the manifold and all the connecting pipes are added to the dead volume of the cylinder. The other reason for such a low pressure is the significant gas leakage from cylinder/piston clearance. The engine used in this study is a general purpose engine that needs a minimum working temperature and pressure for proper sealing.

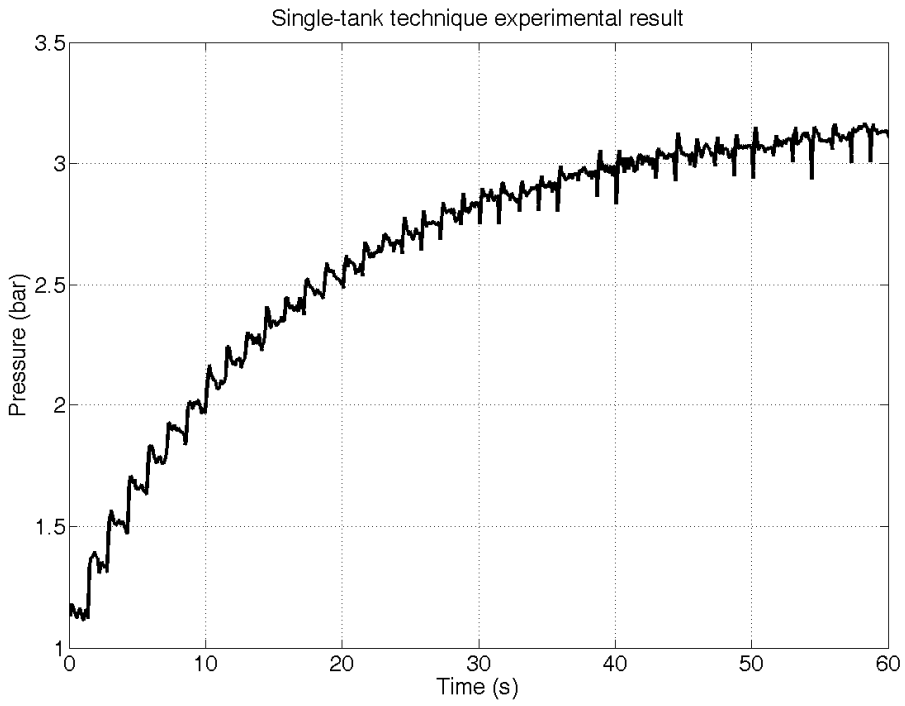

Figure 4-5: HP tank pressure obtained from experiment

The double-tank regenerative braking is tested in the next experiment. Here, the solenoid valves are activated based on Table 4-4. Solenoid '3' is switched on and off twice during each cycle, once in the vicinity of TDC and once in the vicinity of BTC. The results are shown in Figure 4-6 and Figure 4-7.

Table 4-4: Solenoid valves activation

Solenoid '1'	Always closed
Solenoid '2'	Always open
Solenoid '3'	Opens from 170 to 190 and from 5 to 25 CAD
Solenoid '4'	Opens from 290 to 355 CAD

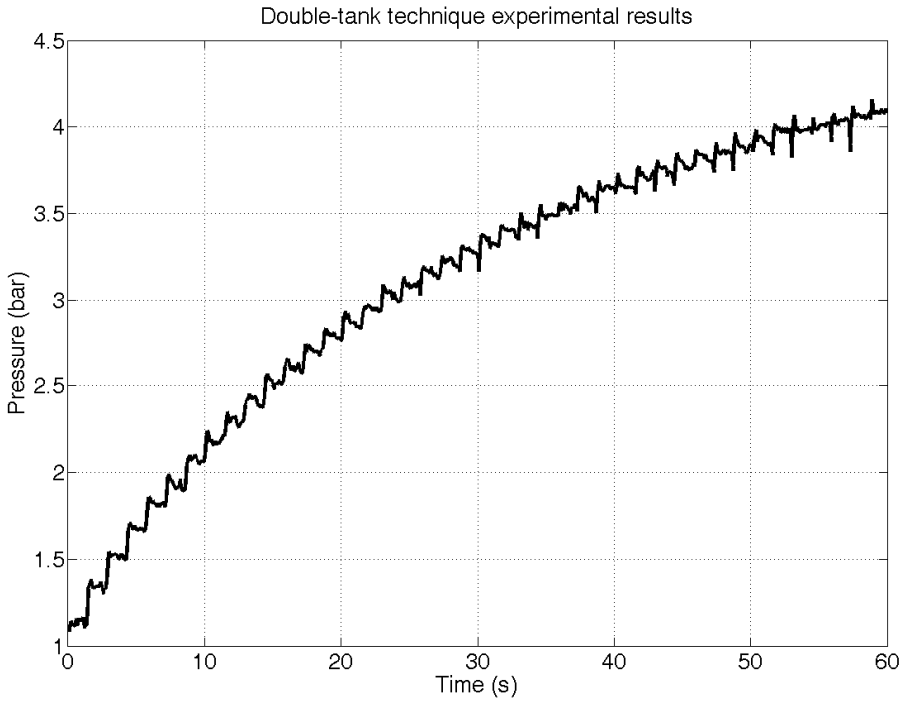

Figure 4-6: HP tank pressure obtained from experiment

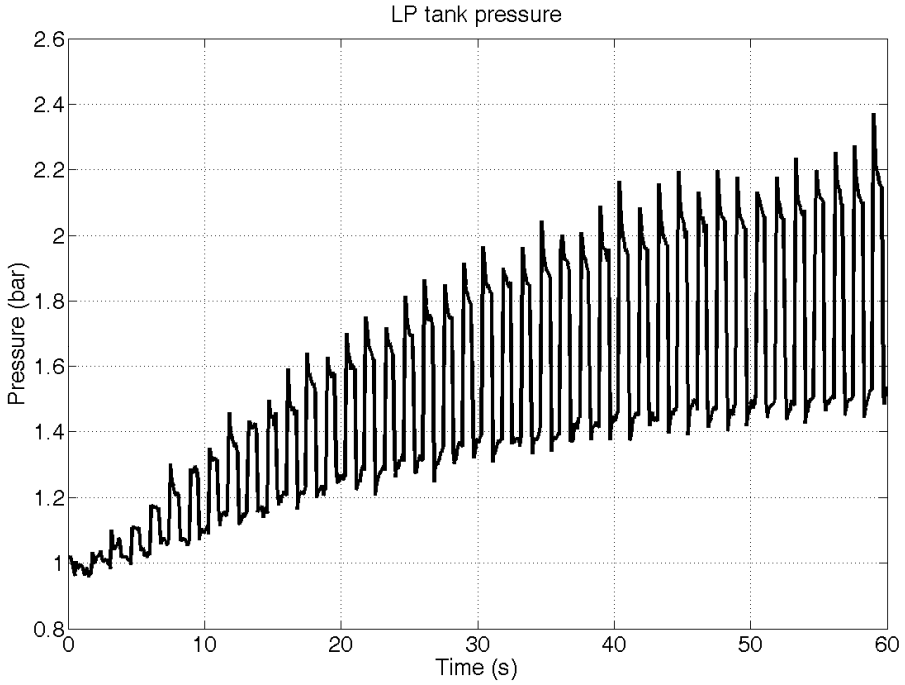

Figure 4-7: LP tank pressure obtained from experiment

As can be seen in Figure 4-6, the HP tank pressure increases to more than 4 [bar] after 60 seconds for the double-tank system. Figure 4-7 illustrates the LP tank pressure variation. As can be seen, the LP tank works as an auxiliary tank which stores the unused pressurized air at TDC and delivers it back to the cylinder at BDC. In this experiment, since the engine is not run in the conventional mode, its temperature is low during the experiment. Thus, there is no need for cooling the LP tank.

Figure 4-8 shows the experimental results for the single-tank and double-tank regenerative braking strategies for a test period of 120 seconds. As this figure illustrates, there is a limit to the air pressure when the single-tank regenerative braking system is used. The pressure remains almost constant after 50 seconds. Using the double-tank regenerative system, not only the pressure increases to more than 4.7[bar], but the rate of pressure change is still positive at t=120[s]. It should be mentioned that the results are obtained with fixed valve timing and a much greater difference between the single-tank and double-tank system performance could be expected if valve timings are optimized based on the LP and HP tank pressures. The experimental results shown in Figure 4-8 indicate about 70% improvement in storing pressure and 120% increase in the energy storing capacity of the regenerative system (based on Eq.(3-2)) after 120 [s] using the double-tank compression strategy over the single-tank method.

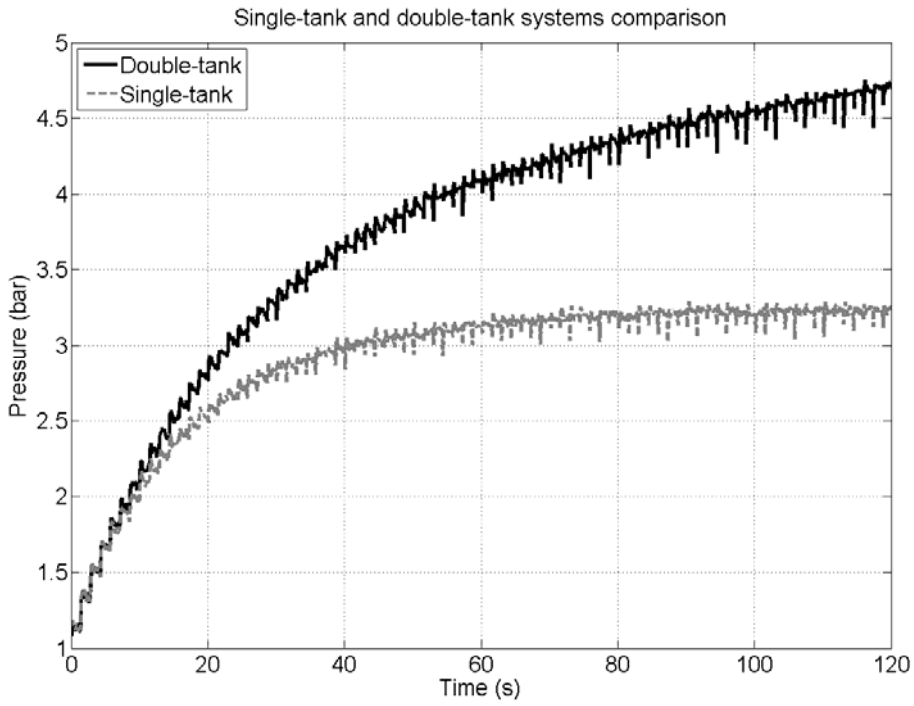

Figure 4-8: HP tank pressure obtained from single-tank and double-tank systems

4.3 Summary

In this chapter the double-tank compression strategy was studied and compared with the conventional type experimentally. The experimental results showed the advantage of the proposed strategy over the conventional single-storage system. In the next chapter a new cam-based valvetrain system that eliminates the need for a fully flexible valvetrain in air hybrid engines is presented.

Chapter 5
Cam-based Air Hybrid Engine

5.1 Background

The most important challenge of implementing an air hybrid engine is the need for a fully flexible valvetrain. There are some efforts described in the literature to avoid using a fully flexible valvetrain in air hybrid engines. Brunel's research group proposed several configurations to avoid camless valves. In 2009 they proposed the configuration shown in Figure 5-1 for a four stoke air hybrid engine [35]. In their first design, all the valves were cam-driven with fixed timings except valve '6' which opens in compression phase in regenerative mode using a cam profile switching system. A solenoid valve ('10' in the figure) was also utilized to control the flow to and from the tank during AM and CB. However, this design needs a high speed solenoid valve (a better than 10 [ms] response time) with relatively large flow capacity. Also, during AM, valves '5' and '6' have the same timing, and the tank pressurized air is expelled to the atmosphere. In their second design (Figure 5-2) both intake valves were switchable with different timings during AM and CB. A butterfly valve ('12') was utilized to control the air flow to the engine during CB. Solenoid valve '10' is always closed during CB and open during AM.

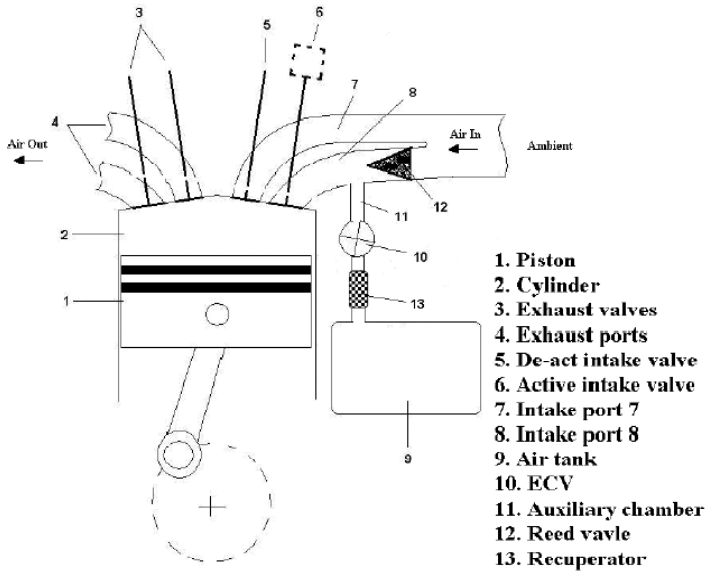

Figure 5-1: Brunel's first proposed air hybrid configuration [35]

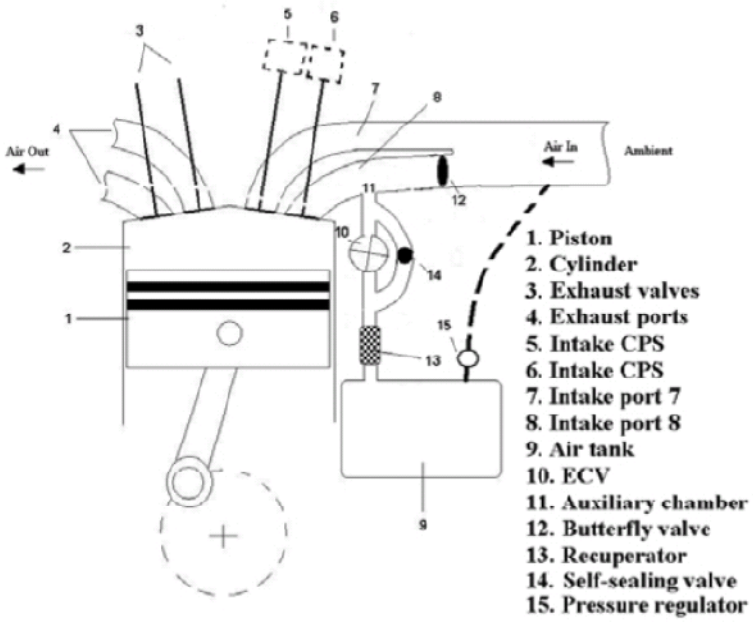

Figure 5-2: Brunel's second proposed configuration for air hybrid engines [36]

This design has also some drawbacks as the butterfly valve cannot hold the pressurized air in the chamber during CB and AM. There is also no control on the flow during AM.

Although in their proposed configuration, cam-driven valvetrain along with cam profile switching system has been proposed, all the experiments are done with an engine rig equipped with camless valvetrain [37].

The ETH research group [23,4] proposed four-stroke AM and CB modes to eliminate the need for a set of fully camless valvetrain. In their proposed configuration, the intake and exhaust valves remained camshaft-driven but an extra camless valve has used to connect the cylinder to the tank. Although this has reduced the number of camless valves and hence the costs, it still needs one extra camless valve.

In spite of all these efforts, a cost-effective, practical, and robust solution to the problem has not yet been proposed. In this section, a novel configuration for the single and double-tank air hybrid engine is proposed and tested. This configuration simplifies the air hybrid engine valvetrain significantly and relaxes the need of a fully flexible valvetrain in air hybrid engines.

5.2 Cam-based Valvetrain

An air hybrid engine should be able to work as a four-stroke conventional engine and also as a two-stroke compressor and air motor. Also, the engine torque has to be regulated at various operational modes. Therefore, the air hybrid engine valvetrain not only has to change the air flow to or from the engine to regulate the engine torque, but also change the engine operation from four-stroke to two-stroke and vice versa.

In this work, a new cam-based flexible valvetrain is proposed which can switch the engine operational mode from four-stroke to two-stroke and vice versa. In this design, shown in Figure 5-3, two cams are mounted for each engine valve on the cam shaft: one two-stroke and one four-stroke. Four-stroke and two-stroke cam followers are in continuous contact with the four- and two-stroke cams, respectively. However, the valves follow the two-stroke or four-stroke cam’s motion selectively utilizing the Vtec technology [38] allowing switching between the two active cam followers. Connecting the four-stroke cam follower to the valve will result in conventional valve timing (i.e., about 280º of CAD opening for intake valves and about 300º of CAD opening for exhaust valves). Since the cam shaft speed is half of the

engine shaft speed, four-stroke cams result in one opening/closing event per two engine revolutions. The two-stroke cams are also in contact with the two-stroke cam followers. The two-stroke cam follower is connected to the valve during compression braking or air motor mode. Activating the two-stroke cam follower results in 180º of CAD opening for the intake and 180º of CAD opening for exhaust valves. The specific design of the two-stroke cams, shown in Figure 5-3, doubles the opening/closing events of the valve per engine revolution compared to the conventional four-stroke cams. This leads to one opening/closing event for the valve per engine revolution and the engine operates in two-stroke mode.

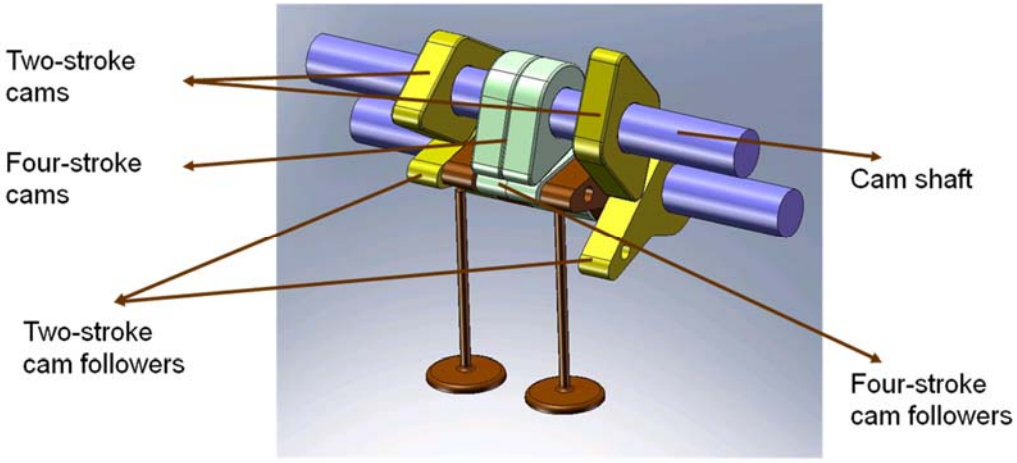

Figure 5-3: Proposed valvetrain based on Vtec

Utilizing the proposed valvetrain system, the engine operational mode can be changed from four-stoke mode with fixed valve timings to two-stroke mode with a different set of fixed valve timings. Although different valve timings for four-stroke can be obtained compared to two-stroke, timings are fixed at each mode because all of the two- and four-stroke cams are fixed on the cam shaft. Even though the proposed valvetrain is capable of switching the engine operational mode between two- and four-stroke, it cannot generate different valve timings required in the compression braking and air motor. To implement different valve timings at different two-stroke modes (i.e., air motor and compression braking), a cylinder head design comprising a set of three-way solenoid valves and unidirectional valves is proposed for both single- and double-tank air hybrid engines.

5.3 Cam-based Single-tank Configuration

To implement the required valve timings and control the engine torque at the two-stroke mode in a single-tank configuration, a cylinder head design comprising a set of three-way solenoid valves and unidirectional valves is proposed as shown in Figure 5-4. The engine operational mode can be changed by changing the arrangement of the three-way solenoid valves. Figure 5-4 shows the arrangement of the three-way valves and the air flow during conventional mode. As can be seen, intake valves (valves '1' and '2') are connected to the intake manifold, and exhaust valves (valves '3' and '4') are connected to the exhaust manifold. The throttle along with the spark angle and fuel injector, are the actuators that can be used for engine torque control. The throttle angle is mostly used to regulate relatively large changes in the engine torque while the spark angle and air fuel ratio are used for rapid changes in the engine torque [39].

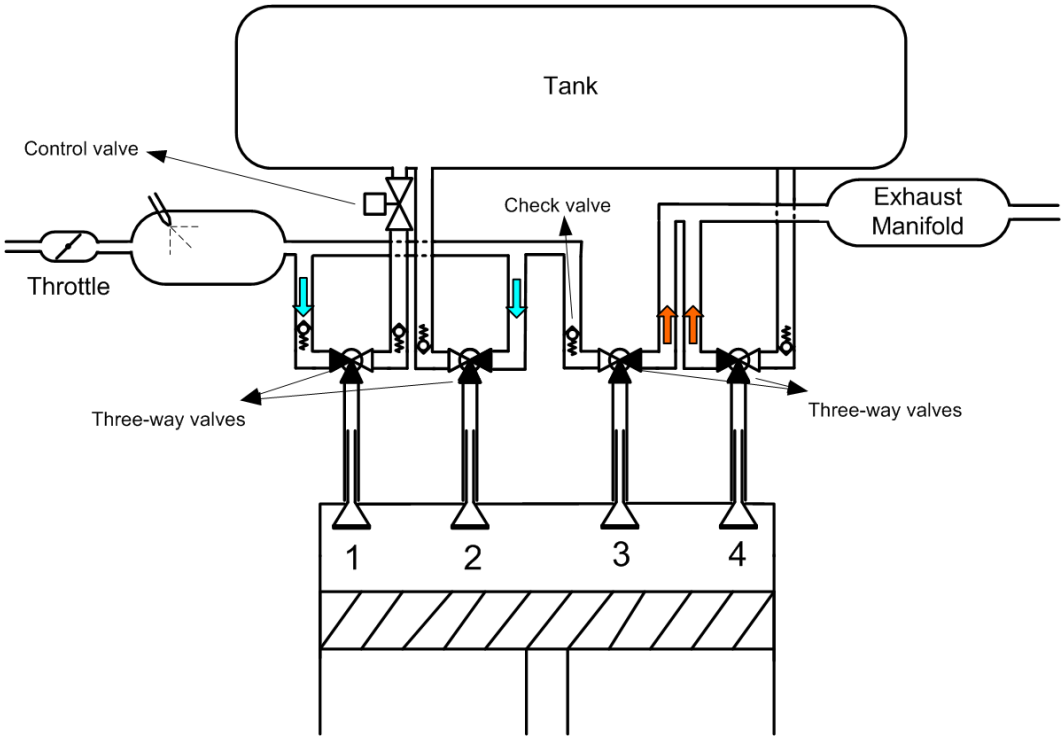

Figure 5-4: Three-way valves arrangement in the conventional mode

Changing the three-way valve arrangement as shown in Figure 5-5 and switching to two-stroke cams allow the implementation of the compression braking. In this mode, valves

follow the two-stroke cams, leading to the valve timings shown in Figure 5-6. One of the intake valves and one of the exhaust valves (i.e., valves ‘1’ and ‘3’) are connected to the intake manifold through the three-way valves and are open from 0º CAD to about 180º CAD. Although valves ‘1’ and ‘3’ are open for 180º CAD, fresh air flows into the engine only if the pressure in the cylinder drops below the atmospheric pressure because the unidirectional valve avoids the flow from the cylinder to the intake. Valves ‘1’ and ‘3’ are closed at 180º CAD and the piston starts going up from BDC to TDC, compressing the air adiabatically. Valves ‘2’ and ‘4’ connect to the engine to the tank and are opened at 180 º CAD and left open to 360º CAD, however, pressurized air enters the tank only if the pressure in the cylinder exceeds the tank pressure.

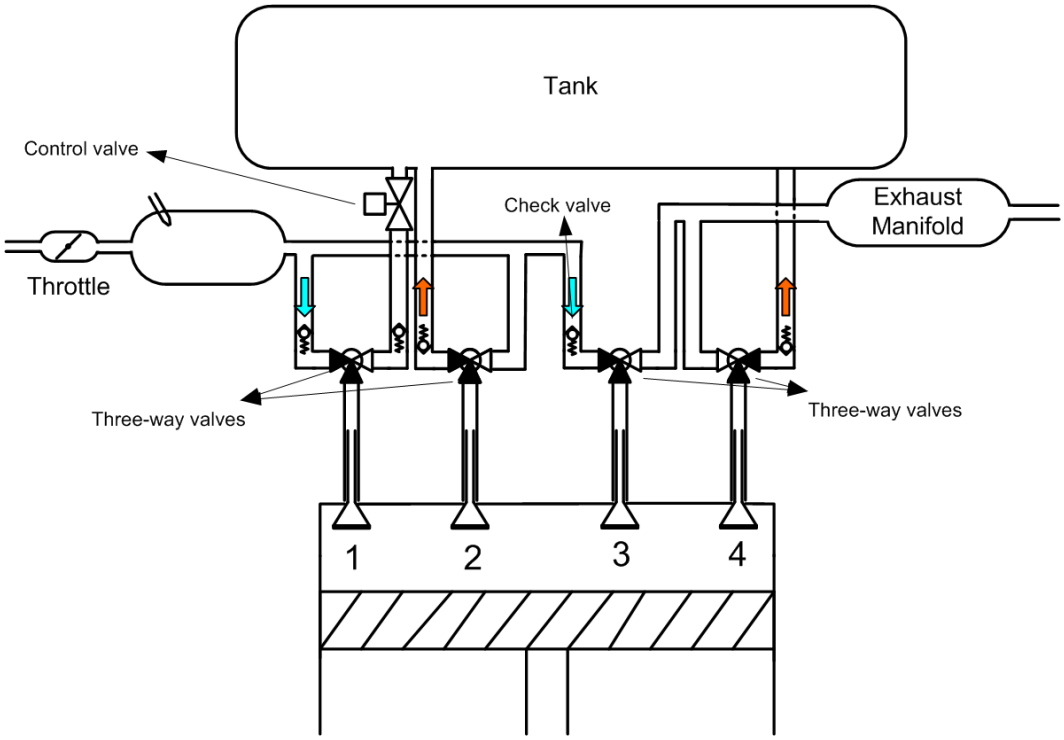

Figure 5-5: Three-way valves arrangement in the CB mode

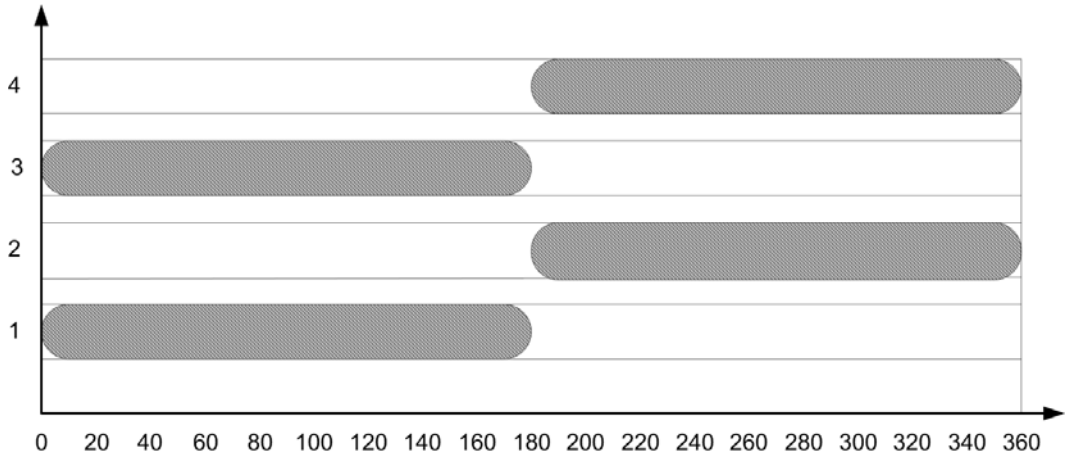

Figure 5-6: Approximate Valve timings in the two-stroke modes

Using unidirectional valves in the air paths, as shown in Figure 5-4, avoids the irreversible mixing of the gases, and consequently, the cylinder and tank are charged through a constant pressure process. In other words, the ideal compression cycle (Figure 3-1) is followed all the time without changing the valve timings. This reduces excessive heat generation during compression process cycle, resulting in a better efficiency. In addition, the engine braking torque can be controlled by the same throttle that controls the engine torque in the conventional mode. Changing the throttle angle in the compression braking mode, changes the air flow to the cylinder and, consequently, the engine braking torque. This simplifies the engine braking torque control significantly because there is no need for an extra actuator or further changes to the conventional torque control system in the engine. However, slower torque control is expected comparing to the conventional mode.

Figure 5-7 shows the three-way valves arrangement during air motor mode. The valve timings are the same as compression braking mode however, the three-way valves arrangement are different in this mode. Valves ‘1’ and ‘3’ are opened at TDC to let the pressurized air enter the cylinder through valve ‘1’. Valves ‘2‘and ‘4’ are opened around 180º CAD and valve ‘2’ expels the air to the intake manifold to avoid cooling down the exhaust after treatment system. Engine torque can be controlled by controlling the air flow to the engine by an electronically controlled flow control valve. Thus, conventional, single-tank

compression braking and air motor modes can be realized using the proposed cylinder head configuration and cam-based valvetrain, relaxing the need for a fully flexible valvetrain.

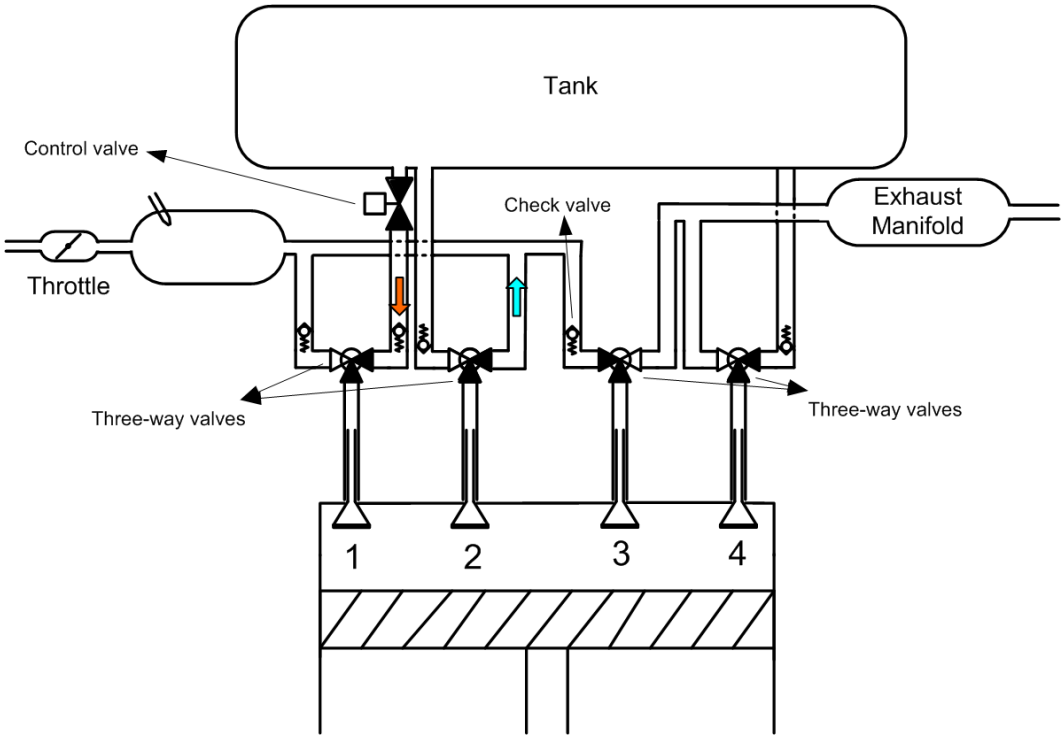

Figure 5-7: Three-way valves arrangement in the AM

5.4 Cam-based Double-tank Configuration

Figure 5-8 shows the proposed cylinder head configuration for implementing the double-tank compression strategy. Similar to the single-tank case, the double-tank air hybrid can be implemented utilizing the switchable valvetrain and a set of three-way and unidirectional valves as shown in Figure 5-8. The engine operational mode can be switched simply by changing the arrangement of the three-way valves. In the conventional mode intake valves (valves ‘1’ and ‘2’) are connected to the intake manifold and exhaust valves (valves ‘3’ and ‘4’) are connected to the exhaust manifold.

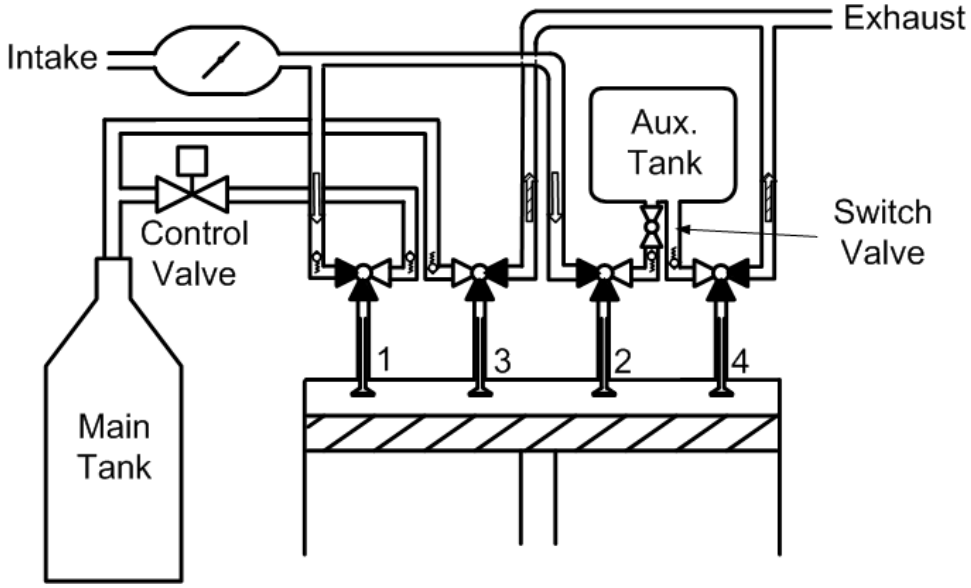

Figure 5-8: Cylinder head design for the double-tank configuration in the conventional mode

For the double-tank configuration, LP tank should be connected to the cylinder two times per revolution during regenerative braking. To meet this requirement, two valves connect the cylinder to the LP tank (i.e., valves ‘2’ and ‘4’).

Changing the arrangement of the three-way valves as shown in Figure 5-9 and switching to two-stroke cams allow the compression braking mode to be implemented. In this mode, valves follow the two-stroke cams, leading to the approximate valve timings shown in Figure 5-10. One of the intake valves (i.e., valve ‘1’) is connected to the intake manifold and is open from 0º CAD to about 180º CAD. Thus, when the piston moves from TDC to BDC, fresh air enters the cylinder from the intake manifold. The engine torque can be regulated by the engine throttle. Valves ‘2’ and ‘3’ are connected to the LP and HP tank respectively and are opened at 180º CAD and left open for the next 180º of CAD. The cylinder pressure starts to increase because of the air flow from the LP and also compression due to the piston upward motion. The air flow from the LP tank to the cylinder stops as soon as the cylinder pressure equals the LP tank pressure. Although valve ‘2’ remains open to 360º CAD, there will be no flow from the cylinder to the LP tank because the unidirectional valve only allows the flow from the LP tank to the cylinder and not vice versa. The HP tank is charged whenever the cylinder pressure exceeds the HP tank pressure. The unidirectional valve placed between

valve ‘3’ and the HP tank avoids irreversible mixing of the air form the HP tank and cylinder and consequently increases the efficiency of the regenerative braking. Valve ‘4’ opens at approximately 350º CAD and allows the LP tank to be charged by the remaining of the pressurized air in the cylinder. Although valve ‘3’ is still open, the unidirectional valve avoids the air blow down from the HP to the cylinder. Valve ‘4’ remains open up to 170º CAD. However, LP tank charging stops whenever the pressure in the cylinder drops below the LP tank pressure. Again, the unidirectional valve avoids the air blow down from the LP tank to the cylinder. This way, the ideal compression cycle shown in Figure 3-4 is implemented without changing the valve timings.

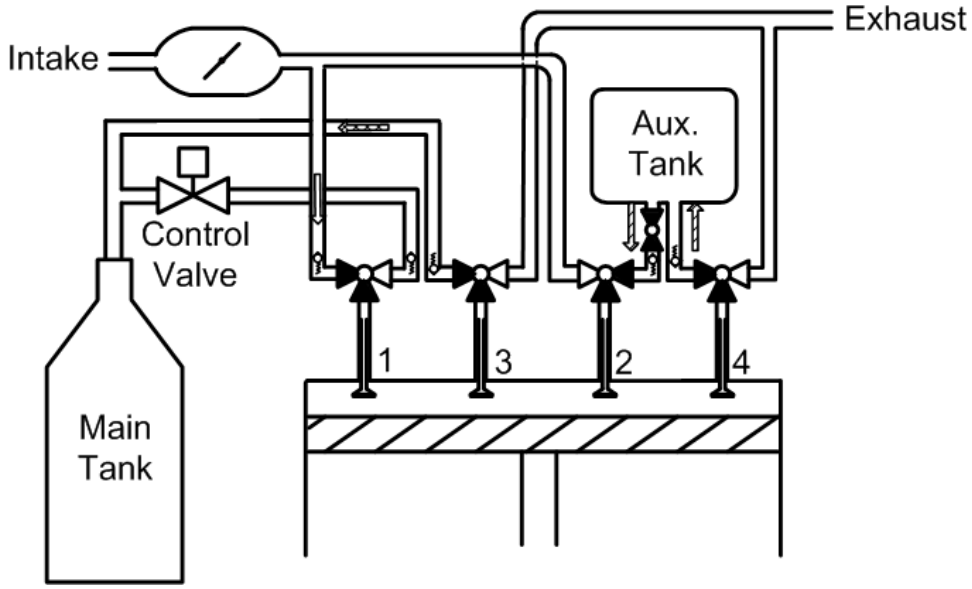

Figure 5-9: Three-way valves arrangement in the compression braking mode

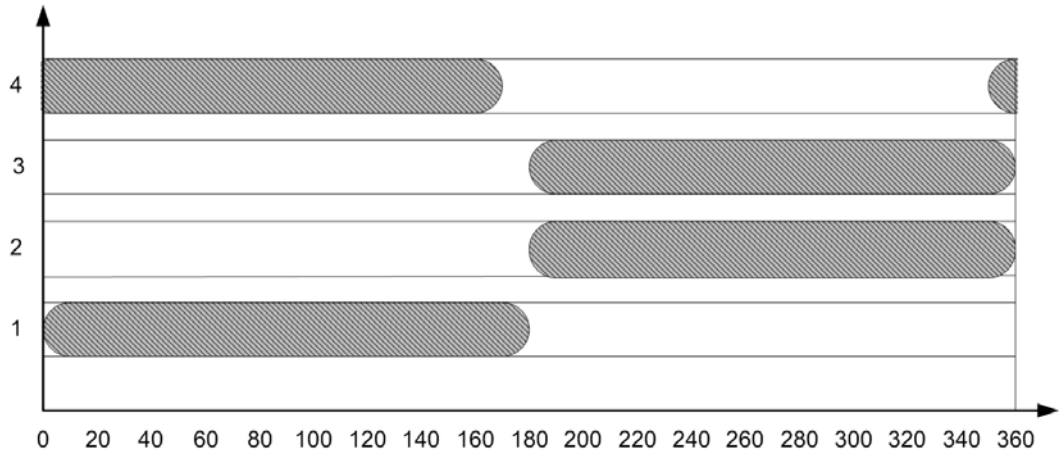

Figure 5-10: Approximate valve timings in the two-stroke modes

Figure 5-11 shows the three-way valves' arrangement in air motor mode. The valve timings are similar to the compression braking mode, however, the three-way valves' arrangement is different in this mode. The pressurized air enters the cylinder when valve '1' is open. A flow control valve, as shown in Figure 5-11, is utilized to control the air flow and, consequently, the engine torque. Although valve '4' is open at almost the same interval as valve '1', there is no flow through this valve because of the unidirectional valve. Valves '2' and '3' open at 180º CAD and the cylinder air is expelled to the intake manifold through valve '2' to avoid cooling down of the exhaust after treatment system.

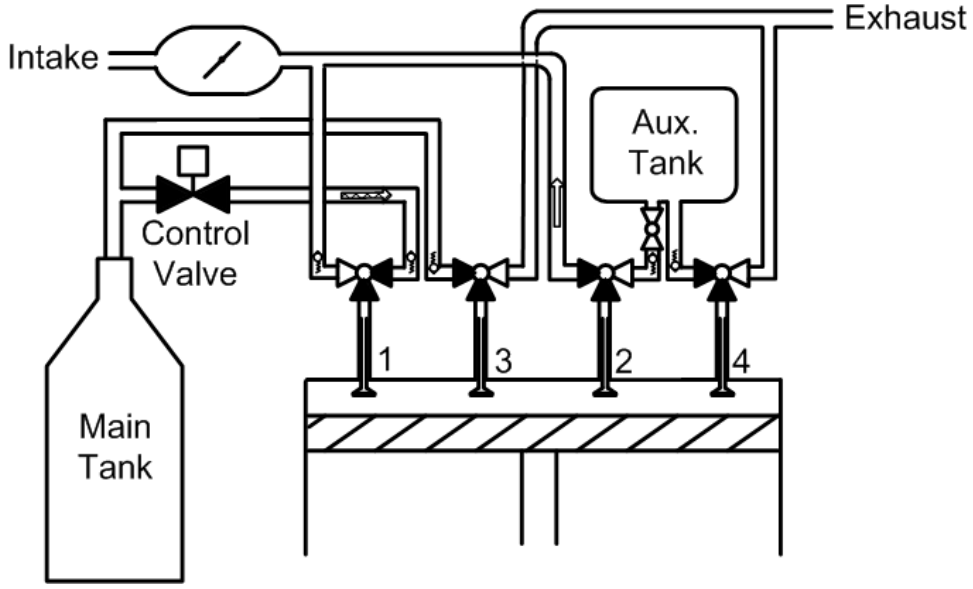

Figure 5-11: Three-way valves arrangement in the air motor mode

Thus, conventional, double-tank compression braking, and air motor modes can be implemented using the proposed cylinder head configuration and valvetrain design, and the need for camless valvetrain to hybridize the conventional engines is eliminated. With reference to Figure 5-9, the regenerative braking operation can be switched to single-tank strategy by deactivating the switching valve located upstream of valve '2'. Therefore, the proposed cylinder head configuration can implement both single-tank and double-tank strategies with the same valve timings.

5.5 Pros and Cons of the Proposed Air Hybrid Configuration

One of the most important advantages of the proposed system is that the regenerative braking, and air motor modes of air hybrid engine can be implemented without using a camless or fully flexible valvetrain or adding an extra valve to the cylinder head. In addition, due to the use of unidirectional valves in the structure, the ideal regenerative cycle is followed and irreversible mixing of gasses, at least between the engine and the main tank, is avoided. The other important benefit of the proposed valvetrain is the simplicity of the engine torque control actuators. The engine braking torque can be controlled by the existing electronic throttle system in the regenerative mode and by a simple flow control valve in the

air motor mode, eliminating the need for a complete valve timing control. Furthermore, both the single- and double-tank compression strategies can be implemented by the proposed double-tank air hybrid engine configuration.

In spite of the above mentioned advantages, there might be some drawbacks associated with the proposed cylinder head design which requires further studies. The configuration of such an intake system and the use of three-way valves and check valves introduce resistance to the air flow and hence results in poor engine performance. Although there is no need for high speed three-way solenoid valves (as they just change the operational mode), they need to have good resistance against high temperature as they are exposed to exhaust gas. In addition, the compression ratio of the engine in regenerative mode could drop as the three-way and check valves volumes are added to the cylinder volume.

5.6 Simulations

5.6.1 Regenerative Braking

To study the performance of the proposed cylinder head design in capturing the kinetic energy of a vehicle, full throttle deceleration of a Ford 150 truck equipped with 5.4[L] V8 engine from 70 [km/hr] down to 10 [km/hr] is modeled in GT-Power. The valvetrain and cylinder head design proposed in Sections 5.3 and 5.4 is utilized to implement the air hybrid engine concept for both single- and double-tank systems. The vehicle and engine specifications are tabulated in Table 5-1. It is noteworthy that all the three-way valves and check valves flow characteristics and their related energy losses are considered in GT_Power.

Table 5-1 Vehicle and engine specifications

Vehicle mass	2800 [kg]
Final drive ratio	3.73
Vehicle initial speed	70 [km/hr]
Vehicle final speed	10 [km/hr]
HP tank volume	60 [l]
LP tank volume	5.4 [l]
Initial HP tank pressure	4 [bar]
Engine displacement volume	5400 [cc]
Engine compression ratio	9
Transmission ratio	1^{st} : 2.36
	2^{nd} : 1.52
	3^{rd} : 1.15
	4^{th} : 0.85

Figure 5-12 shows the tank pressure and temperature during vehicle deceleration for single-tank case. As can be seen, pressure in the air tank increases to more than 17 [bar] after about 15 seconds and remains constant after that. This shows that the maximum pressure in the air tank is limited to 17 [bar] for the single-tank regenerative system. It is noteworthy that there is no limit on the pressure magnitude in the air tank if irreversible mixing of the gases from the cylinder and the tank happens in the cylinder. Irreversible mixing of the gases in the cylinder increases the temperature and, consequently, the pressure (while the maximum amount of air mass is limited based on Eq. (3-13)). However, air tank temperature has to be limited since high temperature air in the tank increases the engine body temperature, which might cause pre-ignition in the cylinder. One of the advantages of utilizing the combination of cam-based valves with unidirectional valves in the cylinder head is that the irreversible mixing of the gases in the cylinder is avoided and, consequently, the air tank temperature remains in an acceptable range as shown in Figure 5-12.

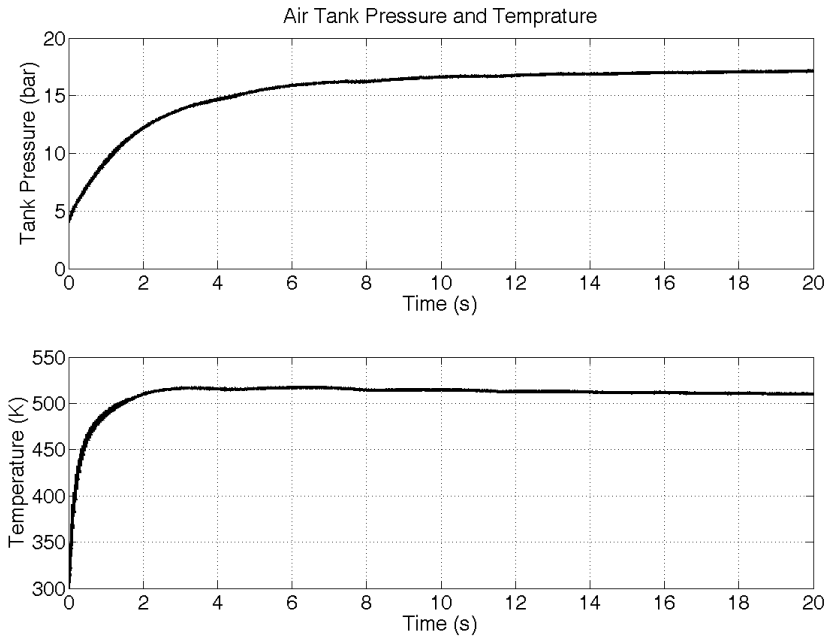

Figure 5-12: Air tank pressure and temperature for the single-tank system

Based on the second law definition for regenerative system efficiency proposed in Eq. (3-2), the overall efficiency of the system in recovering the kinetic energy of the vehicle is about 21.0%.

$$\eta_{\text{startup}} = \frac{\varphi_2 - \varphi_1}{\frac{1}{2} M_{vehicle}\left(v_2^2 - v_1^2\right)} = \frac{111\text{kJ}}{518\text{kJ}} \cong 21\% \,, \qquad 5\text{-}1$$

Since the air tank temperature has to be limited, the energy storing capacity of the system should be increased by an increase in storing pressure. This could be done by employing the double-tank compression strategy. Figure 5-13 shows the pressure and temperature of the main air tank for the double-tank regenerative braking system. As can be seen, air tank pressure increases to more than 31[bar] after only 6.6 seconds while the temperature increases to about 540[K]. This shows that the double-tank braking system offers higher braking torque and higher energy storing capacity compared to the single-tank system. The positive slope of the pressure curve at the end of the simulation also shows that in contrast to the case of the single-tank system, the maximum energy storing capacity of the system has

not been reached yet. The second law efficiency of the double-tank system based on Eq. (3-2) is 46%.

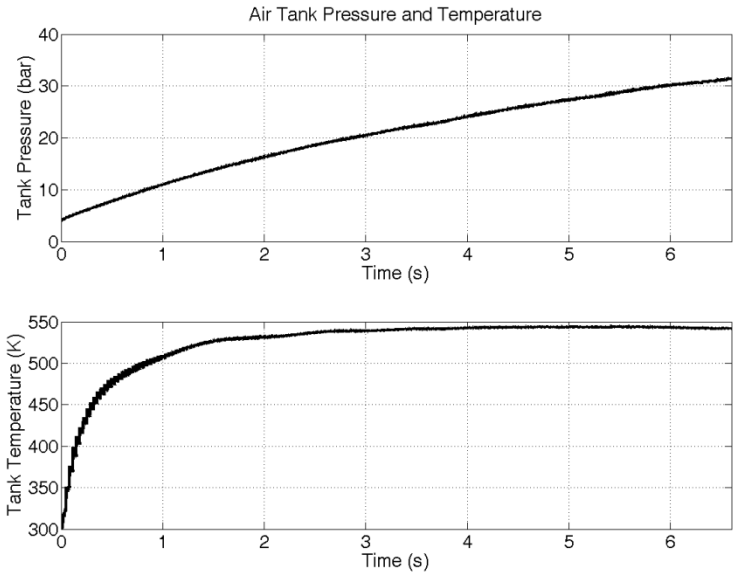

Figure 5-13: Air tank pressure and temperature in for the double-tank system

In the double-tank compression strategy, the main tank temperature is highly dependent on the LP tank temperature. In order to keep the tank temperature at an acceptable level and increase the overall efficiency of the system, the LP tank has to be cooled down similar to the multi-stage compression where pressurized air is cooled down after each compression stage. In this simulation, a higher heat transfer rate for the LP tank is considered to represent the LP tank cooling down process. Simulation results clearly show that the proposed air hybrid engine configurations not only implement the regenerative braking mode, but also limit the temperature in the main tank by following the ideal braking cycles.

5.6.2 Air Motor Mode

As mentioned in Chapter 1, the stored energy in the tank could be used in long-term cruising, accessory assisting mode, supercharged mode, or engine startup mode. With reference to Table 5-2, the energy density of pressurized air even at 300[bar] is not comparable to that of gasoline.

Table 5-2: Energy density of different energy sources [40]

	Energy Density (MJ/kg)
Gasoline	47.4
Compressed air (300 bar)	0.4
Traction battery	0.11~0.25

Considering the fact that the maximum air tank pressure is much lower than 300[bar] in typical air hybrid engines, as opposed to what has been proposed by some researchers, the air motor mode can be activated only for a short period and cannot be used for long-term cruising. This statement is also true for the accessory assisting mode (Appendix I). However, the supercharged and startup modes of an air hybrid vehicle can significantly contribute to improved fuel economy as the first option boosts the engine power and allows a downsized engine to be used [4] and the second one avoids engine idling. Since the supercharged mode cannot be implemented using the engine configuration proposed in Chapter 5, only the startup mode is studied in this thesis.

The startup mode is simulated in GT-POWER and MATLAB/SIMULINK for the same vehicle with the tank pressure stored by single-tank regenerative braking. Figure 5-14 and Figure 5-15 show the tank pressure and vehicle speed versus time. As Figure 5-15 illustrates, the vehicle accelerates to 16 [km/hr] in only 1.5 seconds by employing the stored energy in the air tank. Then, since there is no useful energy left in the tank, the engine conventional mode must be triggered by injecting fuel. The vehicle acceleration rate during the startup mode is managed by controlling the control valve between the tank and the engine. However, in this simulation, the control valve is considered to be fully open. Based on the definition for exergy, the efficiency of the startup mode in recovering the stored energy is determined as follows:

$$\eta_{\text{startup}} = \frac{\frac{1}{2} M_{vehicle}\left(v_4^2 - v_3^2\right)}{\varphi_4 - \varphi_3} = \frac{27\,\text{kJ}}{111\,\text{kJ}} \cong 25\%\,, \qquad 5\text{-}2$$

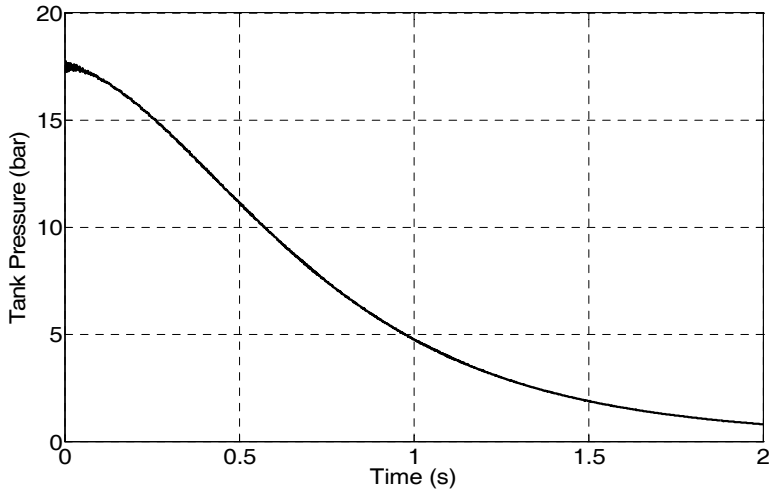

Figure 5-14: Tank pressure in the startup mode

and the roundtrip efficiency of the energy recovery is:

$$\eta_{\text{overall}} = \frac{\frac{1}{2} M_{vehicle} \left(v_3^2 - v_4^2 \right)}{\frac{1}{2} M_{vehicle} \left(v_1^2 - v_2^2 \right)} \cong 5.0\%. \qquad 5\text{-}3$$

Although the overall efficiency of 5.0% in recovering the initial vehicle's kinetic energy seems to be insignificant, a considerable reduction in fuel consumption is achieved by the engine being off during the short stops in a drive cycle. Consequently, a substantial reduction in fuel consumption can be expected if the vehicle's braking energy is used in the subsequent vehicle acceleration because engine idling is avoided due to the stored energy in the tank. Furthermore, the additional fuel consumption caused by restarting the engine is avoided because the engine speed is high enough to switch to the conventional mode at the end of the startup mode (Figure 5-16).

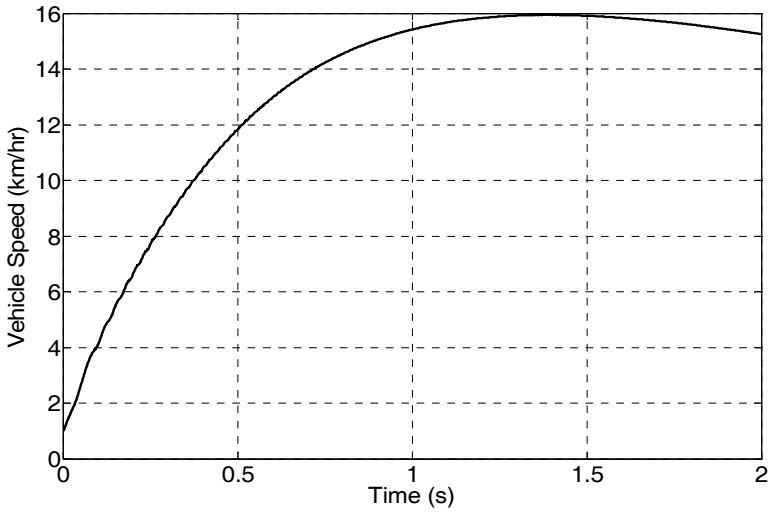

Figure 5-15: Vehicle velocity during startup mode

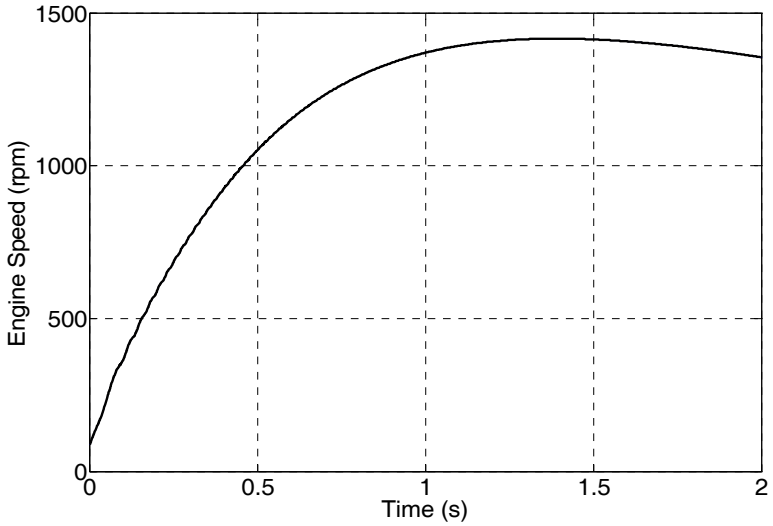

Figure 5-16: Engine speed during startup mode

5.7 Experimental Studies

In order to test the proposed cylinder head configuration the experimental setup has been modified as shown in Figure 5-17.

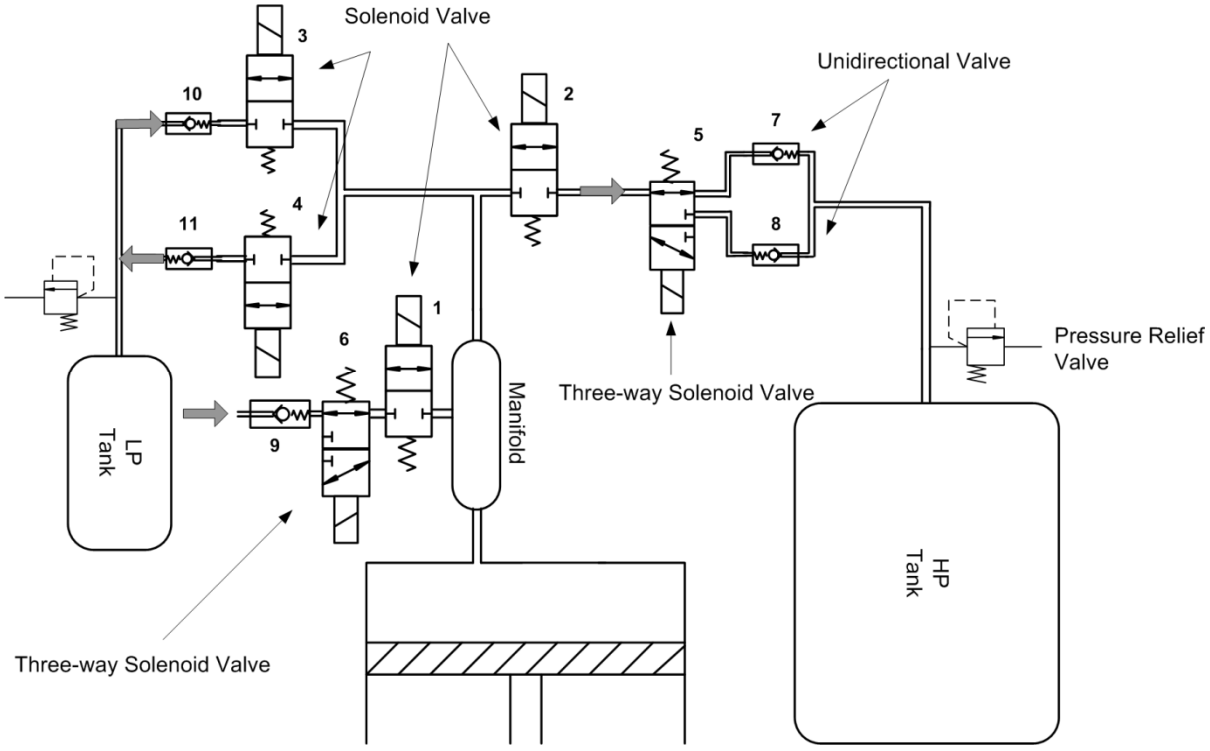

Figure 5-17: Modified experimental setup

Since the switchable cam-based valvetrain was not available for this project, four high speed solenoid valves with fixed opening intervals of 180º CAD were utilized to represent the cam-based valvetrain timings in two-stroke AM and CB modes. The solenoid valves are combined with unidirectional valves as shown in Figure 5-17 and implement the valve timings listed in Table 5-3 for the single- and double-tank systems. Since the engine under study is not run in the conventional mode, only two three-way solenoid valves were employed to change the mode from CB to AM and vice versa.

Table 5-3: Valve timings

Solenoid valve	Operating angle (CAD)		
	Startup	Single-tank	Double-tank
1	170 to 350	350 to 170	360 to 180
2	350 to 170	170 to 350	170 to 350
3	Closed	Closed	170 to 350
4	Closed	Closed	350 to 170

5.7.1 Regenerative Braking Mode

Figure 5-18 shows the tank pressure versus time for the single-tank system. The experimental results indicate that the tank pressure goes up and levels off at about 6.5 [bar] for single-tank system. This is very different from the simulation result in which the maximum pressure was more than 17[bar]. The discrepancy seen in the results involves several factors. Firstly, the compression ratio of the engine with the new engine head was dropped from 8.5 because of a larger dead volume in the new engine head due to added volumes of connecting pipes and solenoid valves (Figure 5-19). Secondly, the engine's temperature was far below its working temperature while running in the CB mode in the experiment. Thus, the piston and cylinder were not sealed properly and there was large air leakage through the piston/cylinder gap.

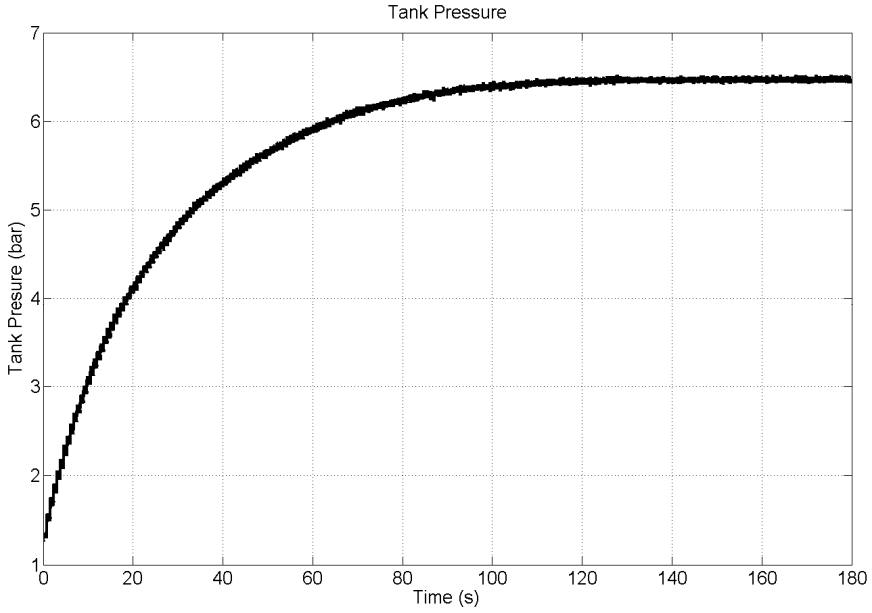

Figure 5-18: Tank Pressure versus time for single-tank system

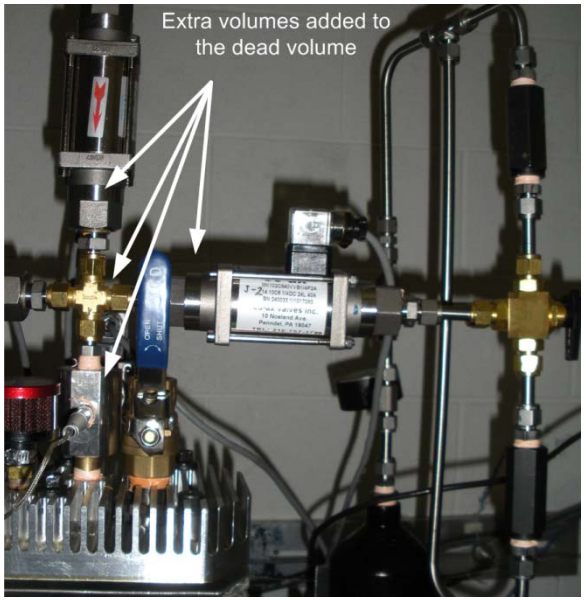

Figure 5-19: Cylinder head

Figure 5-20 illustrates the cylinder P-V cycle for different tank pressures for the single-tank system. This figure shows that the cylinder and the tank are charged through constant pressure processes and no irreversible mixing of gasses occurs in the cylinder. In addition, it can be seen that the enclosed area of the cylinder P-V cycle which represents the generated regenerative braking torque changes with the tank pressure. Thus, the engine braking torque is a function of tank pressure and a controller has to be designed to regulate the engine braking torque against the tank pressure variations.

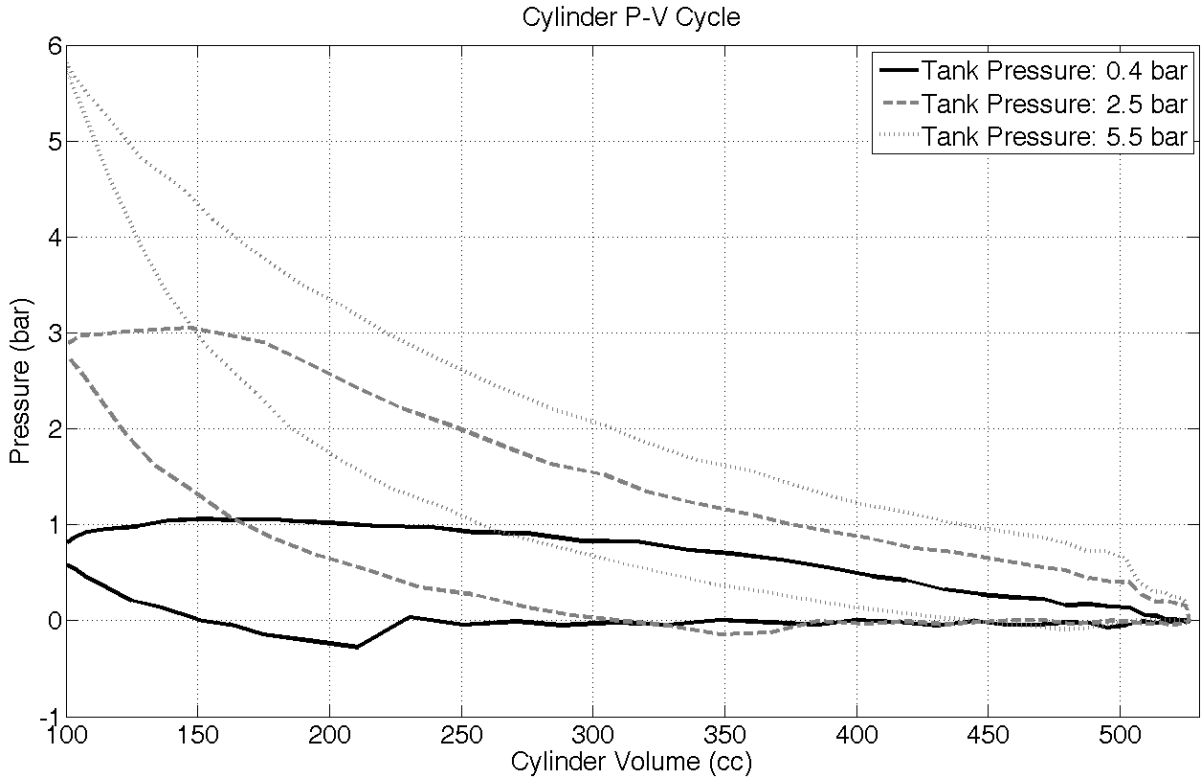

Figure 5-20: Cylinder P-V cycle at various tank pressures

Figure 5-21 shows the cylinder P-V cycle for single-tank and double-tank compression strategies at the tank pressure of 4.5 [bar]. As this figure illustrates, the enclosed area of the double-tank P-V cycle which represents the generated regenerative braking torque is bigger than that of the single-tank. This figure also shows that all the gas exchange events occur reversibly and there is no blow down of the pressurized air from the air tank to the cylinder or vice versa which is the result of using unidirectional valves in the air hybrid engine configuration.

Figure 5-22 shows the pressure variations in HP, LP and cylinder versus engine crank angle for two subsequent cycles for a double-tank system. As can be seen, the cylinder is charged from atmospheric pressure between 0º CAD to 180º CAD whenever the cylinder pressure drops below atmospheric pressure. Although solenoid valve '4' is open during this interval, no air blow down from LP to the cylinder happens because the unidirectional valve '11' avoids the flow from the LP to the cylinder. However, the cylinder is charged with the pressurized air from the LP after solenoid valve '2' is opened around 180º CAD. The

charging of the cylinder from the LP continues until the pressure in the cylinder equals the LP tank pressure. After this point, there will be no flow exchange between the LP and the cylinder; nevertheless, solenoid '2' is still open. Although solenoid valve '3' is open from 180º CAD, air flows into the HP tank whenever the cylinder pressure exceeds the HP tank pressure. The charging of the HP tank continues until the solenoid valve '4' is opened around 350º CAD. At this point, charging of the HP tank stops because the cylinder pressure drops below the HP pressure and the LP tank is charged with the remainder of the pressurized air in the cylinder. Charging of the LP tank continues until the pressure in the cylinder drops below the LP pressure. From this point on, although solenoid valve '4' is still open, there is no flow exchange between the LP and the cylinder and the cylinder is charged with the fresh air coming from the intake manifold. Thus, the double-tank compression strategy is implemented using the proposed configuration.

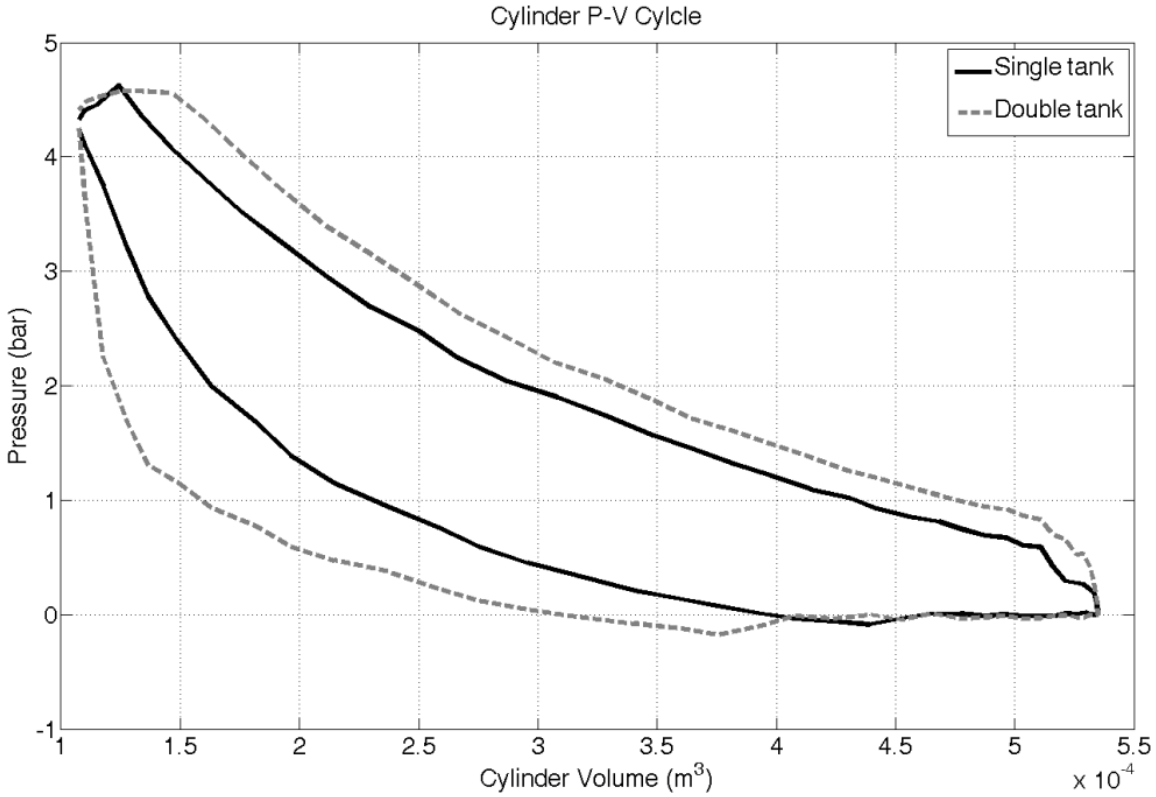

Figure 5-21: Cylinder P-V cycle for single-tank and double-tank systems

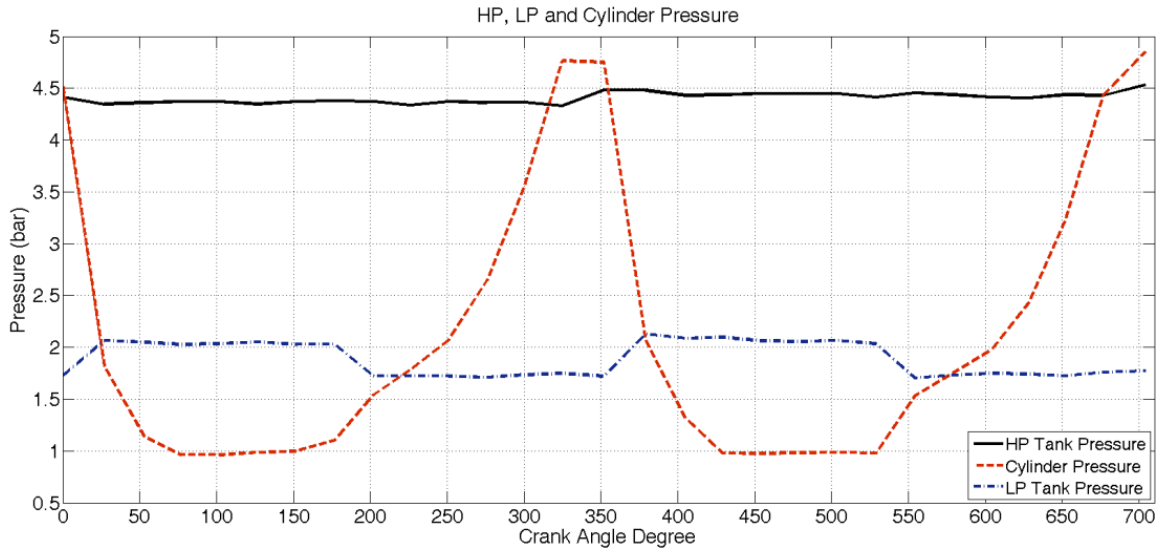

Figure 5-22: HP, LP and cylinder pressure for two subsequent cycles

Figure 5-23 shows the HP tank pressure for single- and double-tank systems at an engine speed of 42 [rpm]. As this figure shows, the tank pressure goes up to about 5.5 [bar] for the single-tank system whereas it goes up to more than 8 [bar] for the double-tank regenerative system. This is an almost 55% improvement in the storing pressure, which consequently increases the energy storing capacity of the system. This confirms that the double-tank compression strategy, implemented with the proposed engine configuration, stores more energy than the single-tank system. As can be seen in this figure, the slopes of the graphs for both cases were still positive at the end of the experiment. This implies that both systems were still able to store more energy. In order to find the upper limit for the pressure in the main tank for both cases, the experiment was repeated at 82 [rpm]. The results are illustrated in Figure 5-24. For an engine speed of 82 [rpm], the HP pressure goes up to more than 9.4 [bar] for double-tank and and about 6.4 [bar] for single-tank. This implies a 55% and 87 % increase in storing pressure and the stored energy (based on Eq.(3-2)) respectively, employing the double-tank compression strategy.

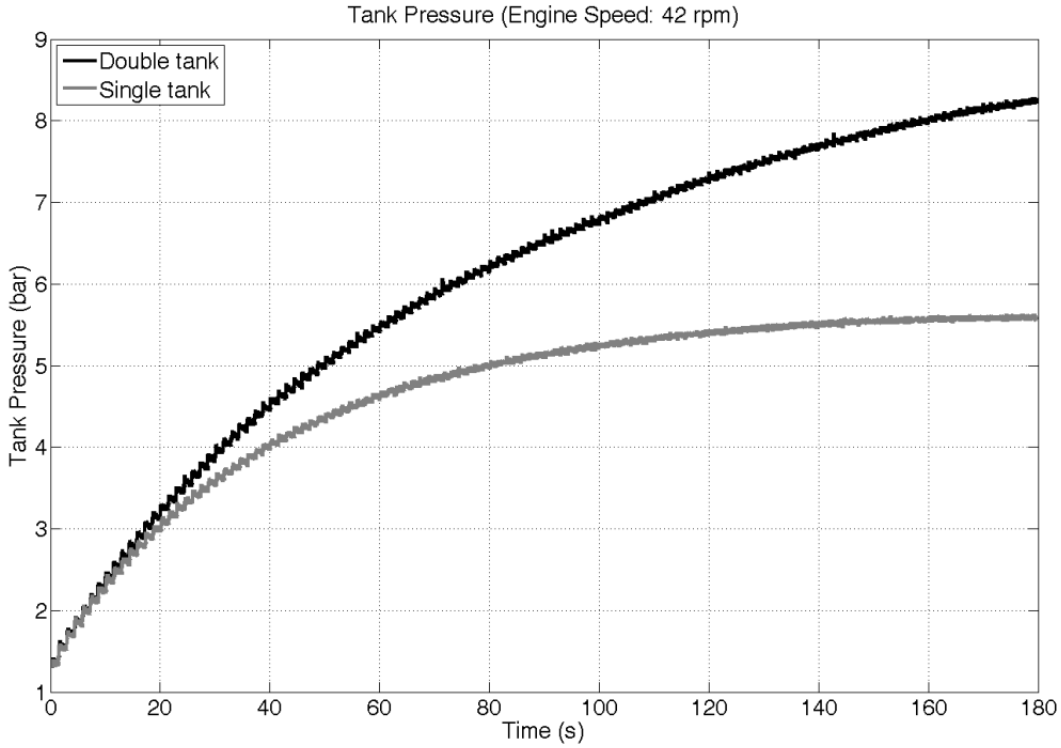

Figure 5-23: HP tank pressure versus time (42 [rpm])

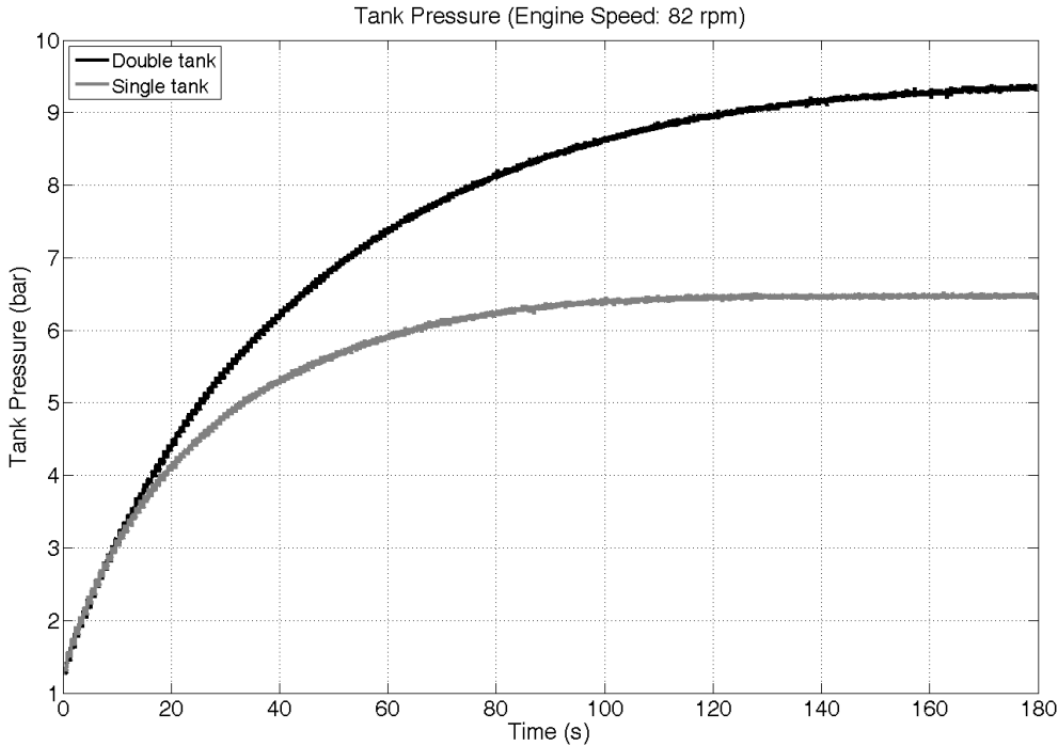

Figure 5-24: HP tank pressure versus time (82 [rpm])

The experimental results clearly show that the regenerative braking mode can be implemented; however, since the switchable cam-based valvetrain was not available, the effects of impulsive motion of unidirectional valves on the poppet valve dynamic have not been addressed yet. More experiments and investigations are needed to study all the technical and practical challenges of utilizing the proposed cam-based valvetrain for air hybrid engines.

5.7.2 Air Motor Mode

The experimental setup is modified by replacing the 2-litre tank with a 30-litre tank to extend the air motor mode duration. The air tank is fed at 6 [bar] and the engine piston is brought to the top dead centre. Then the engine is run using the solenoid valve timing listed in Table 5-3.

Figure 5-25 shows the engine speed as the charging valve between the tank and the engine opens. The engine is connected to a tractor flywheel with the moment of inertia of 5 [$kg.m^4$] with a pulley ratio of 2.14. As can be seen, the pressurized air in the air tank increases the engine speed to approximately 70 [rpm] in 20 seconds which corresponds to a kinetic energy of 615 [J]. This kinetic energy is equivalent to the kinetic energy of a 1400 [kg] vehicle equipped with a four cylinder engine and a 120 [litre] air tank, accelerating to a speed of 6.7 [km/hr]. It is notable that this result was obtained with a tank pressure of 6 [bar] and for a single-cylinder engine with only one power stroke per engine revolution. As a result, higher vehicle speeds and shorter startup duration are expected if the storing pressure and the number of cylinders are higher than the experiment. With reference to Figure 5-26, the tank pressure decreases from 6 [bar] to 4 [bar] in the first 20 seconds. After that, the air motor cannot generate enough torque to counteract the mechanical friction and the engine speed drops as depicted in Figure 5-25.

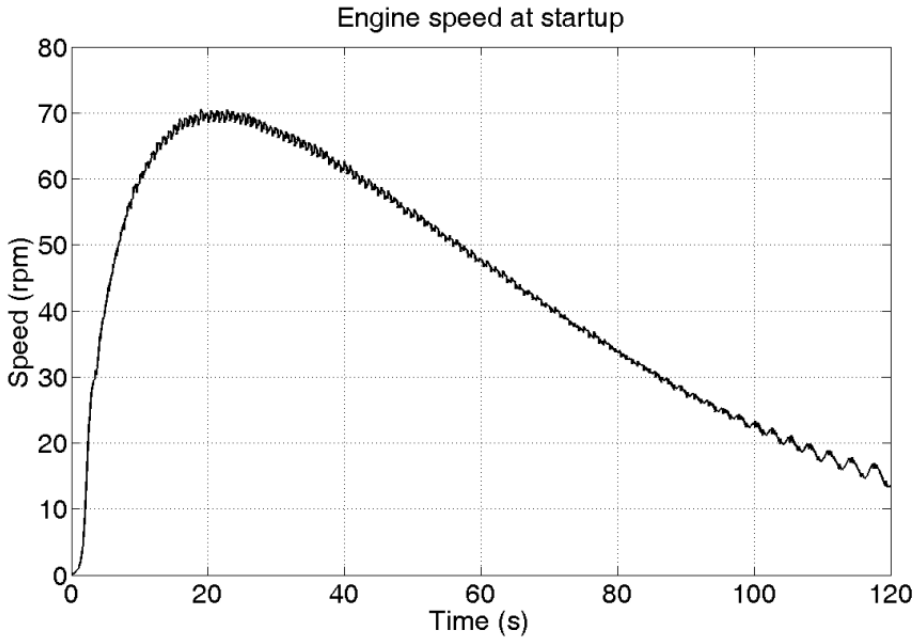

Figure 5-25: Engine speed at startup

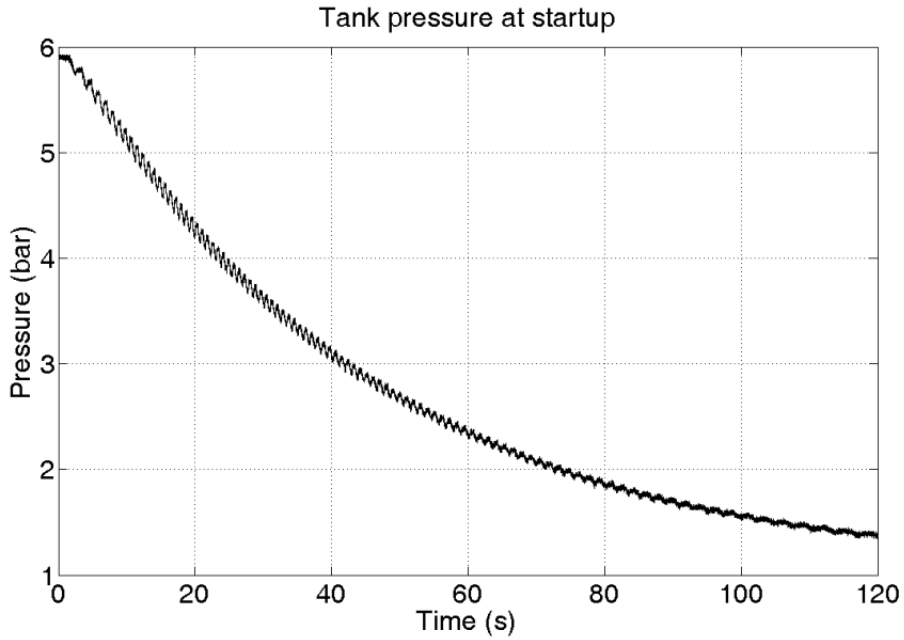

Figure 5-26: Tank pressure in startup mode

Based on the definition of exergy or useful work, the initial exergy of the tank with the volume of 30 [litre] and initial pressure of 6 [bar] is 15.9 [kJ]. The engine indicated power during startup is shown in Figure 5-27, where the engine power drops with the tank pressure.

The regenerated energy by the air motor is 4.87 [kJ] in 120 seconds. By considering the initial tank exergy, the overall efficiency of air motor mode is:

$$\eta_{\mathrm{AM}} = \frac{4.87kJ}{15.9kJ} \cong 30\%. \qquad 5\text{-}4$$

The cylinder/piston leakage is one of the important factors in the low air motor efficiency.

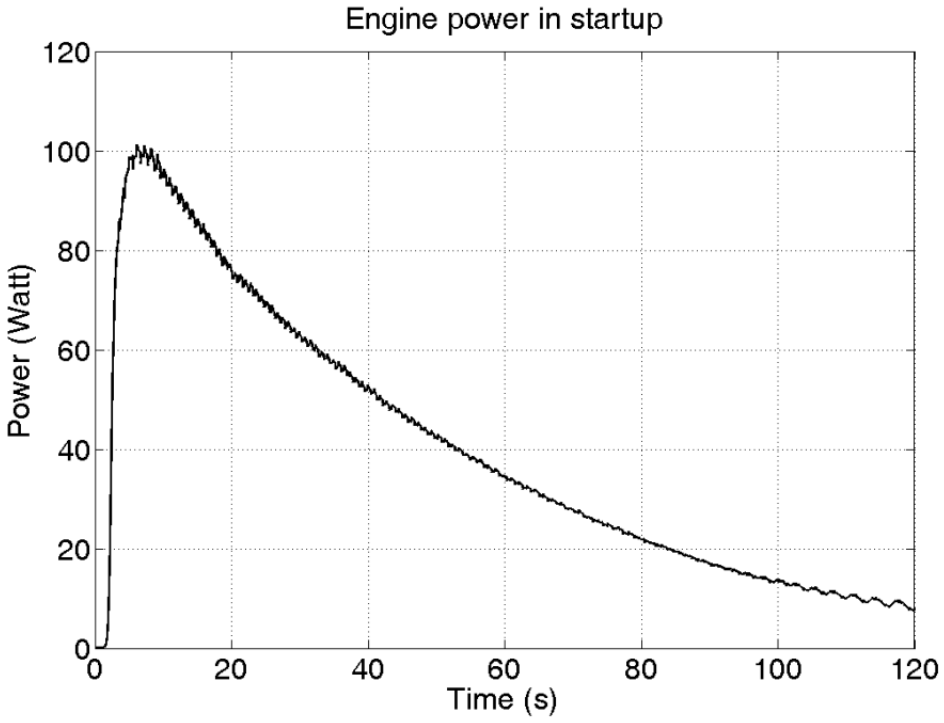

Figure 5-27 Engine power in startup

5.8 Summary

A new cam-based valvetrain configuration for air hybrid engines was proposed which eliminates the need for a fully flexible valvetrain. A set of unidirectional valves along with three-way valves were utilized to implement conventional, CB and AM modes. The feasibility and performance of the proposed configuration was tested using simulation and experiment studies for both regenerative and air motor modes. As mentioned, the engine torque during regenerative mode can be controlled by the existing electronic throttle system. The next chapter shows the feasibility of the regenerative braking torque control with the

throttle and presents the design and implementation of model-based and model-free controllers for this purpose.

Chapter 6
Regenerative Braking Torque Control

6.1 Background

When the driver pushes the brake pedal, linear to the applied force, the hydraulic pressure and hence the braking torque is increased. In an air hybrid engine, the braking system is comprised of friction brake and regenerative braking system (Figure 6-1). The regenerative braking torque is dependent on parameters such as tank pressure and engine speed and therefore a controller is needed to provide the ride experience as in a conventional friction braking system.

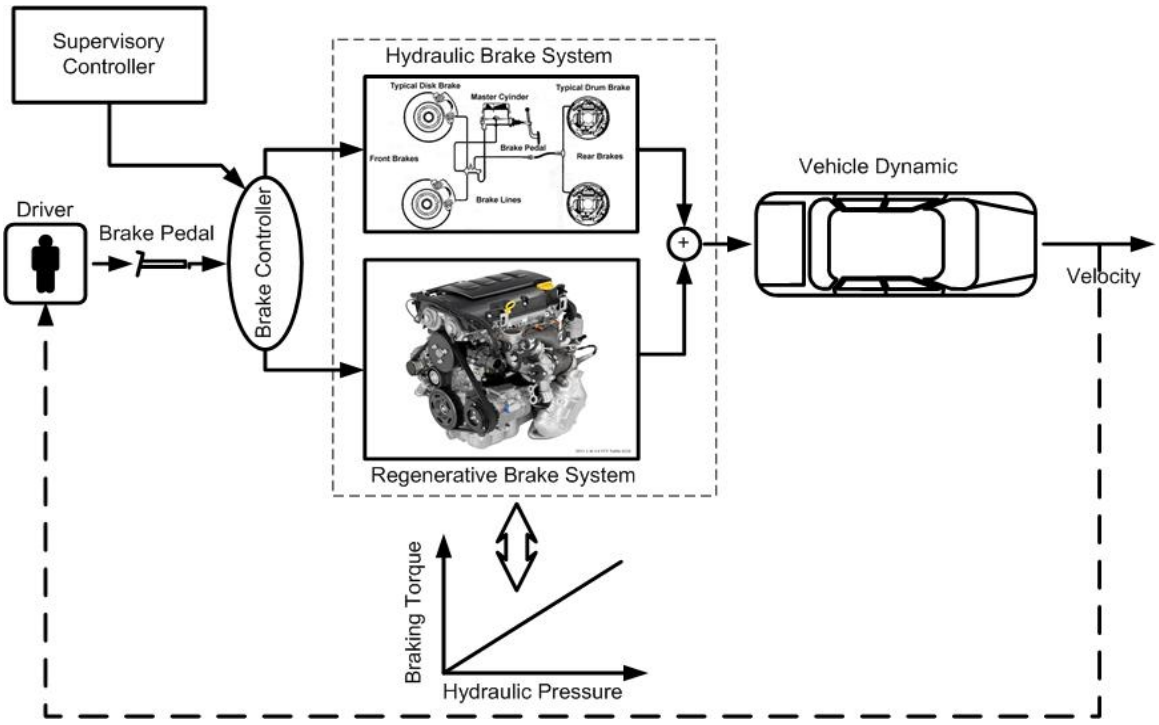

Figure 6-1: Hybridized brake system

To control the regenerative torque, the amount of air entering the cylinder should be regulated. Although it is shown that by regulating the air flow to the engine by controlling the valve timings, the braking torque can be controlled, the braking torque control of air hybrid engines has not been studied thoroughly in the literature. In the air hybrid engine

configuration proposed in Chapter 5, the regenerative braking torque is controlled by regulating the throttle angle. By controlling the throttle angle, one can control the manifold pressure and consequently the engine braking torque. The main objective of this chapter is to develop a throttle-based braking torque control for the proposed air hybrid engine. This controller should be robust and be able to track the desired braking torque.

Model free controllers such as proportional-integral (PI) controllers along with lookup tables are usually used in engine controls [41]. Although these control strategies offer satisfactory performance, the wide range of engine operating conditions, inherent non-linearity and controller calibrations have motivated researchers to conduct many studies on model-based controllers [41]. For instance, Souder et al [42] designed an adaptive sliding mode controller based on the mean value model of the engine to control the air-fuel ratio. Wagner et al. [41] designed a backstepping controller for simultaneous air to fuel ratio and engine speed control. Tang et al. [43] designed an adaptive feedback linearization based controller to control the air fuel ratio in spark ignition engines. The authors showed that, using nonlinear controllers leads to better closed-loop performance than conventional model-free or lookup table controllers.

There are several techniques for controlling nonlinear dynamic systems. However, the robust sliding mode controllers (SMC) have widely been used in many practical applications due to their capability to deal with uncertainties, good transient performance and their simplicity [44]. Furthermore, these control techniques could provide a systematic approach to maintain both stability and performance in the presence of modeling uncertainties [44].

In this chapter, the adaptive sliding mode controller is used for the engine regenerative braking torque control. This controller plus other model-free controllers are used in simulation and experiments for evaluation.

6.2 Regenerative Braking Mean Value Model (MVM)

The first step in designing a model-based controller for the engine in compression braking mode is deriving a control oriented model. This section is devoted to deriving an MVM for the engine during braking.

An MVM is a dynamic model of an engine that requires little engine data [45]. For a typical SI engine, MVM is comprised of three main subsystems [45], [46]: the fueling dynamics, the crank shaft dynamics and the manifold air dynamics. However, for an air hybrid engine in the regenerative mode, only the latter two subsystems are needed for the mean value model.

Air mass flow rate through the throttle in MVM is a function of manifold pressure and throttle angle that can be expressed by [47]:

$$\dot{m}_{throttle} = \rho_{air} A(\theta) \psi(P_r), \tag{6-1}$$

where $\psi(P_r)$ is:

$$\psi(P_r) = \begin{cases} \left(\frac{2}{\gamma+1}\right)^{\frac{1}{\gamma-1}} \sqrt{\gamma \frac{R}{M_{air}} \upsilon_{man} \frac{2}{\gamma+1}} & P_r < 0.53 \\ (P_r)^{\frac{1}{\gamma}} \sqrt{\frac{R}{M_{air}} \upsilon_{man} \frac{2\gamma}{\gamma-1}\left[1 - P_r^{\frac{\gamma-1}{\gamma}}\right]} & P_r \geq 0.53 \end{cases}, \tag{6-2}$$

and $A(\theta)$ is the throttle effective area and is estimated by :

$$A(\theta) = A_0 C_d(\theta), \tag{6-3}$$

where A_0 is the throttle reference area and $C_d(\theta)$ is the discharge coefficient which is defined experimentally as a function of throttle angle. Mass flow rate to the engine is defined by speed-density equation as:

$$\dot{m}_{engine} = \frac{P_{atm} M_{air}}{R \upsilon_{atm}} V_d \frac{\omega}{2\pi} \eta(P_m, \omega, P_{\text{tank}}), \tag{6-4}$$

where $\eta_{vol}(P_m, \omega, P_{\text{tank}})$ is the engine volumetric efficiency and is a function of manifold pressure and engine speed for typical engines [47]. However, in the case of air hybrid engines in the compression braking mode, tank pressure has a direct effect on the value of volumetric efficiency. As the tank pressure increases, the volumetric efficiency drops because the leftover pressurized air in the cylinder decreases the air flow rate to the engine. Thus, engine volumetric efficiency in the regenerative mode is considered to be a function of

the manifold pressure, engine speed and tank pressure. The manifold pressure dynamic, assuming constant manifold temperature is derived using the conservation of air mass in the intake manifold and the ideal gas law:

$$\dot{P}_m = \frac{R\upsilon_{man}}{V_{man}M_{air}}\left(\dot{m}_{throttle} - \dot{m}_{engine}\right). \tag{6-5}$$

Now, we need to derive an expression for the engine torque as a function of air mass flow rate to the engine. In the MVM for SI engines, the engine torque is related to the air mass flow rate by considering the engine thermal efficiency map and the heat content of the injected fuel. However, there is no fuel injection during the CB mode. Therefore, a new model is needed to relate the air mass flow rate to the engine torque. In the regenerative braking mode, the engine can be considered in a steady state mode which receives air at the manifold pressure and compresses it adiabatically to the tank pressure. Thus, the engine braking torque can be estimated by:

$$T_{engine} = \dot{m}_{engine}\upsilon_{man}C_p\frac{\left(\left(\frac{P_{\text{tank}}}{P_{atm}}\right)^{\frac{\gamma-1}{\gamma}} - 1\right)}{\omega}. \tag{6-6}$$

In the above equation, the engine friction and heat transfer from the cylinder are ignored. To incorporate both of these parameters, the above equation is modified to:

$$T_{engine} = \frac{\dot{m}_{engine}\upsilon_{man}C_p\left(\left(\frac{P_{\text{tank}}}{P_{atm}}\right)^{\frac{\gamma-1}{\gamma}} - 1\right)}{\omega} + T_f\left(\omega, P_m, P_{\text{tank}}\right), \tag{6-7}$$

where, $T_f\left(\omega, P_m, P_{\text{tank}}\right)$ accounts for the engine friction and heat transfer that can be found through experiment. Replacing $\dot{m}_{engine}$ from Eq. (6-4) results in:

$$T_{engine} = \left(\frac{P_{atm}M}{R\upsilon_{atm}}V_d\frac{1}{2\pi}\eta_{vol}\right)\upsilon_{man}C_p\left(\left(\frac{P_{\text{tank}}}{P_{atm}}\right)^{\frac{\gamma-1}{\gamma}} - 1\right) + T_f\left(\omega, P_m, P_{\text{tank}}\right), \tag{6-8}$$

Differentiating the above equation with respect to time and assuming that $\partial\omega/\partial t$ and $\partial P_{\text{tank}}/\partial t$ are negligible compared to the manifold pressure dynamic (the air tank is at least two order of magnitude larger than the manifold) leads to:

$$\dot{T}_{engine} = \left(\frac{P_{atm} M}{R \upsilon_{atm}} V_d \frac{1}{2\pi} \frac{\partial \eta_{vol}}{\partial P_m} \right) \upsilon_{man} C_p \left(\left(\frac{P_{atm}}{P_{\text{tank}}} \right)^{\frac{-\gamma+1}{\gamma}} - 1 \right) \dot{P}_m + \frac{\partial T_f}{\partial P_m} \dot{P}_m . \qquad 6\text{-}9$$

For convenience, the above equation can be written as:

$$\dot{T}_{engine} = f_1 \dot{P}_m , \qquad 6\text{-}10$$

where, $f_1 = \left(\frac{P_{atm} M}{R \upsilon_{atm}} V_d \frac{1}{2\pi} \frac{\partial \eta_{vol}}{\partial P_m} \right) \nu_{man} C_p \left(\left(\frac{P_{atm}}{P_{\text{tank}}} \right)^{\frac{-\gamma+1}{\gamma}} - 1 \right) + \frac{\partial T_f}{\partial P_m}$. Substituting $\dot{P}_m$ from Eq. (6-5) in Eq. (6-10) yields:

$$\dot{T}_{engine} = f_1 \frac{R \upsilon_{man}}{V_{man} M} \left(\rho_{air} A(\theta) \psi(P_r) - \frac{P_m M}{R \upsilon_{atm}} V_d \frac{\omega}{2\pi} \eta_{vol} \right). \qquad 6\text{-}11$$

Now, the above equation can be written as the following control affine system (for more information on control affine systems see [44]):

$$\dot{T}_{engine} = g_1 A(\theta) + g_2 , \qquad 6\text{-}12$$

where, $g_1 = f_1 \frac{R \upsilon_{man}}{V_{man} M} \left(\rho_0 \psi(P_r) \right)$ and $g_2 = -f_1 \frac{R \upsilon_{man}}{V_{man} M} \left(\frac{P_m M}{R \upsilon_{atm}} V_d \frac{\omega}{2\pi} \eta_{vol} \right)$.

Now, the engine braking torque is related to the control input, θ, by a non-linear first order differential equation in a canonical controllable form, Eq. (6-12). In order to check the validity of the MVM model, a control signal as shown in Figure 6-2.a is applied to both a detailed engine model in GT-Power with the specifications shown in Table 6-1 and its mean value model in Matlab/SIMULINK. The mean value model parameters such as volumetric efficiency maps are obtained from GT-Power detailed model.

Table 6-1: Engine specification

Number of cylinders	4
Displacement	1800 [cc]
Compression ratio	8.5
Throttle diameter	50 [mm]

Figure 6-2.b and Figure 6-2.c show air mass flow rate to the engine and the manifold pressure obtained from the two models with respect to time. As can be seen, there is a good agreement between the detailed model and MVM. However, a non-negligible difference between engine braking torque obtained from GT-Power and MVM can be seen in Figure 6-2.d. The discrepancies seen between the detailed model and MVM can be explained as follows:

1. MVM is an average model. Thus, the fluctuations caused by the reciprocal operation of the cylinders cannot be seen in the MVM.

2. Engine volumetric efficiency map ($\eta_{vol}(P_m, \omega, P_{\text{tank}})$), shown in Figure 6-3 for engine speed of 3000 rpm, is obtained at discrete engine speeds of 500, 1000, 2000, 3000 and 4000 rpm. The value of volumetric efficiency at the engine speeds different from these values is obtained by interpolation. This introduces a source of error to the mean value model.

3. The term $T_f(P_m, \omega, P_{\text{tank}})$ in Eq. (6-7) is neglected in the mean value model. This is the main source of the discrepancy seen between the detailed model and MVM in Figure 6-2.d. This difference can be minimized by obtaining a $T_f(P_m, \omega, P_{\text{tank}})$ map and considering it in the MVM. However, in this thesis, it is assumed that $T_f(P_m, \omega, P_{\text{tank}}) = 0$.

It is a well-known fact that the dynamic model of a system is an approximation of the real system, due to the presence of complex phenomena and disturbances. Therefore, even though the derived mean value is not an exact model of the system, it can be used in the design of a robust model-based controller. Furthermore, the differences between the detailed model and MVM can be minimized by acquiring the engine operating maps such as $\eta(P_m, \omega, P_{\text{tank}})$ at a higher number of operating points and including $T_f(P_m, \omega, P_{\text{tank}})$ in the MVM, but in this

work, the discrepancies between the detailed model and the derived MVM are considered as model uncertainties that had to be compensated by the controller.

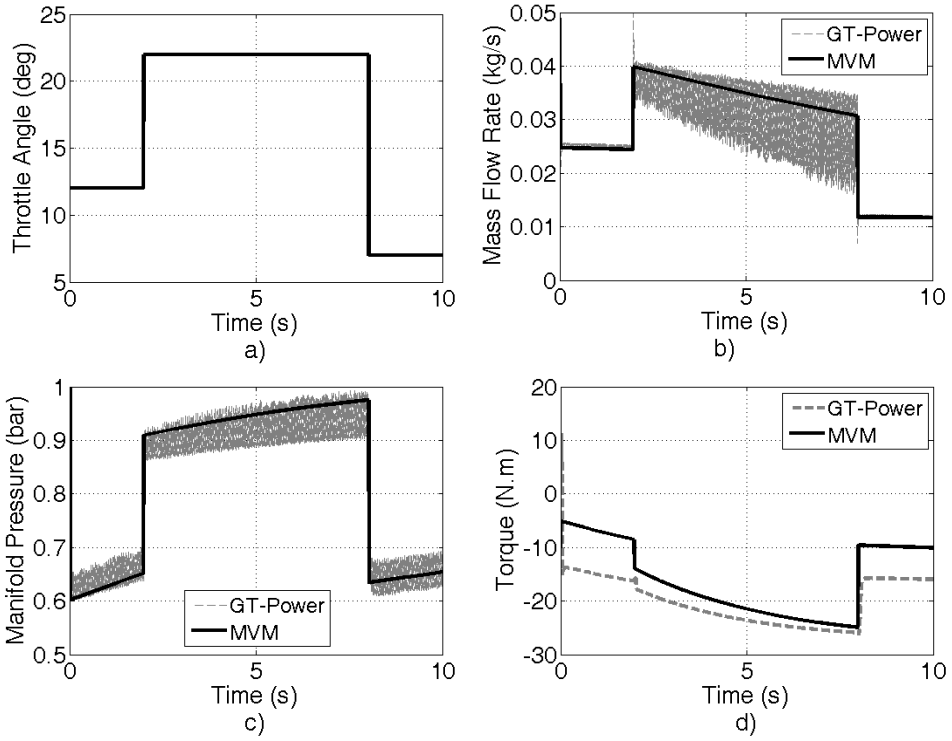

Figure 6-2: Comparison between the detailed model and MVM, a) throttle angle signal, b) mass flow rate, c) manifold pressure, d) braking torque.

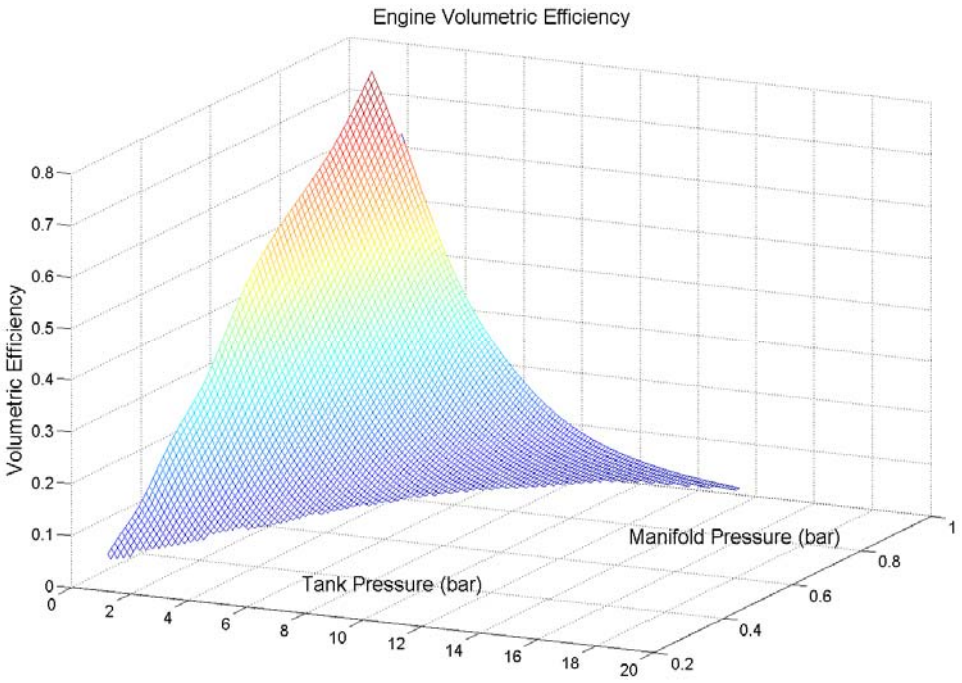

Figure 6-3: Engine volumetric efficiency in CB mode (@ 3000 [rpm]).

6.3 Robust Regenerative Torque Controller Design

The advantage of employing a non-linear control scheme is that all the operating points of the system can be considered and there is no need to linearize the nonlinear system about some operating points. Sliding mode controllers are attractive due to their capability to deal with uncertainties, good performance and fast response. But, the discontinues nature of this type of controller creates chattering in the control signal that may excite un-modeled high frequency modes of the system. The boundary layer method, which attempts to eliminate the chattering in the control signal, also requires a trade-off between tracking performance and chattering [44]. In this section, a nonlinear adaptive sliding mode scheme is designed and adapted to the system (Eq. (6-12)) based on reference [48] to control the engine torque during regenerative braking mode. The Adaptive sliding mode control scheme is chosen due to its ability in estimating the unknown parameters of the system and also dealing with the un-modeled dynamics and disturbances. The control objective is to track the desired torque, set by the supervisory controller. Thus, assuming the engine regenerative torque is available for measurement the error term is defined as follows:

$$e = T_{engine} - T_d. \tag{6-13}$$

The first step in designing the SMC is to define/design the sliding surface. In this study, the integral type sliding surface [44] is chosen to ensure a zero steady-state error.

$$S = \left(\frac{d}{dt} + \lambda\right)^n \int e dt = 0, \tag{6-14}$$

where n is the order of the system. Based on Eq. (6-12), the order of the system is one, thus, the sliding surface is defined as follows:

$$S = e + \lambda \int e dt = 0. \tag{6-15}$$

The control law that guarantees achieving the above goal is designed systematically in two steps, which is described next.

6.3.1 Controller Design for Nominal System

In the first step, the design of the SMC for the case of the nominal system (i.e., Eq. (6-12)) is considered. Then, the control law is designed for the actual system where there are model uncertainties and external disturbances. Let's suppose that the system dynamics and all the model parameters are known at each instant and there are no unknown external disturbances. One method to design a control law that derives the system trajectories to the sliding surface is the Lyapunov direct method. Therefore, the following Lyapunov function is considered for the single-input single-output system defined by Eq. (6-12) as:

$$\mathrm{Y} = 1/2\, SS. \tag{6-16}$$

To guarantee the stability of the system, the derivative of Lyapunv function should satisfy the following relation:

$$\dot{\mathrm{Y}} = S\dot{S} \le 0. \tag{6-17}$$

If we set $\dot{\mathrm{Y}}$ equal to a negative value such as $\dot{\mathrm{Y}} = S\dot{S} = -SKS$ where K is a positive constant, inequality (6-16) is satisfied. Thus,

$$S\dot{S} = -SKS \Rightarrow S\left(\dot{S} + KS\right) = 0. \qquad 6\text{-}18$$

From Eq. (6-15) the derivative of S with respect to time is:

$$\dot{S} = \dot{e} + \lambda e = \dot{T}_{engine} - \dot{T}_d + \lambda e. \qquad 6\text{-}19$$

Replacing $\dot{T}_{engine}$ from Eq. (6-12) and plugging $\dot{S}$ in $\dot{S} + KS = 0$, results in:

$$g_1 A(\theta) + g_2 - \dot{T}_d + \lambda e + KS = 0. \qquad 6\text{-}20$$

Thus, the control law for the nominal system is derived as follows:

$$\theta = A^{-1}\left(g_1^{-1}\left(-g_2 + \dot{T}_d - \lambda e - KS\right)\right). \qquad 6\text{-}21$$

The standard SMC control law for this system is:

$$\theta = A^{-1}\left(g_1^{-1}\left(-g_2 + \dot{T}_d - \lambda e - K\,\mathrm{sgn}(S)\right)\right). \qquad 6\text{-}22$$

Comparing Eq. (6-21), to the standard SMC control law, Eq. (6-22), shows that the discontinuous signum function, $\mathrm{sgn}(S)$, which causes chattering in standard SMC, is replaced with the continuous function, KS. This removes the chattering from the control input. However, the smooth control law of (6-21) still needs to be modified as it is not robust to the model uncertainties and disturbances. There are some other techniques to remove chattering from the control signal. One of them is the boundary layer method. In the case of boundary layer method, the control law of (6-22) is replaced with following control law:

$$\theta = A^{-1}\left(g_1^{-1}\left(-g_2 + \dot{T}_d - \lambda e - Ksat(S/\varepsilon)\right)\right), \qquad 6\text{-}23$$

where ε is the layer thickness. It can be shown that using the boundary layer method is a tradeoff between the performance and control discontinuity (Appendix F). Although for a given system, an optimum value for the thickness can be obtained, the closed-loop system may not be robust to the plant uncertainties and external disturbances [49].

6.3.2 Controller Design for System with Uncertainty

The control law obtained above is valid for a completely known system without any model uncertainties or external disturbances. However, in the presence of unknown external disturbances, model and parameters uncertainties, functions g_1 and g_2 are of the form:

$$g_1 = \hat{g}_1 + \Delta g_1,\ g_2 = \hat{g}_2 + \Delta g_2, \tag{6-24}$$

where $\hat{g}_1$ and $\hat{g}_2$ are the known parts and Δg_1 and Δg_2 are the unknown parts of g_1 and g_2. Therefore, if the model uncertainties and external disturbances are considered, Eq. (6-12) is written as:

$$\dot{T}_{engine} = \hat{g}_1 A(\theta) + \Delta g_1 A(\theta) + \hat{g}_2 + \Delta g_2 + d(t). \tag{6-25}$$

Now, all the uncertain terms can be lumped as follows [48]:

$$\tilde{g} = \Delta g_1 A(\theta) + \Delta g_2 + d(t), \tag{6-26}$$

and Eq.(6-12) is rewritten as:

$$\dot{T}_{engine} = \hat{g}_1 A(\theta) + \hat{g}_2 + \tilde{g}. \tag{6-27}$$

For the above system, the control law in Eq. (6-21) has to be modified to:

$$\theta = A^{-1}\left(\hat{g}_1^{-1}\left(-\hat{g}_2 + \dot{T}_d - \lambda e - KS - \tilde{g}\right)\right), \tag{6-28}$$

however, $\tilde{g}$ is unknown and not available in general. Thus, $\tilde{g}$ should be replaced by its estimate, $\tilde{g}_{est}$. Consequently, the control law can be written as:

$$\theta = A^{-1}\left(\hat{g}_1^{-1}\left(-\hat{g}_2 + \dot{T}_d - \lambda e - KS - \tilde{g}_{est}\right)\right), \tag{6-29}$$

where $\tilde{g}_{est}$ is the online estimate of $\tilde{g}$, and is derived in the next section.

6.3.3 Stability and Robustness Analysis

In order to prove the stability of the controller law of (6-29) and to derive an estimation law for unknown $\tilde{g}$, the following Lyapunov function is considered:

$$\mathrm{Y} = \frac{1}{2}\left(S^2 + E^2/\Gamma\right), \tag{6-30}$$

where Γ is a positive constant and $E = \tilde{g}_{est} - \tilde{g}$ is the estimation of error. Derivative of the above function is:

$$\dot{\mathrm{Y}} = S\dot{S} + E\dot{E}/\Gamma\,. \tag{6-31}$$

From Eq.(6-19), $\dot{S} = \dot{T}_{engine} - \dot{T}_d + \lambda e$, $\dot{T}_{engine} = \hat{g}_1 A(\theta) + \hat{g}_2 + \tilde{g}$ and $A(\theta) = \hat{g}_1^{-1}\left(-\hat{g}_2 + \dot{T}_d - \lambda e - KS - \tilde{g}_{est}\right)$. Thus,

$$\dot{V} = S\left(-KS - E\right) + \Gamma^{-1}E\dot{E} = -SKS - SE + \Gamma^{-1}E\left(\dot{\tilde{g}}_{est} - \dot{\tilde{g}}\right), \tag{6-32}$$

now, if the following update law is chosen:

$$\dot{\tilde{g}}_{est} = \Gamma S, \tag{6-33}$$

the adaptive control law for the system with uncertainties and external disturbances is defined as:

$$\begin{cases} \theta = A^{-1}\left(\hat{g}_1^{-1}\left(-\hat{g}_2 + \dot{T}_d - \lambda e - KS - \tilde{g}_{est}\right)\right) \\ \tilde{g}_{est} = \int \Gamma S dt \end{cases}. \tag{6-34}$$

The proposed control law of (6-34) and the dynamic system given in Eq. (6-27) lead to the following closed-loop dynamics:

$$\dot{S} + KS = -\tilde{g}_{est} + \tilde{g}, \tag{6-35}$$

where $\tilde{g}_{est}$ can be replaced by Eq. (6-33) as follows:

$$\dot{S} + KS + \int \Gamma S dt = \tilde{g}. \tag{6-36}$$

Assuming K to be constant, the derivative of the above equation is:

$$\ddot{S} + K\dot{S} + \Gamma S = \dot{\tilde{g}}. \tag{6-37}$$

The stability of the above second order system, which is a constant-coefficient Lineard equation, is studied in[50]. The global asymptotic stability of $\ddot{x}+f(x)\dot{x}+g(x)=0$ can be proved if all the conditions listed below are satisfied:

I) $xg(x)>0$,

II) $f(x)>0$,

III) $\lim_{x\to\infty}\int_0^x g(\xi)d\xi=\infty$. 6-38

Now for the asymptotic stability of the closed-loop system under study (6-35), all of the above conditions have to be satisfied. The first condition leads to the following inequality:

$$S^2\left(\Gamma-\dot{\tilde{g}}/S\right)>0\Rightarrow S^2\Gamma-S\dot{\tilde{g}}>0\Rightarrow S^2\Gamma>S\dot{\tilde{g}}$$
$$\Rightarrow S^2\Gamma>S\dot{\tilde{g}}\Rightarrow\begin{cases}S>0\Rightarrow S\Gamma>\dot{\tilde{g}}\Rightarrow\Gamma>\dot{\tilde{g}}S^{-1}\\ S<0\Rightarrow S\Gamma<\dot{\tilde{g}}\Rightarrow\Gamma>\dot{\tilde{g}}S^{-1}\end{cases}. \quad 6\text{-}39$$

Thus, if $\Gamma>\dot{\tilde{g}}/S$ is valid, the first condition for global asymptotic stability of the system is satisfied. If the rate of change of lumped uncertainties is bounded, $\left|\dot{\tilde{g}}\right|<\delta<\infty$, then $\Gamma>\frac{\dot{\tilde{g}}}{S}$ can be satisfied for the whole state space except a small neighborhood of the sliding surface where $|S|<\varepsilon$, if $\Gamma=\frac{\delta}{\varepsilon}$. Thus, we can conclude that there exists a Γ for which the first condition of asymptotic stability of the closed loop system is satisfied everywhere in the state space, except a small neighborhood of the sliding surface if the rate of change of lumped uncertainties is bounded. The second and third conditions are satisfied because: II) $K>0$ and III) $\lim_{S\to\infty}\int_0^S \xi\left(\Gamma-\frac{\dot{g}}{\xi}\right)d\xi=\infty$. Thus, it can be concluded that the closed-loop system (6-35) can be brought to any small neighborhood of the sliding surface by choosing a proper set of control parameters.

6.4 Simulation and Numerical Results

In this section, two model-based controllers, the ASMC developed in Section 6.3.3 and a smooth SMC along with a model-free lookup table/ high gain PID controller are applied to the braking torque control problem of the single-tank regenerative system. The engine and vehicle specifications are shown in Table 6-1 and Table 6-2.

Table 6-2 Vehicle specifications

Vehicle mass	1400 [kg]
Final drive ratio	3.73
Vehicle initial speed	55 [km/hr]
Tank volume	100 [l]
Initial tank pressure	1.5 [bar]
Transmission ratio	1st : 2.36
	2nd : 1.52
	3rd : 1.15
	4th : 0.85

It is assumed that a constant regenerative braking torque at the vehicle wheels is requested by the driver. In other words, the desired engine torque is constant and changes only at the time of gear shifting to compensate for the change in the overall gear ratio between the engine output and the vehicle wheels. The closed-loop dynamic of the throttle is modeled by [39]:

$$0.05\dot{\theta}_{throttle} + \theta_{throttle} = \theta_{throttle,com}. \quad 6\text{-}40$$

The clutch slip dynamic is also modeled by the following equation:

$$0.2\dot{\omega}_{engine} + \omega_{engine} = \omega_{clutchoutput}. \quad 6\text{-}41$$

It is assumed that the initial throttle position is 20º and the controller is activated at T=3[s]. The controller parameters are tuned as listed in Table 6-3. The air hybrid engine is modeled in GT-Power software and the controller is simulated in Simulink7.7© software. GT-Power

and Simulink are coupled and run simultaneously. It is assumed that the engine output torque is available for measurement. The control task is to control the throttle angle in such a way that the engine braking torque meets the braking torque requested by the driver. For the case of model-based controller, manifold pressure is obtained at each instant using MVM. The obtained manifold pressure is used to determine $\hat{g}_1$ and $\hat{g}_2$. Then the control signal is obtained at each instant based on Eq. (6-23), i.e., smooth SMC, and Eq. (6-34), i.e, ASMC. With reference to Figure 6-4 the control signal (i.e. commanded throttle angle) along with the computed engine speed, obtained from vehicle dynamics, are sent to the air hybrid engine model in GT-Power. Tank pressure and engine torque are also obtained from GT-Power model at each instant and used as the controller inputs.

Figure 6-5 shows the closed-loop control structure with lookup table/PID controller. A lookup table is developed from the steady state simulation of the engine in GT-Power as the feedforward part of the controller which determines the throttle angle according to the desired torque, engine speed and tank pressure.

Table 6-3: Controllers' parameters

PID	Proportional gain	10
	Integral gain	0.6
	Derivative gain	0.2
Smooth SMC	λ	0.1
	K	4
	ε	0.5
Adaptive SMC	λ	0.1
	K	2
	Γ	10

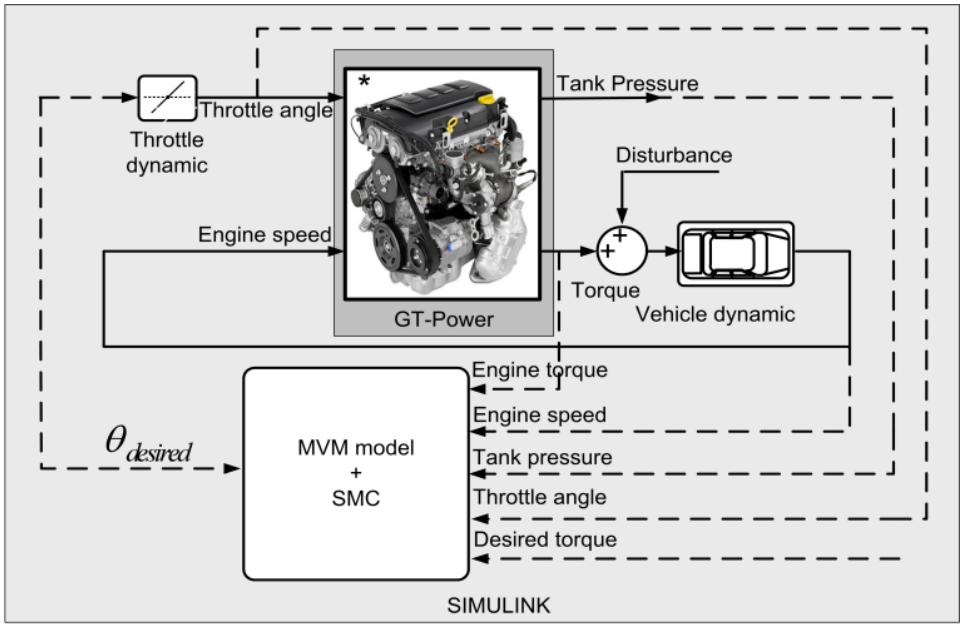

* http://www.treehugger.com/files/2008/09/gm-chevy-volt-engine-flint-michigan.php

Figure 6-4: Sliding mode controller scheme

A high gain PID controller is also tuned to compensate for all the uncertainties related to the lookup table and external disturbances and to generate a desired transient performance for the closed-loop system. As the engine mode is shifted to regenerative braking, the engine starts working as an air compressor, stores the kinetic energy of the vehicle in the air tank and applies braking torque at the vehicle wheels. This leads to the decrease in the vehicle speed. It is assumed that the automatic transmission changes the transmission ratio when vehicle speed drops below 50 [km/hr]. Thus, the sudden change in the engine speed around T=8 [s] (Figure 6-6) is due to the gear shifting. Because of the sudden change in the engine speed, the desired engine torque should be shifted to keep the braking torque at a constant level. This introduces a step input to the system (Figure 6-7). It is assumed that the desired braking torque is set at -20 [Nm] at the beginning of the simulation and is shifted to about -15 [Nm] after gear shifting to maintain the braking torque at the vehicle wheels unchanged.

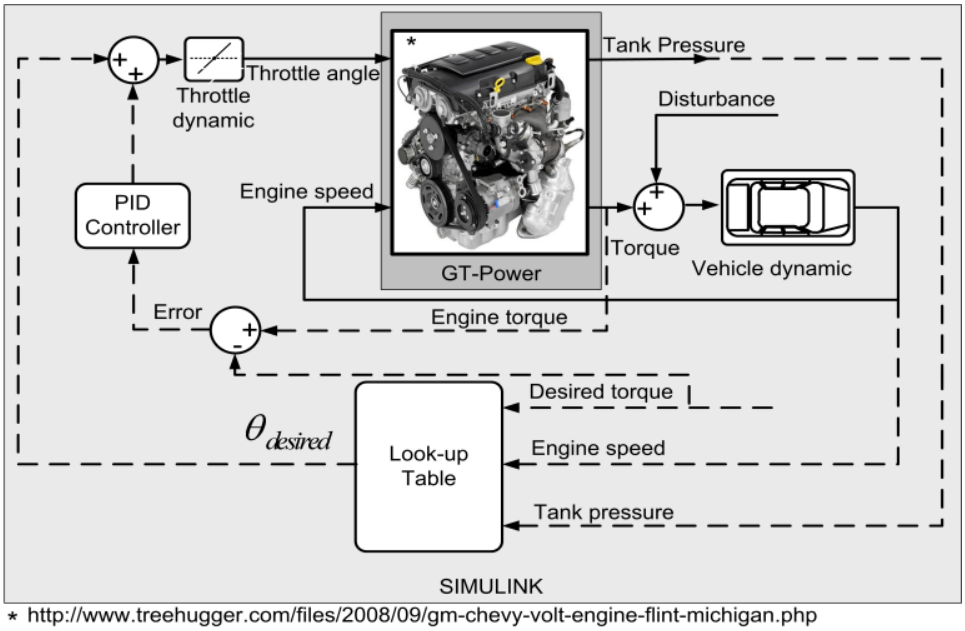

Figure 6-5 Lookup table/PID controller scheme.

Figure 6-7 shows the closed-loop tracking performance of the system and the commanded throttle angle for ASMC controller. The closed-loop system starts with 1.5 [N.m] tracking error and it takes about 1 second for the error to decay to 0.1 [N.m]. This relatively long time is because the relation between the throttle angle and the engine torque is highly non-linear and the engine torque varies slowly with the throttle angle at the angle of 20º, initial error is relatively large and the engine speed and tank pressure are changing continuously. Engine torque tracks the desired trajectory within 0.5% (i.e, $\left|T_{eng} - T_{des}\right| / T_{des} \times 100$) from T=4[s] to T=8[s] for ASMC. Tracking error increases to about 6% at the time of gear shifting and decays to less than 1% in less than 0.5 [s] and remains within 0.5% for the rest of the simulation. Thus, the designed ASMC is not only successful in removing the chattering, but also in following the reference trajectory.

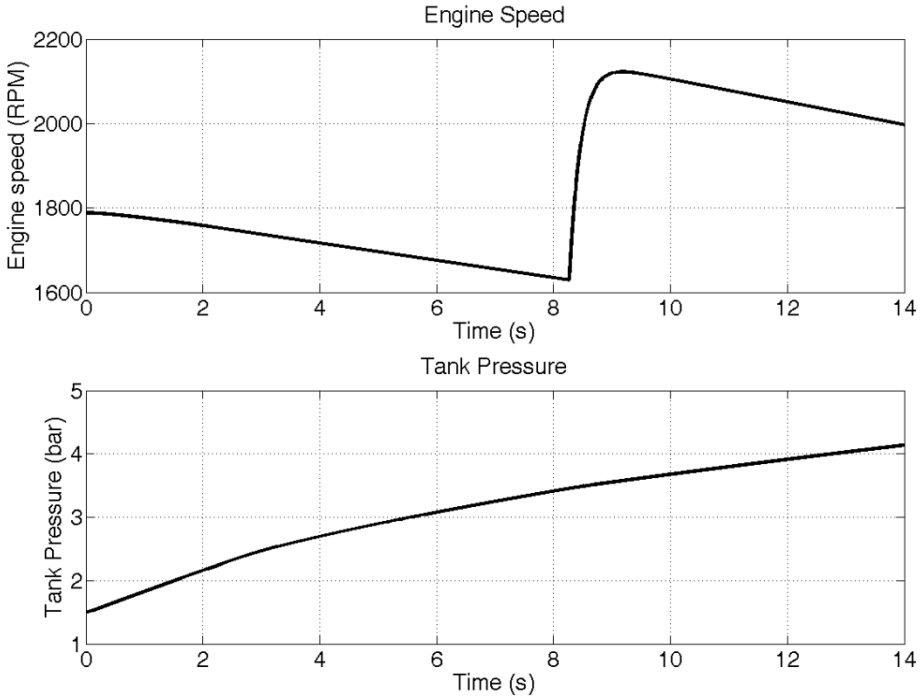

Figure 6-6: Engine speed and tank pressure versus time

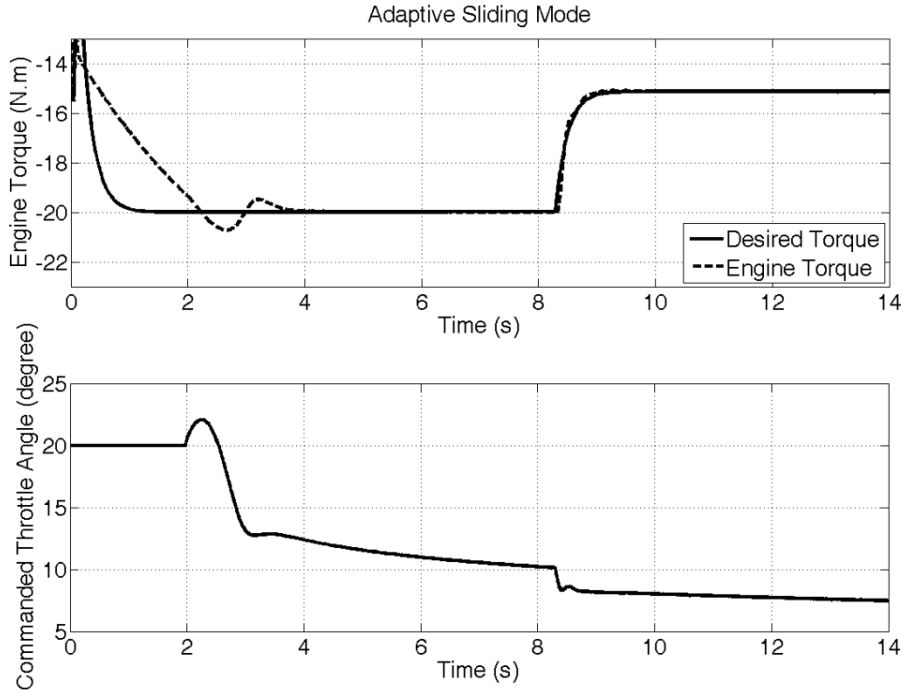

Figure 6-7: Closed-loop tracking performance and controller commanded signal

Figure 6-8 compares the tracking error obtained by the three controllers. As can be seen, ASMC has the best tracking properties in terms of the settling time and steady state error. As

this figure illustrates, there is a steady state error when smooth SMC controller is employed. Despite the fact that using the boundary layer method can remove the chattering, it only guarantees the performance to a certain precision [44] and perfect tracking cannot be obtained in general. High gain PID also shows satisfactory performance; however, it should be mentioned that PID controllers are usually tuned for some desired operating points. Thus, in spite of their time taking tuning process, they may not show a satisfactory performance and robustness in a wide range of operating points specifically for a highly non-linear system such as an engine. Secondly, although increasing the PID gains leads to a better tracking performance, it shrinks the stability margin of the closed-loop system. Having the derivative term in the controller structure also helps the stability of the system only to a certain level. As a general rule, tuning a PID is always a tradeoff between the stability margin and the performance. According to Koktovic and Marnino [51], as the feedback gains are increased, the stability margin is reduced in size and ultimately is limited to the equilibrium point.

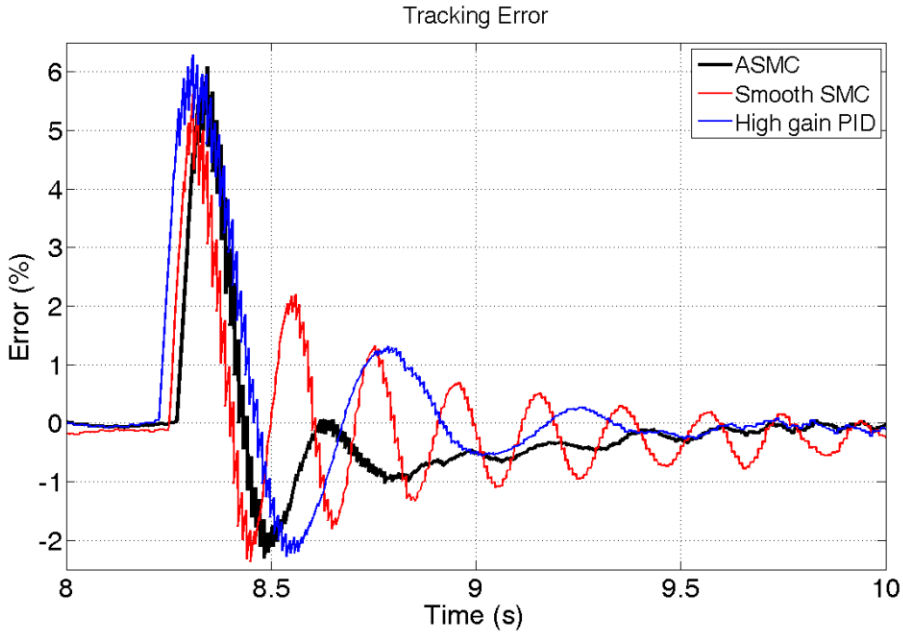

Figure 6-8: Tracking error of ASMC, smooth SMC and high-gain PID without external disturbance

In the next step, the performance and robustness of the three controllers are studied by adding an external disturbance of $T_{dist} = -0.5 + \sin 3t$ [Nm] to the GT-Power model output (Figure 6-4 and Figure 6-5). Figure 6-9 shows the tracking error of the three controllers. In

this case, ASMC controller has almost similar tracking performance to the case of no external disturbance (Figure 6-8) with the steady state error of less than 0.5%, which clearly implies that the controller is robust to disturbances and has adaptive capability. However, PID and smooth SMC controllers exhibit higher tracking error (up to 4%). As Figure 6-9 clearly shows, introducing an external disturbance to the system causes chattering in the system output when smooth SMC is used. This shows that the chosen a boundary layer thickness of $\varepsilon = 0.5$ is not enough to remove the chattering in the presence of external disturbances. Choosing a thicker boundary layer removes the chattering as seen in the output, however, it deteriorates the closed-loop tracking performance.

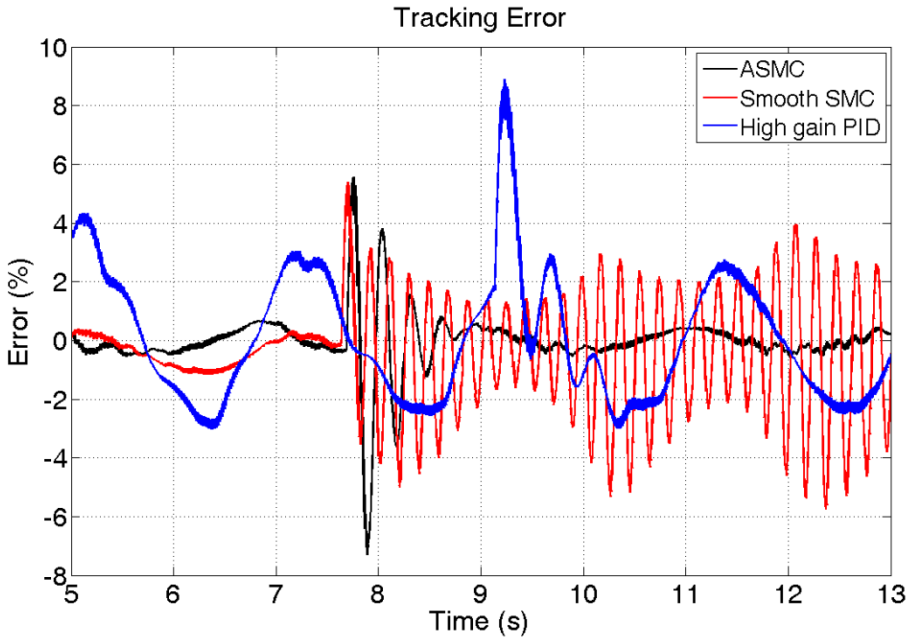

Figure 6-9: Tracking error of ASMC, smooth SMC and high-gain PID with external disturbance

The steady state tracking performance of each controller from T=8 to T=14 is summarized in Table 6-4. The average tracking error $\bar{e}$, standard deviation of error σ_e, and integral of absolute tracking error are presented for the three controllers. With reference to Table 6-4, ASMC has the best tracking performance among all the studied controllers. Lookup table/PID controller also depicts satisfactory performance. The performance of all the

controllers deteriorates by the external disturbance; however, the adaptive SMC shows the best robustness against the external disturbance.

Table 6-4: Torque Controller Performance

Controller Description	$\bar{e}$	σ_e	$\int \lvert e \rvert dt$
No External Disturbance			
Lookup table/PID	0.01 N.m	0.16	0.29
Smooth SMC	0.063 N.m	0.15	0.38
Adaptive SMC	0.001 N.m	0.13	0.23
With External Disturbance			
Lookup table/PID	0.003 N.m	0.36	1.698
Smooth SMC	0.033 N.m	0.55	1.93
Adaptive SMC	0.007 N.m	0.22	0.964

To avoid redundancy, the developed adaptive SMC is only applied to the single-tank system in simulation. However, the controller is applied to both single- and double-tank systems in the experiments.

6.5 Experiments

6.5.1 Experimental Procedure

The experimental setup was modified by adding a proportional valve to the intake manifold as shown in Figure 6-10. This valve is used to control the engine braking torque by controlling the air flow to the engine instead of an electronic throttle system. Some sensors are also installed to measure pressure and the temperature of the inlet manifold, cylinder and the tank. Due to the slow response time of the solenoid valves, the engine speed was fixed at 140 [rpm] by a servo motor. The cylinder pressure is measured by a pressure sensor, directly mounted on the cylinder head. The data from this pressure sensor is used to determine the engine mean effective pressure and indicated braking torque. The proportional valve has the characteristics listed in Table 6-5 and is controlled by a voltage to current converter drive

(Appendix G). The proportional valve effective area, $A(\theta)$, varies with the control signal as shown Figure 6-11.

Table 6-5: Proportional valve characteristics

Make	SMC
Orifice size	4 [mm]
Flow	0-85 [lpm]
Max operating pressure	1.2 [bar]

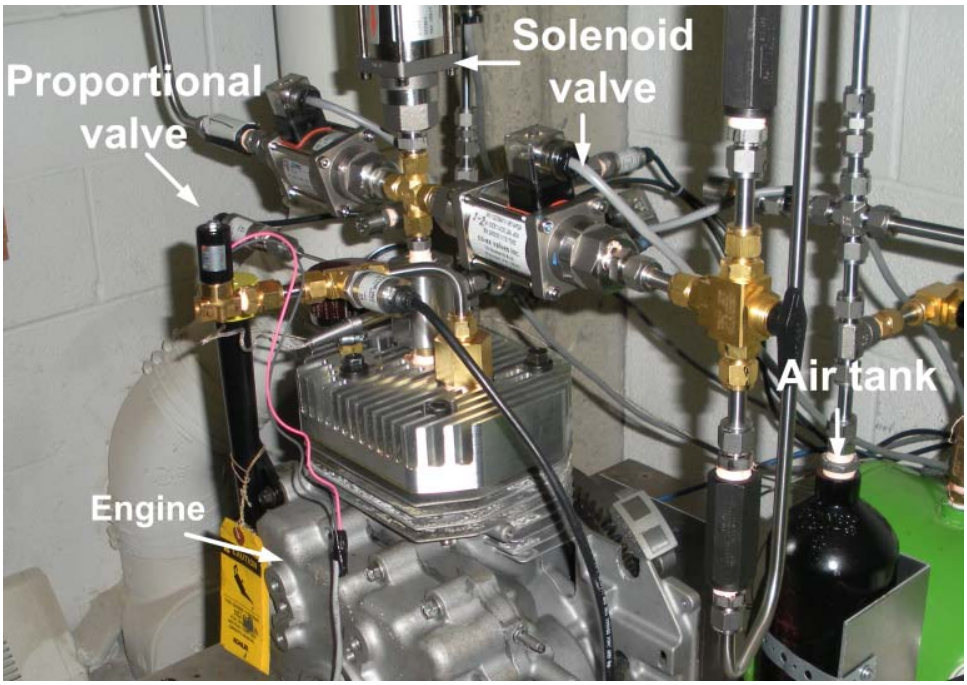

Figure 6-10: Experimental setup

6.5.2 Single-tank Regenerative Torque Control

The engine braking torque is proportional to the tank pressure and the inlet valve control signal. Figure 6-12 shows the engine regenerative torque versus tank pressure for various proportional valve effective areas. The engine braking torque drops as the tank pressure increases and the valve control signal decreases. As can be seen, the engine torque is not zero when the valve is almost closed because of the piston/cylinder leakage.

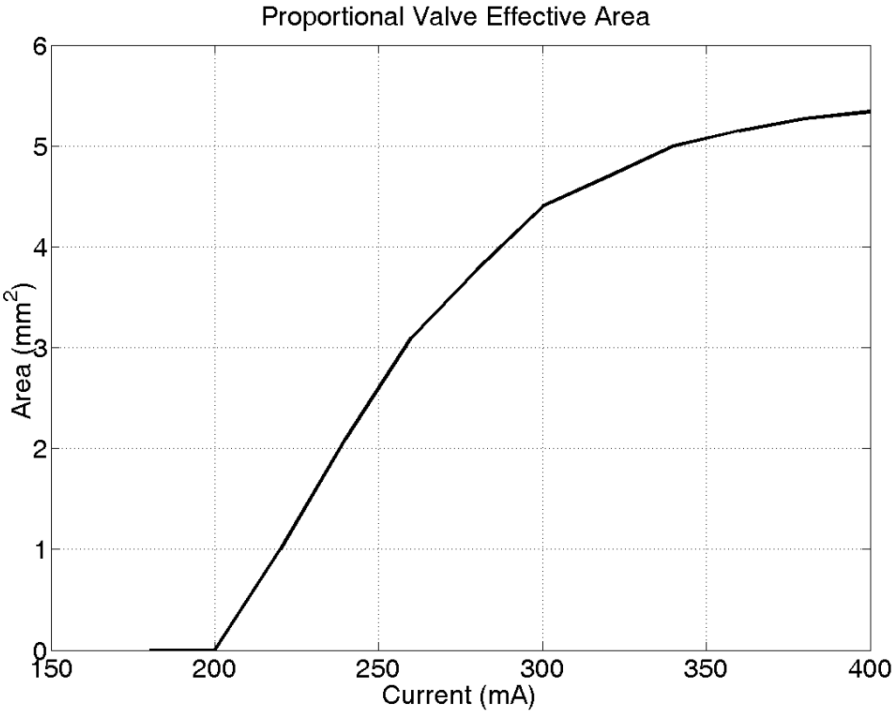

Figure 6-11: Proportional valve effective area (suggested by manufacturer)

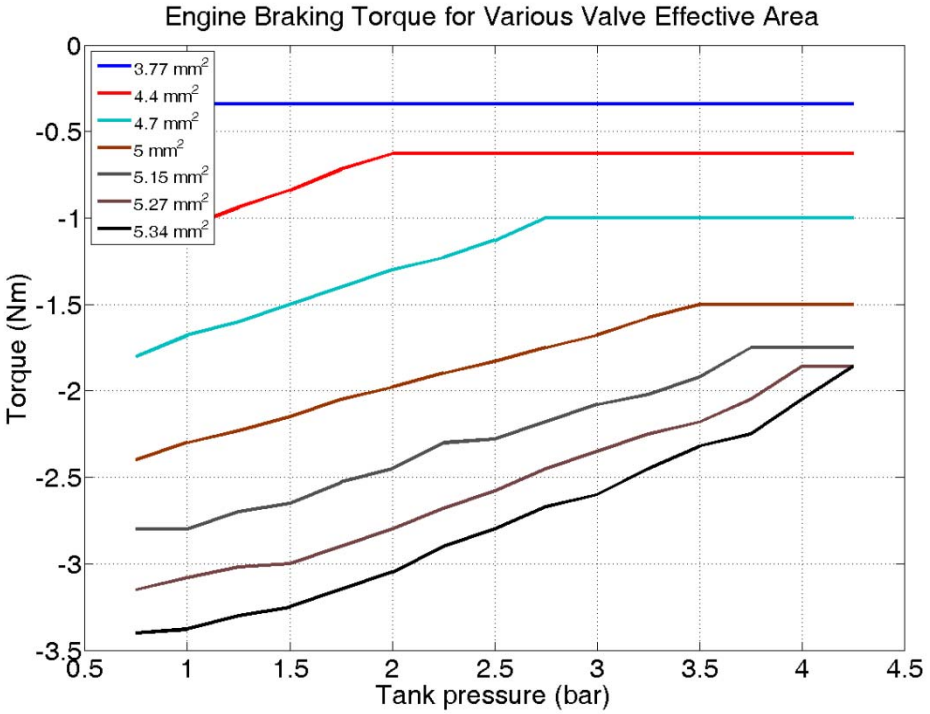

Figure 6-12: Engine braking torque versus tank pressure for various control signals

In order to apply the adaptive SMC to the system, g_1 and g_2 in Eq.(6-12) are required. To define these parameters engine volumetric efficiency maps, along with the online measurement of the manifold pressure are required. However, since the flow to the engine and to the tank cannot be measured in the available test bed, the volumetric efficiency maps cannot be obtained. In addition, the pressure sensor mounted on the inlet manifold did not show a meaningful pressure offset form atmospheric pressure which is mainly because of the low engine speed. As a result, parameters required for defining g_1 and g_2 could not be measured or identified. As a result, g_1 and g_2 were identified directly by measuring $\dot{T}_{engine}$ at various operating points by the least square method (more details in Appendix H).

Three different controllers, adaptive SMC, smooth SMC and a PI controller are tuned and used for the engine torque control. It is noteworthy that ASMC was tuned after only 4 trials; however, PI and smooth SMC were tuned after 16 and 30 trials respectively. Controllers' parameters are listed in Table 6-6.

Figure 6-13 shows the closed-loop tracking performance of the controllers. All the controllers show satisfactory performances, however, ASMC and PI have the best tracking performance as they track the desired torque within 5% (Figure 6-14), despite the continuous change in the tank pressure and unfiltered sensor noises (Figure 6-15). For smooth SMC, the overshoot is about 7%, however, the performance deteriorates with time and the steady state error rises to about 13%.

Settling time for ASMC and PI is about 5 seconds (about 11 engine cycles) which is mainly due to the slow engine speed (140 [rpm]). Figure 6-16 shows the actuator control signal for ASMC controller. As can be seen, chattering is removed from the control signal employing ASMC. The closed-loop performances of the three controllers are listed in Table 6-7.

Table 6-6: Controllers' parameters

Adaptive sliding	λ	0.001
	K	0.003
	Γ	0.0002
Smooth sliding	λ	0.001
	K	0.003
	ε	1
PI	Proportional gain	0.1
	Integral gain	0.75
Controller sampling rate		10 [ms]

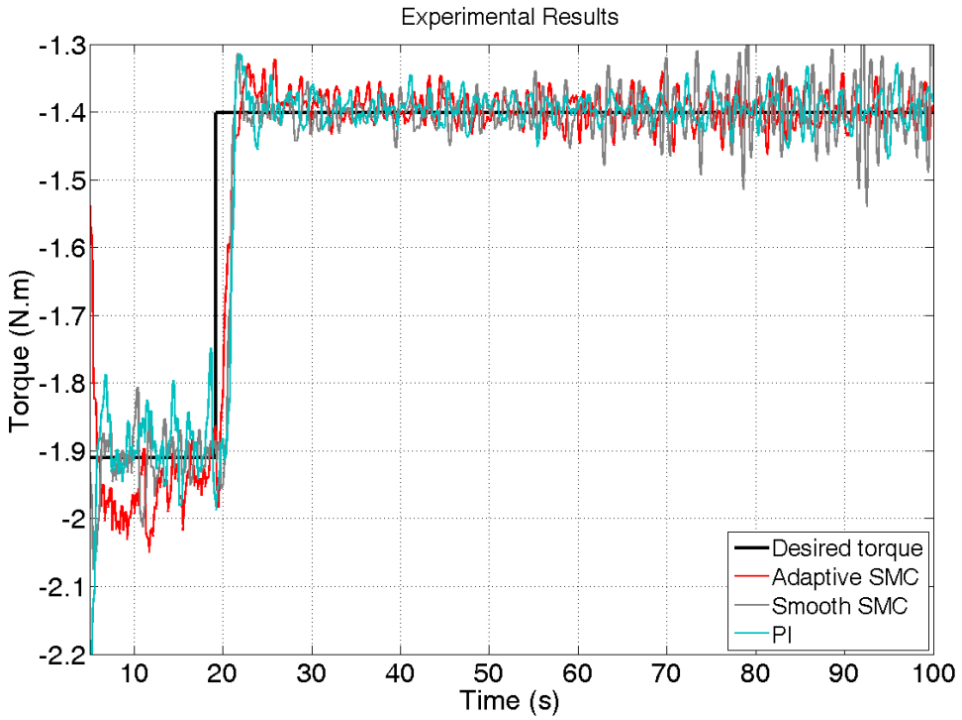

Figure 6-13: Experimental closed-loop tracking performance for ASMC, smooth SMC and PI

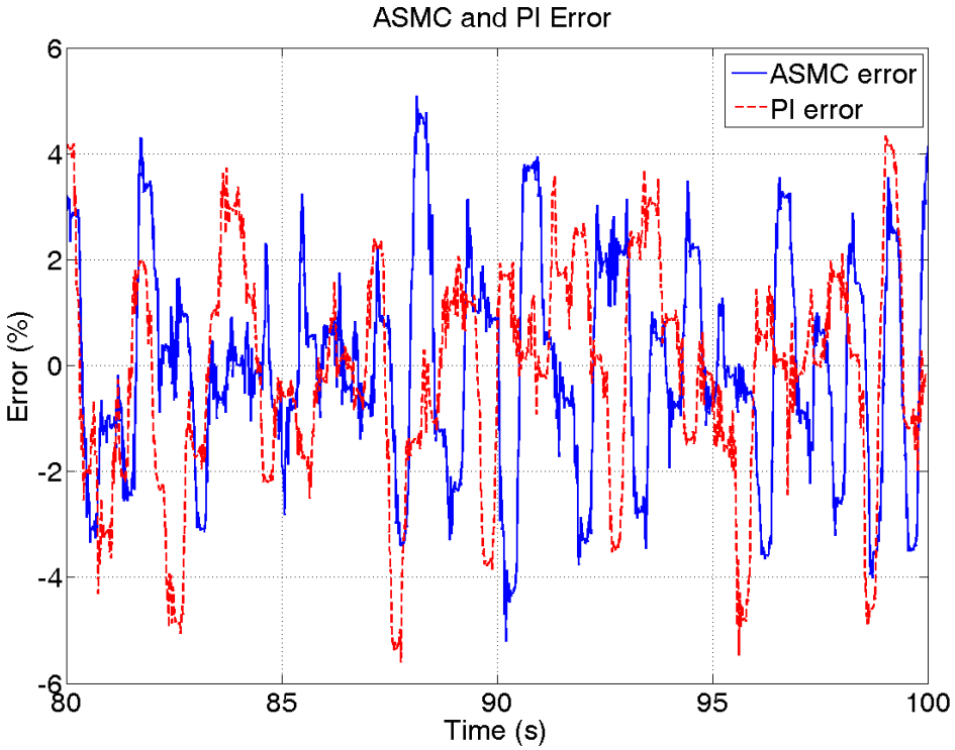

Figure 6-14: Experimental closed-loop tracking performance for ASMC and PI

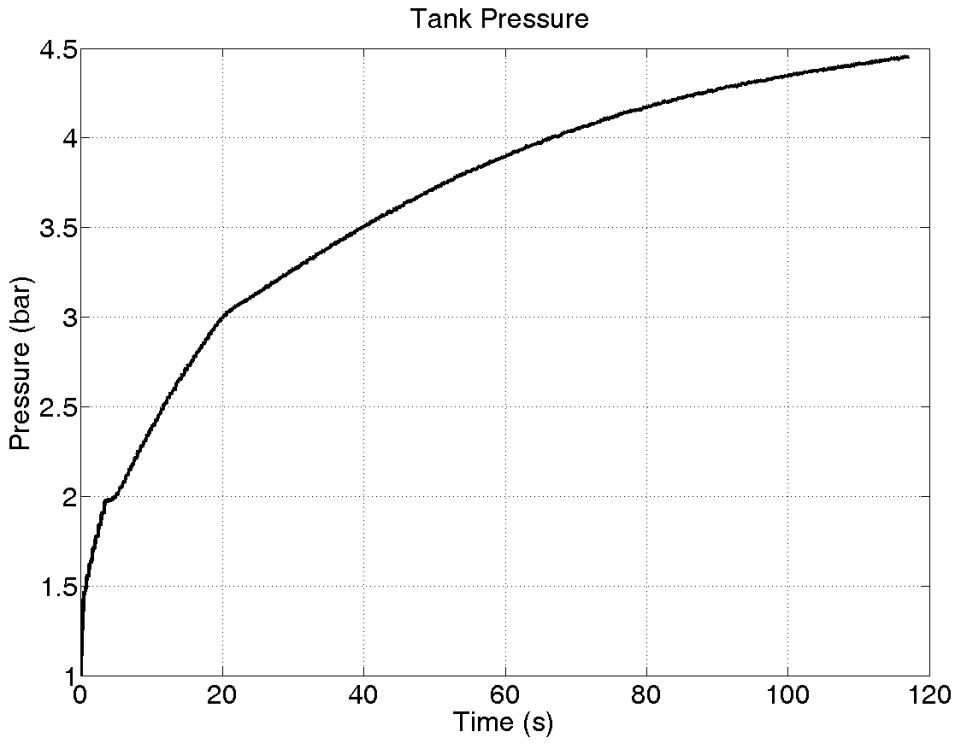

Figure 6-15: Change in the tank pressure throughout the experiment

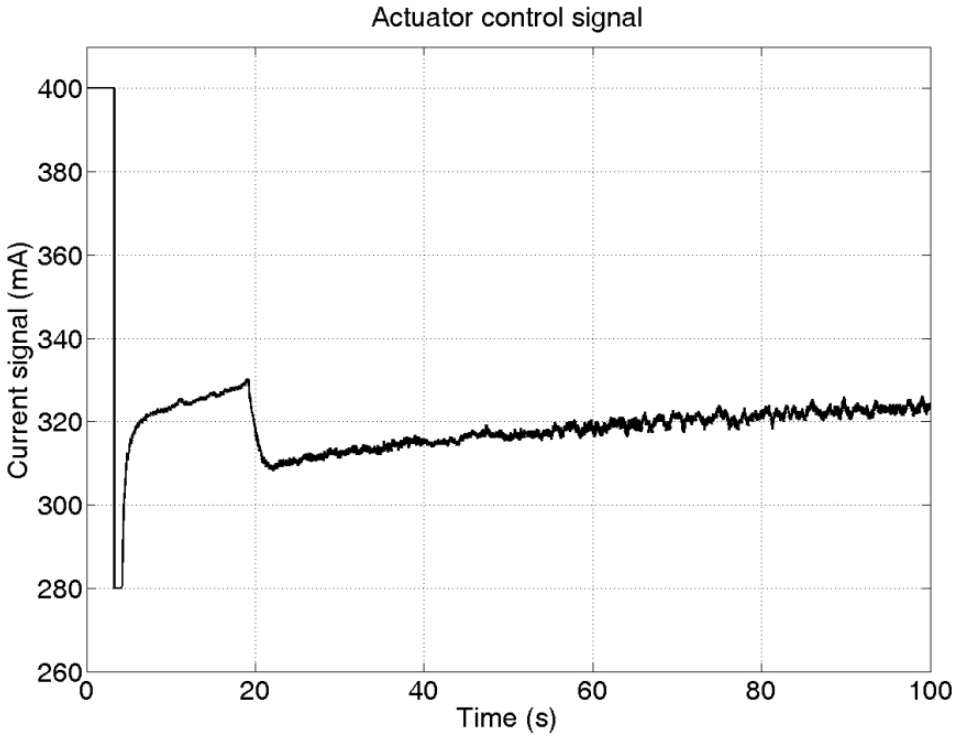

Figure 6-16: Actuator control signal

Table 6-7: Controllers' performances

Controller	Rise time [s]	Overshoot (%)	Steady state error (%)
Smooth SMC	5	7	13
PI	5	6.5	5
ASMC	5	6	5

To compare the robustness of the controllers against perturbations, the plant is perturbed by connecting the cylinder to atmospheric pressure for 0.5 [s] in the next set of experiments. As Figure 6-17 shows, ASMC and PID controllers show satisfactory performance regarding the perturbations; however, the smooth SMC performance deteriorates in spite of its time taking tuning process.

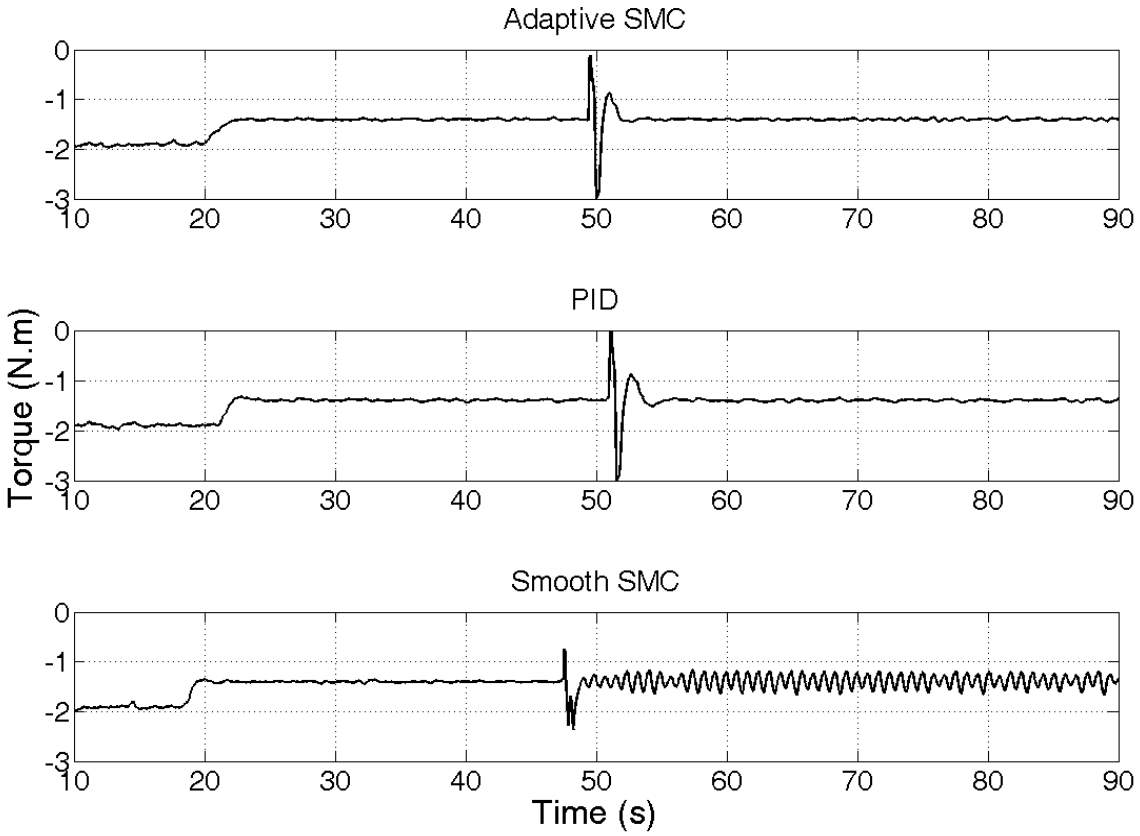

Figure 6-17: Experimental closed-loop tracking performance of ASMC, smooth SMC and PI

6.5.3 Double-tank Regenerative Torque Control

In the next set of experiments, braking torque control of the double tank system is investigated. Figure 6-18 shows the double-tank regenerative system torque versus tank pressure for various valve effective areas for the engine speed of 140 [rpm]. In contrast to the single-tank case, the engine braking torque increases with the tank pressure. This can be explained with reference to the thermodynamic cycle of the double-tank case (Figure 3-4) in which the P-V cycle enclosed area is not zero even when the main tank is full.

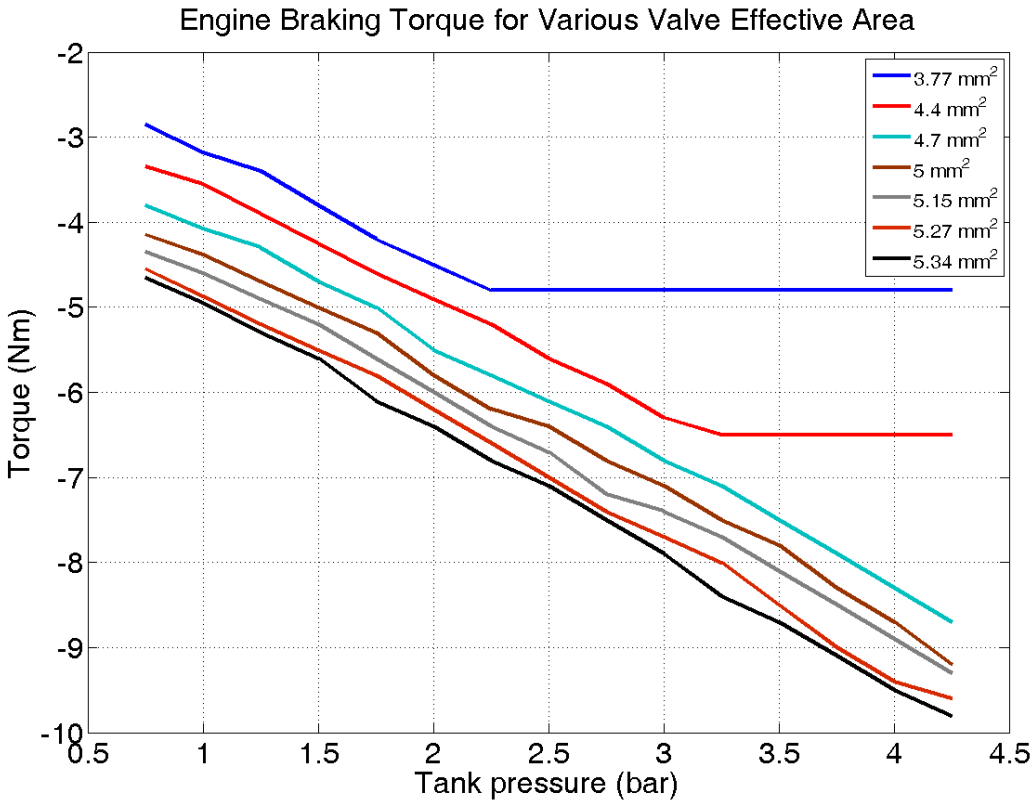

Figure 6-18: Engine torque versus tank pressure for different control signals

Figure 6-19 shows the LP tank pressure variation versus HP tank pressure for two effective areas of the valve. As can be seen, the LP tank pressure varies in a certain range for each tank pressure and control signal. Thus, it can be concluded that for a certain HP tank pressure and throttle angle, there is a certain range for LP tank pressure variation. Thus, as the throttle angle changes, the LP pressure range also changes and is adjusted for the new throttle angle after a limited number of cycles. As a result, a separate control of LP tank flow is not required and the engine torque can be controlled by controlling the inlet flow to the engine.

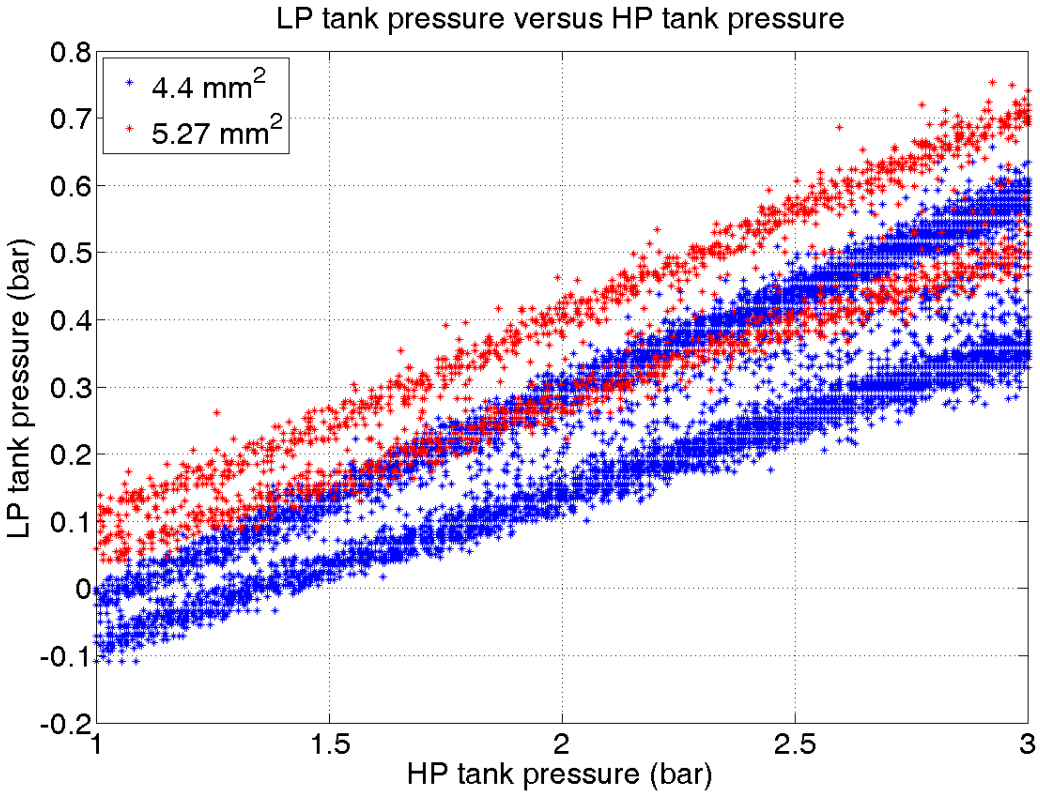

Figure 6-19: Steady state LP tank pressure variation versus HP tank pressure

For the case of the double-tank regenerative system, only PI controller and ASMC were implemented. The only difference between single-tank and double-tank systems is the engine volumetric efficiency maps. Thus, the same system dynamic, i.e, Eq.(6-12), is considered and identified for ASMC design.

Figure 6-20 shows the closed-loop step response of the system using the two controllers. The closed-loop system has an overshoot of 4% and 7% and steady state error of 2% and 3% in tracking the desired torque for ASMC and PI controllers, respectively. However, the settling time for this case is about 8 seconds (about 18 cycles) for both cases. The reason for the longer settling time compared to the single tank case is the LP tank pressure variation (Figure 6-21). As can be seen, the operating pressure range of LP tank changes as the throttle angle increases. A faster settling time could be expected at engine normal operating speed.

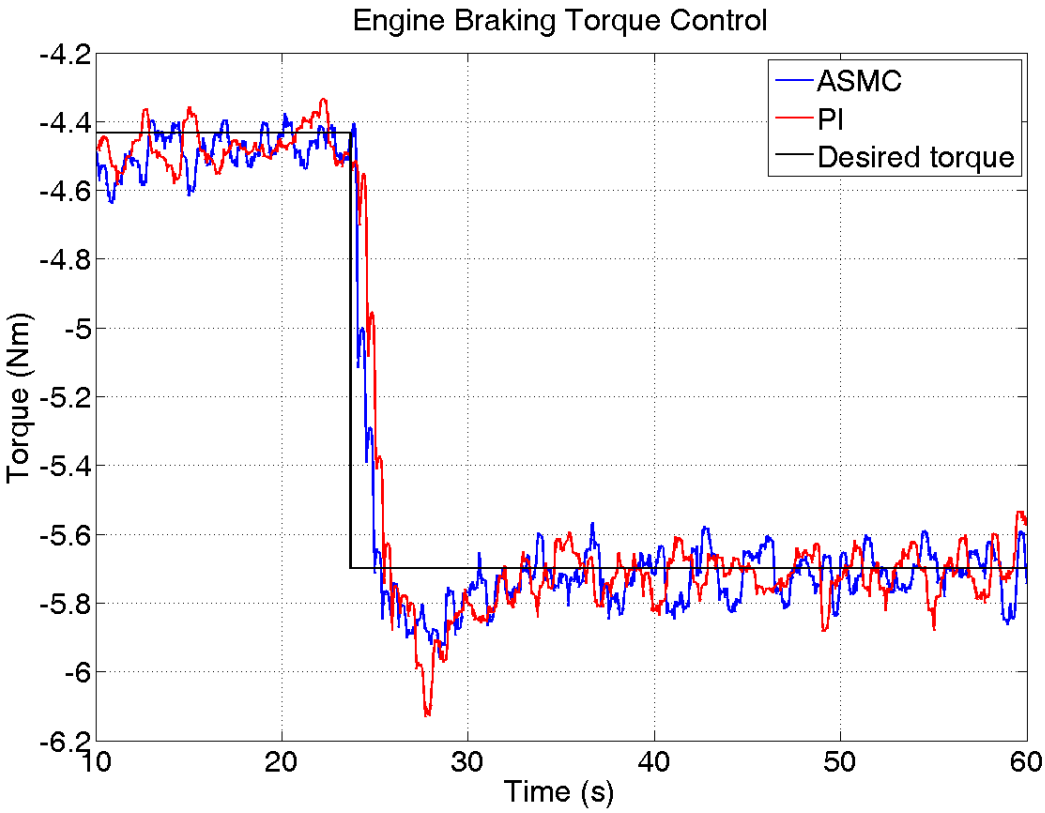

Figure 6-20: Experimental closed-loop tracking performance for ASMC and PI

Figure 6-22 shows the HP tank pressure for the step input in the engine torque. As can be seen, the flow rate to the HP tank increases as a higher torque is required.

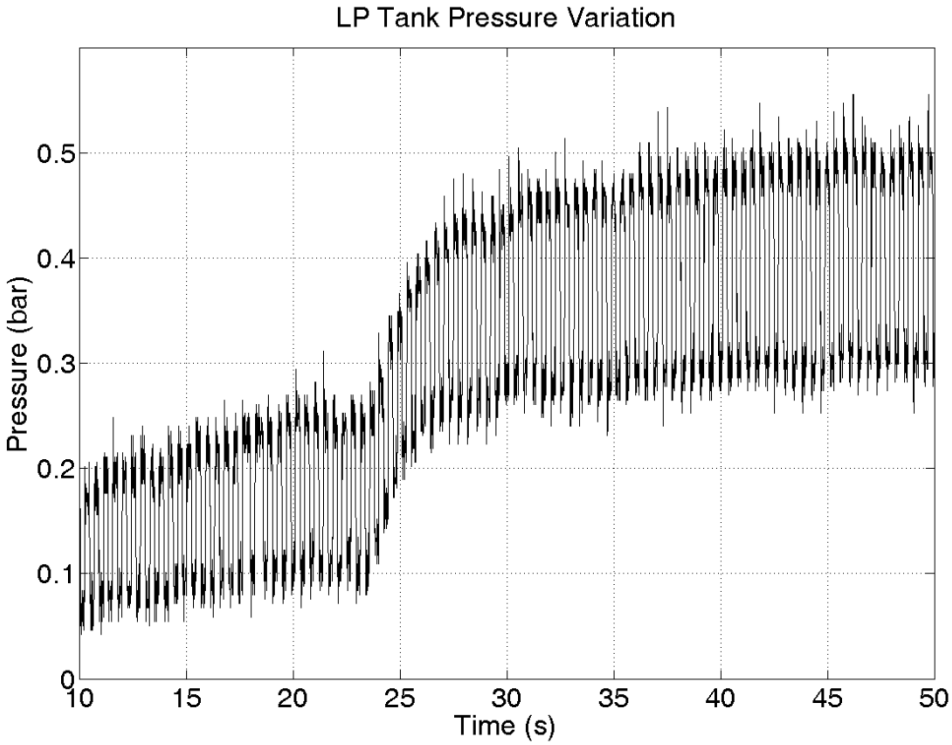

Figure 6-21: LP tank pressure

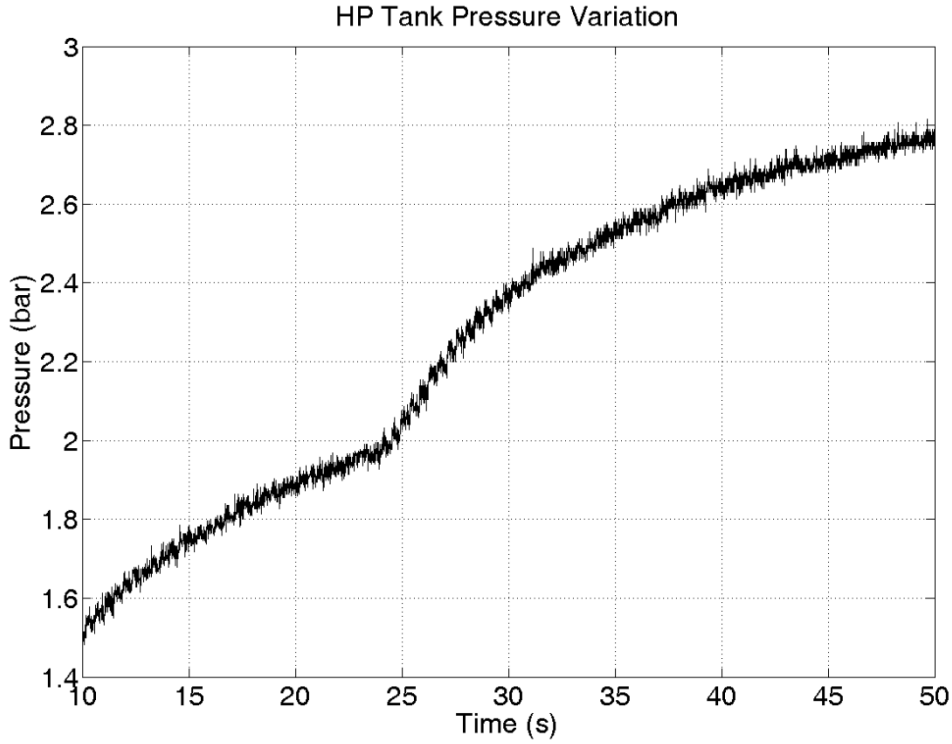

Figure 6-22: HP tank pressure for step input

6.6 Summary

In this chapter, a throttle-based regenerative braking torque control for air hybrid engines was developed. A new mean value model for the engine during braking was derived and an adaptive sliding mode was implemented for this particular application. The robustness and performance of the controller was investigated and compared using simulation and experiments with that of a high-gain PID and a model-based smooth sliding mode controller. The experimental results showed that a throttle-based controller could be used efficiently to regulate the regenerative braking torque in air hybrid engines.

Chapter 7
Drive Cycle Simulations

7.1 Background

An air hybrid vehicle uses two energy sources for propulsion: pressurized air and fossil fuel. The air hybrid vehicle powertrain also has different modes of operation while accelerating and braking. In practice, the performance of a hybrid engine is highly dependent on the power management strategy for mode-schedule planning. Therefore, a supervisory control or power management strategy should be designed to choose between the different modes of operation. There are many studies in the literature addressing power management strategies in hybrid vehicles. Typically, heuristic controllers are employed for power management in vehicles.

In this chapter, the optimal power management strategy using Dynamic Programming (DP) to minimize the vehicle fuel consumption for both the single and double-tank hybrid engines are studied and compared. This study is conducted for two standard drive cycles.

7.1.1 Dynamic Programming

Dynamic programming can be applied to the following discrete dynamic systems [11]:

$$x_{k+1} = F(x_k, \alpha_k), \qquad 7\text{-}1$$

where $x_k \in X = \{x^1,...,x^i\}$ and $\alpha_k \in \mathrm{A} = \{\alpha^1,...,\alpha^j\}$ are the system state and control action respectively (k is the step index) to find the optimal set of control actions that minimizes the cost function, $\Omega(x_0)$, subjected to both state and control action constraints. The solution to this DP problem is the set of control actions, $\mathrm{A} = \{\alpha_0, \alpha_1, \alpha_2,..., \alpha_{f-1}\}$, that minimizes the cost function such that:

$$\Omega_{optimum}(x_0) = \min_{A} \Omega(x_0). \qquad 7\text{-}2$$

The notion $\min_{A}$ is used to indicate the minimum of a function taken over all the possible values of the variable A. The cost function for the discrete dynamic system (7-1) is defined as [11]:

$$\Omega(x_0) = \pi_f(x_f) + \sum_{k=0}^{f-1} \pi_k(x_k, \alpha_k). \qquad 7\text{-}3$$

In the above equation, $\pi_f(x_f)$ is the cost associated with the final state and is usually set to impose the constraint on the state final value and $\pi_k(x_k, \alpha_k)$ is the cost of applying α_k at x_k. The DP method is applied backward in time, and is most useful for offline optimization where the final state of the system is known a priori. Figure 7-1, shows how the method can be applied to a system that is discretized both in space and time. The idea is to start from the final states and define the cost associated with each final state of the system. A high cost is assigned to those final states that are unlikely to occur or are constrained. Consequently, the associated cost to each of the final states is defined as:

$$\Omega(x_f^i) = \pi(x_f^i), \qquad 7\text{-}4$$

where x_f^i is the ith state at t_f. Once the cost associated with each final state is determined, the solution continues backward in time by calculating $\Omega(x_{f-1}^i)$, as follows:

$$\Omega_{optimum}(x_{f-1}^i) = \min_j \pi(x_{f-1}^i, \alpha_{f-1}^j) + \Omega_{optimum}(F(x_{f-1}^i, \alpha_{f-1}^j)). \qquad 7\text{-}5$$

Figure 7-1 shows the case where $\alpha_{f-1} \in \{\alpha^1, \alpha^2\}$, and the two control actions, α^1 and α^2 that can be applied to x_{f-1}^i at t_{f-1}, take the system to $x_f^i = F(x_{f-1}^i, \alpha_{f-1}^1)$ and $F(x_{f-1}^i, \alpha_{f-1}^2)$ at t_{f-1}. In this case, the optimum cost associated with x_{f-1}^i is expressed as:

$$\Omega_{optimum}(x_{f-1}^i) = \min(\pi(x_{f-1}^i, \alpha_{f-1}^1) + \Omega_{optimum}(x_f^i), \pi(x_{f-1}^i, \alpha_{f-1}^2) + \Omega_{optimum}(F(x_{f-1}^i, \alpha_{f-1}^2))) . \qquad 7\text{-}6$$

Since the space is discritized in space, $F(x_{f-1}^i, \alpha_{f-1}^2)$ is not associated with any state. Thus, $\Omega_{optimum}(F(x_{f-1}^i, u_{f-1}^2))$ should be calculated by interpolating $\Omega_{optimum}(x_f^{i-1})$ and $\Omega_{optimum}(x_f^{i-2})$.

This way, by the progress of the method backward in time, the minimum cost associated with each state is defined and finally, $\Omega_{optimum}(x_0)$, which is the optimum cost of going from x_0 to x_f, is determined.

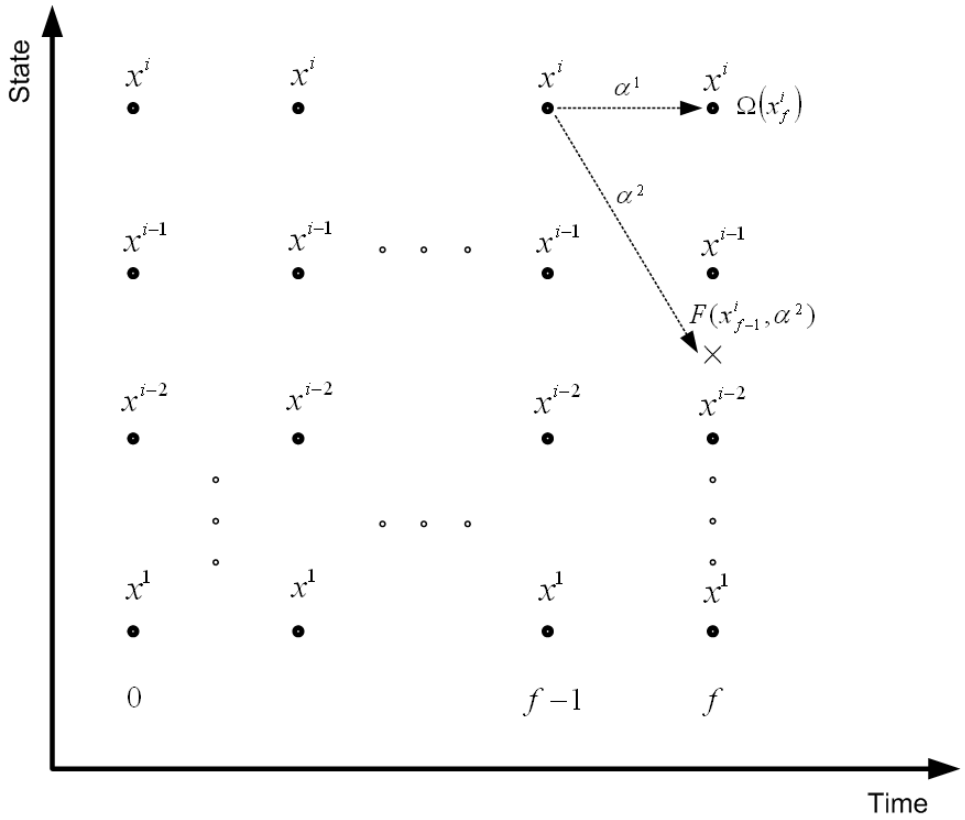

Figure 7-1: Dynamic programming

7.1.2 Application of Dynamic Programming

As mentioned earlier, DP is a numerical approach that can be applied to discrete dynamic systems to find the optimal control action that minimizes a chosen cost function. This method is specifically suitable for optimization problems with constraint both on the system states and control actions [11]. Thus, it is an attractive method for drive cycle optimization problems, since the drive cycle is known a priori. Researchers adopted this method for powertrain optimization problems in [24],[52], [53], and [54]. According to Guzzella [11] "dynamic programming is a useful tool as it can be used to provide an optimal performance benchmark". As a result, it can be useful for comparing the performances of the single-tank and double-tank regenerative systems in standard drive cycles.

7.2 Implementation of the Dynamic Programming

In this section, dynamic programming algorithm is applied to find the optimum set of control actions for the single-tank and double-tank air hybrid engines in standard drive cycles. For this particular application, the State of Charge (SoC) of the air tank is chosen as the system state. The SoC of the tank and time are discritized with the step sizes listed in Table 7-1.

Table 7-1: Parameters of dynamic programming algorithm

State variable	Tank pressure
State step size	0.1 [bar]
State range	1-25 [bar]
Stage variable	Time
Stage step size	0.25 [s]
Initial tank pressure	11 [bar]
Final tank pressure	>11 [bar]
Lowest allowed tank pressure	5 [bar]

For each state, there are four control actions: 1. engine off, 2. engine on, 3. air motor on and 4. regenerative braking on. Thus, $\mathrm{A}=\left\{\alpha^{1},\alpha^{2},\alpha^{3},\alpha^{4}\right\}$ is the set of control actions with four members and $X=\{1,1.1,1.2,...,24.9,25\}$ is the set of states. To determine $\pi\left(x_k^i,\alpha_k^j\right)$, which is the cost of applying $\alpha_k^j \in A$ to $x_k^i \in X$ at the time step k, and the discrete function F, a single-tank and double-tank air hybrid engine with the head configuration proposed in Chapter 5 are simulated in GT-Power and their operating maps at various operational modes are obtained. The specifications of the vehicle and the engine under study are listed in Table 7-2.

Table 7-2: Vehicle and engine specification

Vehicle mass	1800 [kg]
Engine displacement	2 [litre]
Final drive ratio	4.2
Tank volume	60 [l]
Drag coefficient	0.32
Tire radius	38 [cm]
Transmission ratio	1st : 3.3
	2nd : 1.96
	3rd : 0.97
	4th : 0.78

Figure 7-2 and Figure 7-3 show the single-tank and double-tank operating maps for the tank pressure of 1 to 25 [bar] and throttle angle of 0 to 90. As can be seen, the double-tank system has higher mass flow rate to the tank. This is mainly due to its higher volumetric efficiency. It also produces a higher braking torque range, because of the larger enclosed area on the P-V diagram (Figure 3-4). Figure 7-4 shows the air motor operating map. As can be seen, the required mass flow rate out of the tank increases by speed increase. The conventional mode operating map is also derived. The obtained operating maps are used to train three neural networks, $\Phi_{j=1,..,3}$, representing the fuel flow rate to the engine for the conventional, air flow rate to the tank for regenerative and air flow rate out of tank for air motor mode. The offline speed and torque profile of the vehicle in two standard drive cycles (i.e., FTP75 and UDDS) are also derived. At each instant of time and for each state of charge, the fuel or air mass flow rate is determined as follows:

$$\dot{m}_{\mathrm{j}} = \Phi_j\left(x_k^i, \alpha_k^j, T_k, \omega_k\right). \qquad 7\text{-}7$$

The obtained mass flow rate is used to determine the subsequent state, $x_{k+1} = F\left(x_k^i, \alpha_k^j\right)$, and also the cost associated with the control action, $\pi\left(x_k^i, \alpha_k^j\right)$. If the engine is on (control action '2'), the cost is equal to the fuel consumption and if the engine is off (control actions '1', '3'

and ‘4’), the cost is set to zero. However for each state, one or two control actions are feasible. For instance, when the required engine torque is positive, only control actions ‘2’ and ‘3’ are feasible. Thus, a high cost is assigned to the unfeasible control actions at each state. In addition, if the required braking or traction torque is out of the regenerative braking or air motor torque range at a particular state and time, the corresponding control action cost is set to a high cost.

The initial tank pressure is set at 11 [bar]. To determine the benefit of the regenerative system, the final tank pressure should be equal to or higher than its initial pressure. This introduces a constraint on the final state of the system. To impose this constraint, the cost associated with final tank pressures of less than 11 [bar] is set to a large cost. This way, those paths that end up with these states are not chosen as the minimum cost path. Also, the minimum allowable tank pressure is set at 5 [bar] for the intermediate states by assigning a large cost to the states with pressures less than 5 [bar] to ensure that the tank is not depleted in the drive cycle.

a) Single-tank

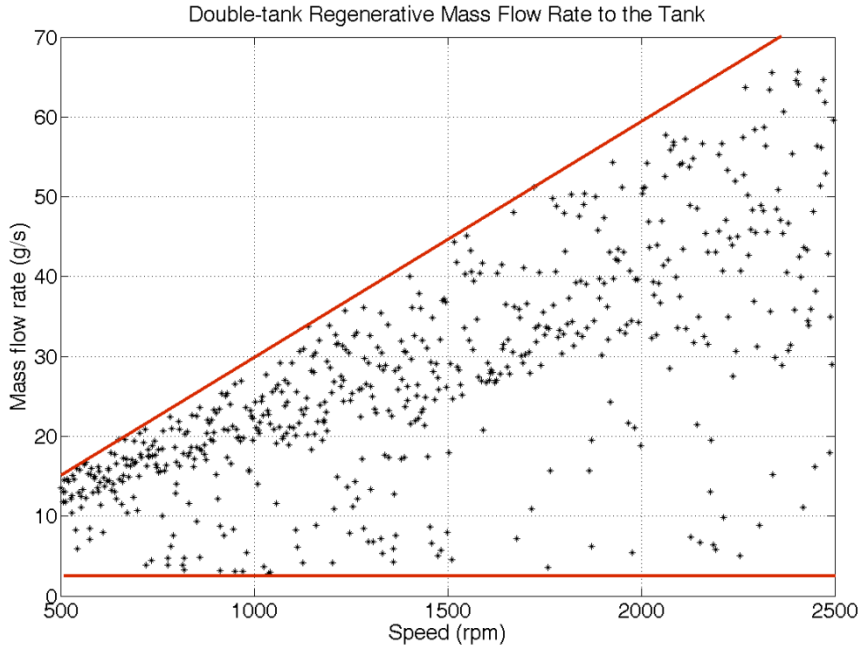

b) Double-tank

Figure 7-2: a) Single-tank and, b) double-tank flow rate to the tank

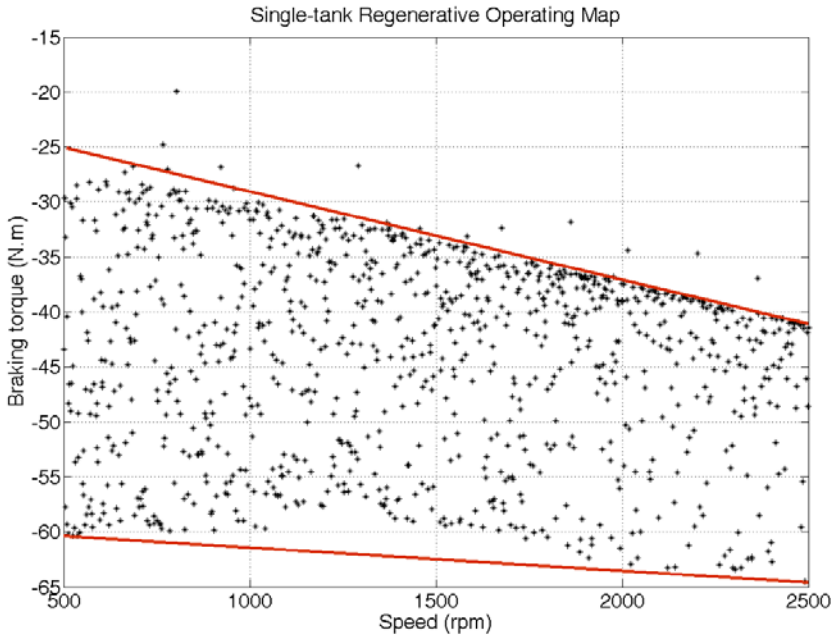

a) Single-tank

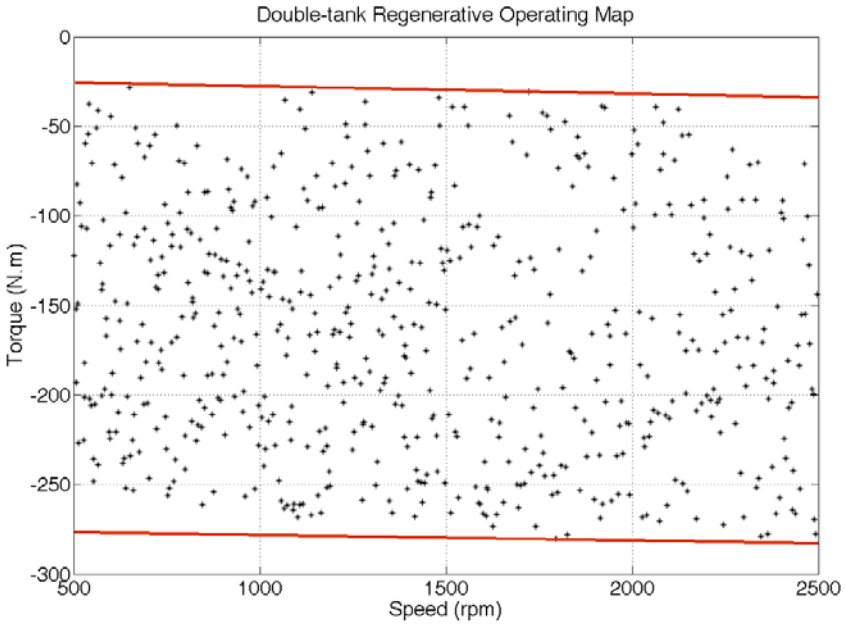

b) Double-tank

Figure 7-3: a) Single-tank and, b) double-tank braking torque

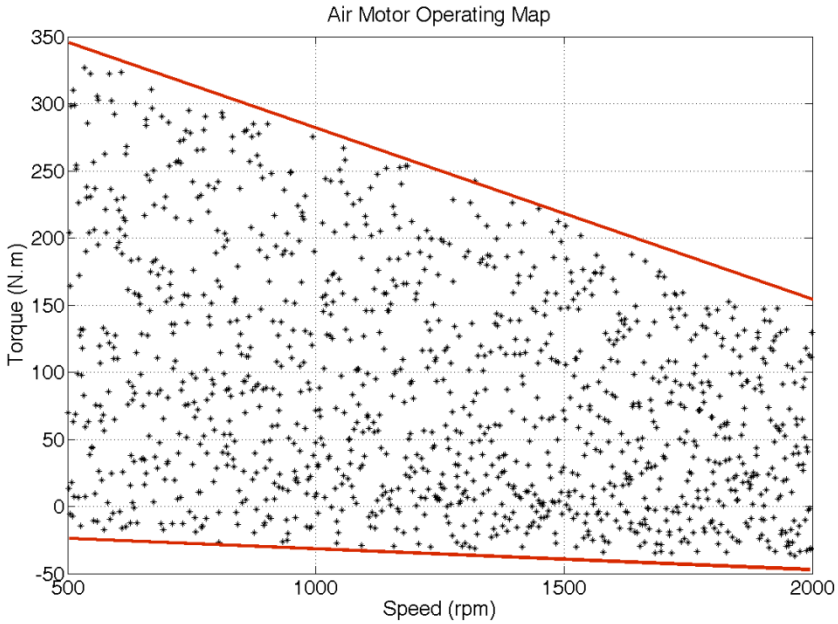

a) Engine torque

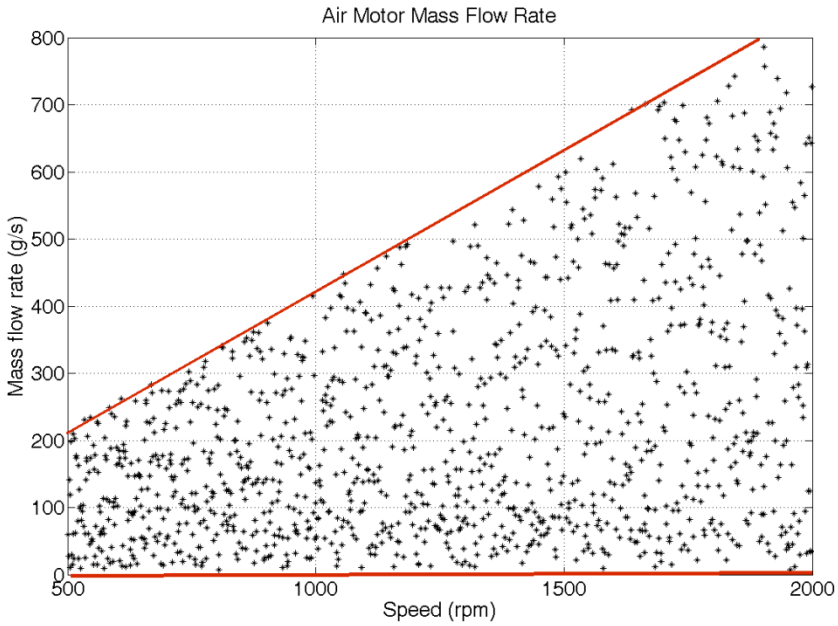

b) Mass flow rate out of tank

Figure 7-4: Air motor operating maps

7.2.1 UDDS Drive Cycle

Figure 7-5 shows the UDDS operating map in the braking phase and the operating range of the single-tank regenerative system. With reference to Figure 7-7, three different regions on the map can be recognized. The required braking torque range in region 'I' is lower than the single-tank regenerative torque lower bound. Thus, the vehicle's kinetic energy in region 'I' cannot be captured. However, the regenerative system is able to capture the braking energy in region 'II' where the required braking torque is in the range of the regenerative system. In region 'III', the regenerative system is only able to capture the kinetic energy of the vehicle, partially, since the required braking torque range exceeds its operating range. Thus, in addition to the regenerative system, the friction brakes should be also employed in region 'III'.

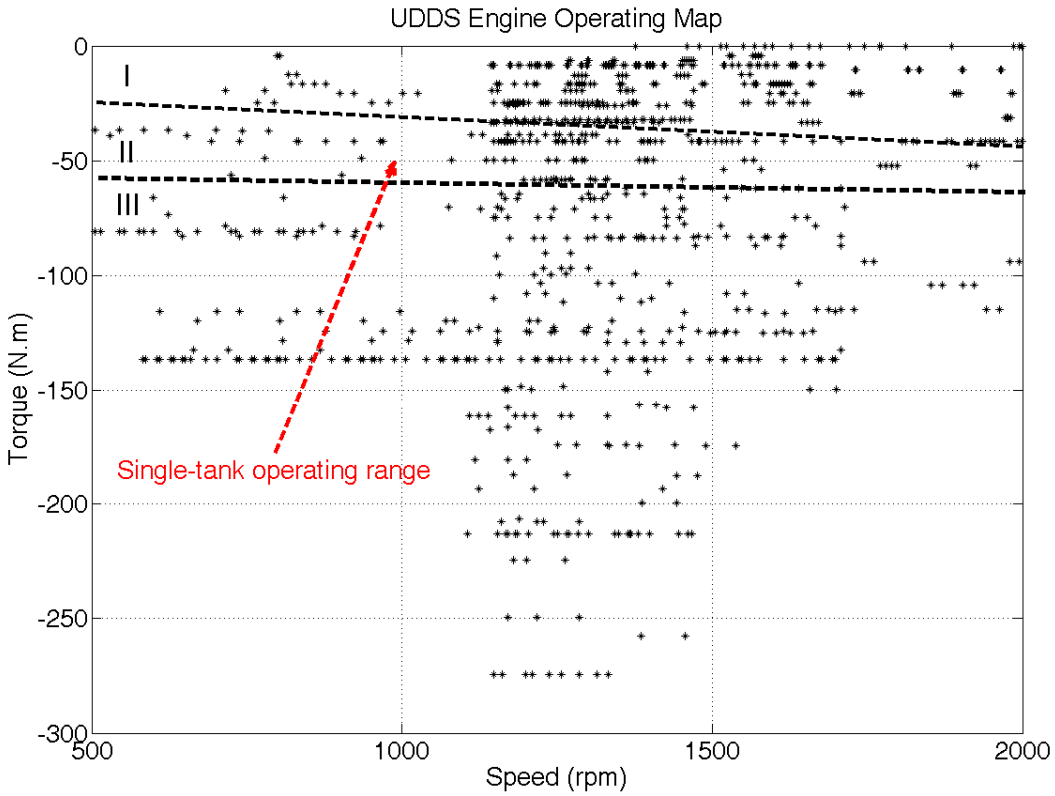

Figure 7-5: UDDS operating map and single-tank regenerative operating range

Figure 7-6 compares the UDDS operating map in the braking phase and the operating range of the double-tank regenerative system. Here, the regenerative system operating range

covers a larger area than that of the single-tank (region 'II' is larger). Thus, the regenerative system is capable of capturing a larger portion of the vehicle kinetic energy.

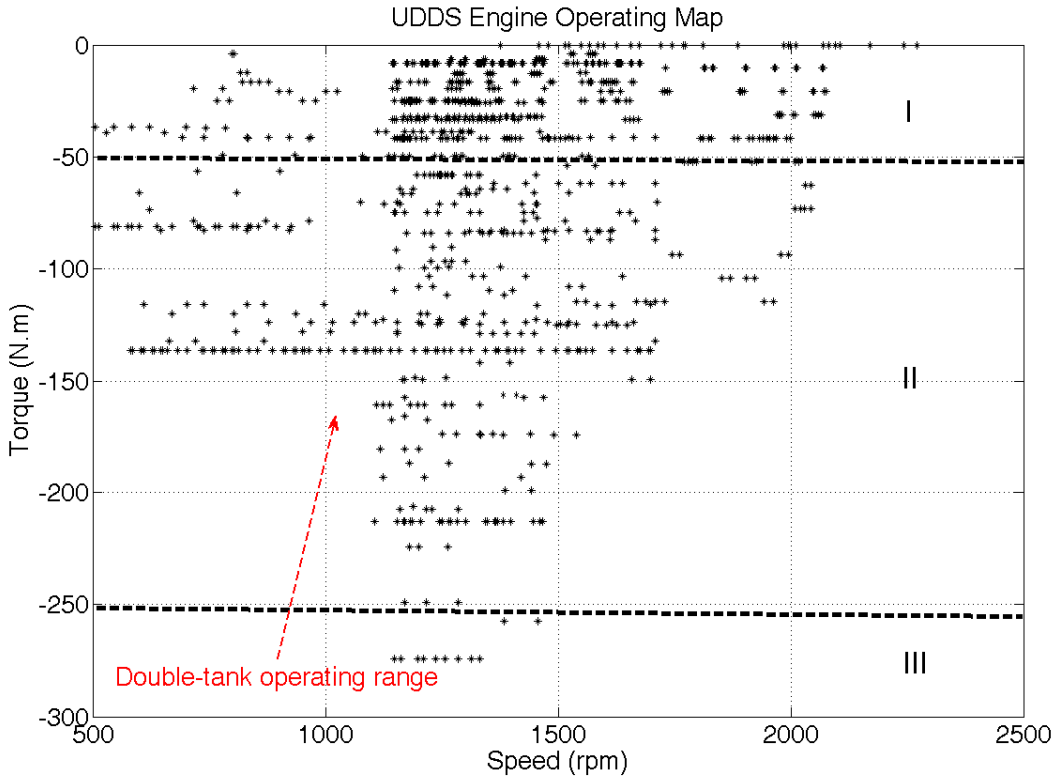

Figure 7-6: UDDS Operating map and double-tank regenerative operating range

Figure 7-7 depicts the SoC of the tank if the set of optimized control actions, obtained by the DP algorithm, is followed for both the single- and double-tank systems. As can be seen, employing the double-tank strategy, pressure fluctuates between 5 to 20[bar] while for the single-tank system, the tank pressure fluctuates between 9 to about 16.5 [bar]. The bigger range of fluctuations shows that the stored energy in the tank was used more frequently for the double-tank system. Thus, higher efficiency is expected for the double-tank air hybrid engine. The actual fuel consumption of both systems will be discussed later in this chapter.

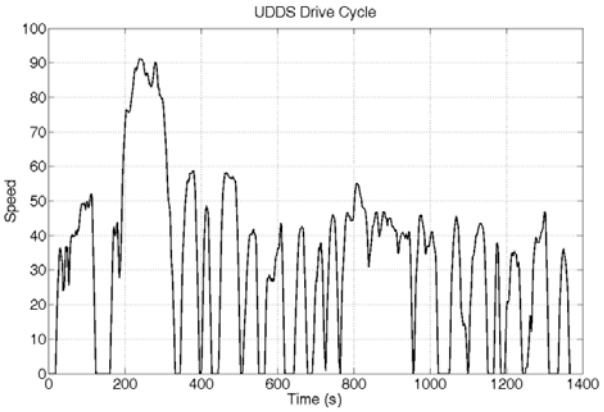

a) Drive cycle

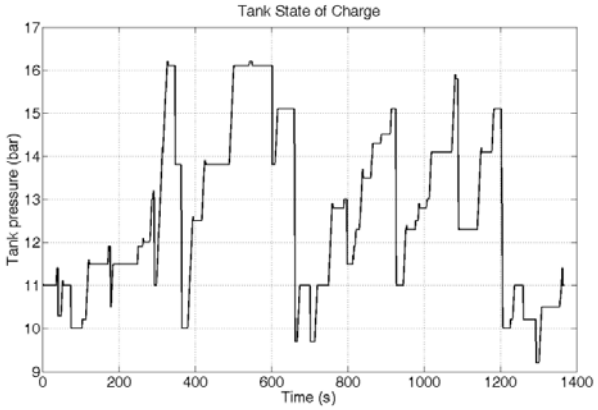

b) Single-tank SoC profile

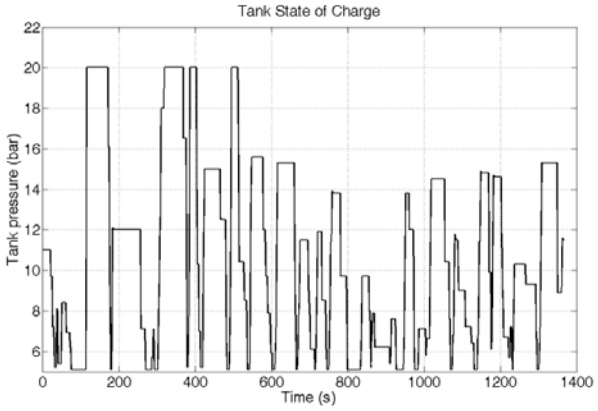

c) Double-tank SoC profile

Figure 7-7: UDDS cycle a) speed profile, b) single-tank SoC profile, c) double-tank SoC profile

7.2.2 FTP75 Drive Cycle

Figure 7-8 shows the FTP75 operating map in the braking phase and operating range of a single-tank regenerative system. Again, the same three operating regions can be recognized: region 'I' where the regenerative system cannot be employed, region 'II' where the regenerative system can be employed and region 'III' where the regenerative system can capture the vehicle energy partially. In contrast with the UDDS, region '2' covers a large portion of the map in the case of the FTP75 drive cycle.

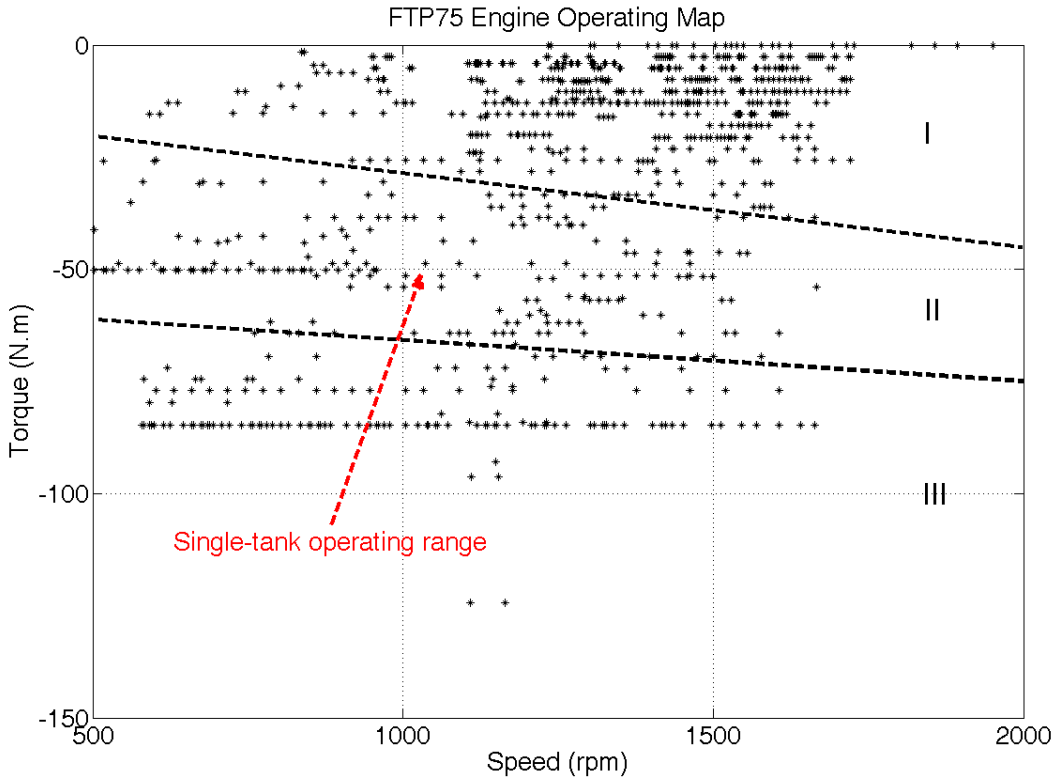

Figure 7-8: FT75 Operating map and single-tank regenerative operating range

Figure 7-9 compares the FTP75 operating map in the braking phase and the operating range of the double-tank regenerative system. As can be seen, region 'I' covers a large portion of the map. This means that the required braking torque range in this cycle is below the lower bound of the double-tank system. Thus, compared with the UDDS cycle, the double-tank regenerative system, if used alone, can capture a small portion of the vehicle

kinetic energy (however, the proposed air hybrid engine configuration can switch between single-tank and double-tank strategies).

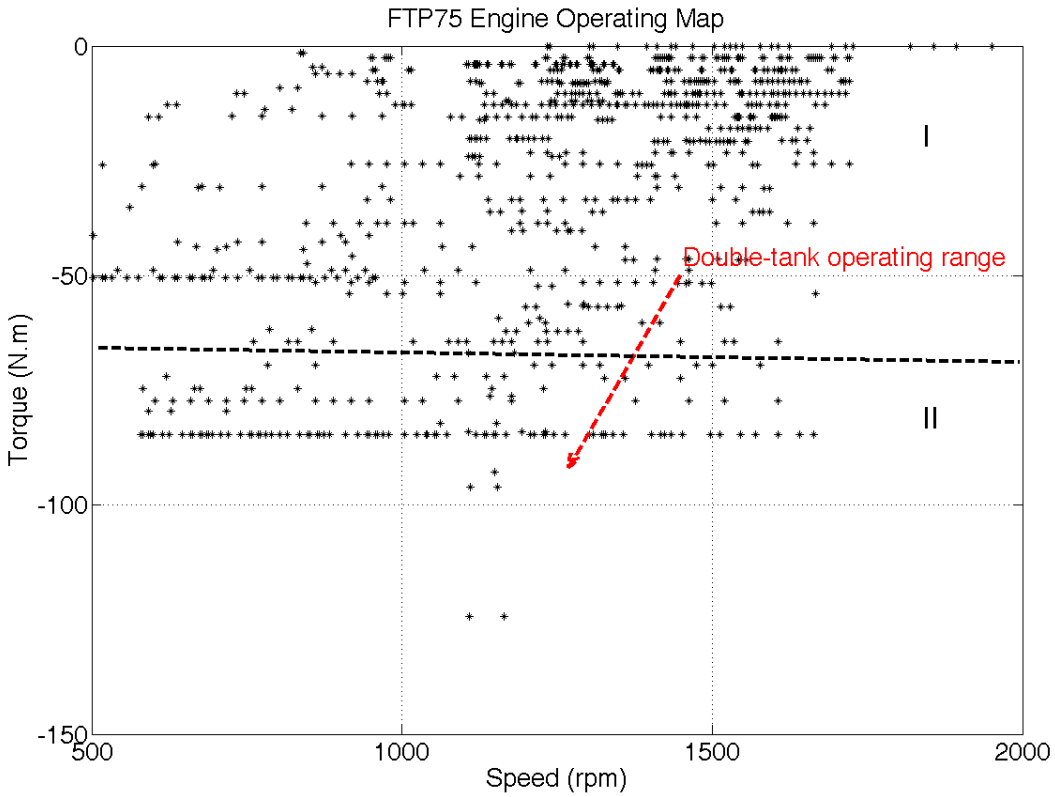

Figure 7-9: FT75 Operating map and double-tank regenerative operating range

The results of DP algorithm, shown in Figure 7-10, confirm this conclusion. The air tank is not charged when the optimal control action set is followed. Thus, compared with the single-tank, the double-tank regenerative system has a lower fuel economy in the FTP75 drive cycle. This conclusion is valid if only the double-tank system is used. With reference to Figure 5-8, the single-tank regenerative strategy is implemented with the double-tank regenerative system by deactivating the LP tank solenoid valve. In this way, the double-tank system can recover the vehicle kinetic energy even at low decelerating rates. The drive cycle fuel consumption of both systems, following the optimum mode scheduling is followed.

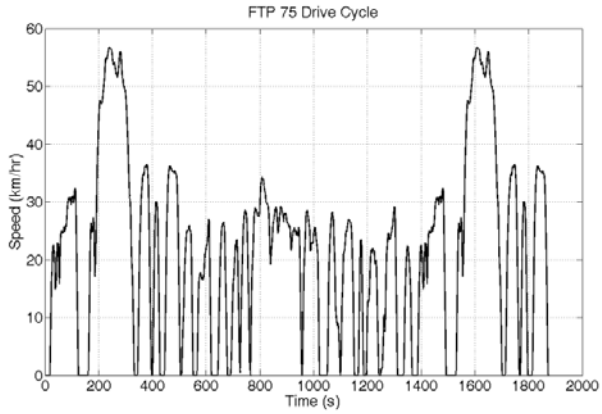

a) Drive cycle

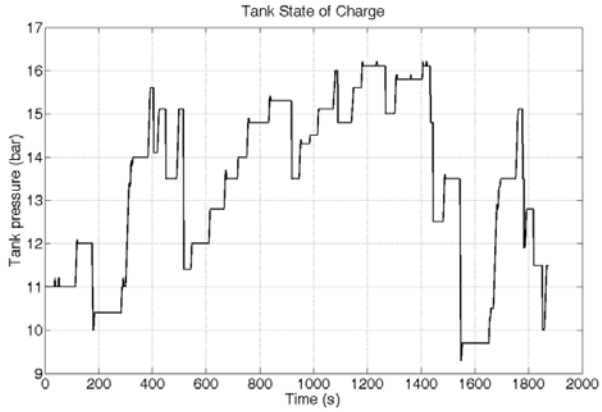

b) Single-tank SoC profile

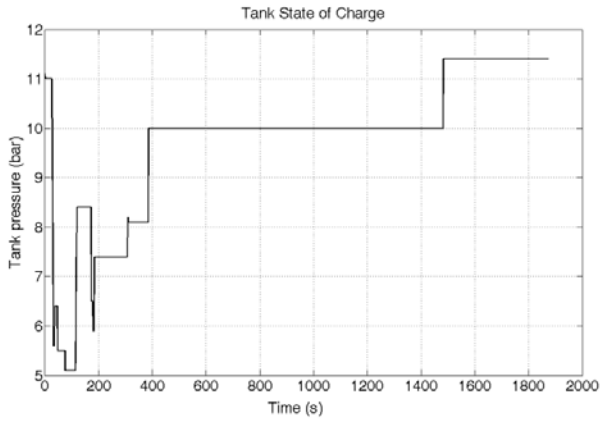

c) Double-tank SoC profile

Figure 7-10: FTP75 cycle a) speed profile, b) single-tank SoC profile, c) double-tank SoC profile

7.3 Optimum Fuel Consumption

In this stage, the sets of the optimized control actions for each configuration are fed into the vehicle model to define the vehicle fuel consumption. The engine fuel consumption for control actions '3' and '4' is zero. Control action '1' is activated only if it is followed by air motor mode (control action '2'). Table 7-3 summarizes the fuel economy for each configuration. By utilizing the single-tank regenerative strategy, the fuel consumption drops by 6% and 14% in the UUDS and FTP75 respectively, whereas, the double-tank strategy decreases the fuel consumption by 19% in the UDDS and 6% in the FTP75. Since the double-tank regenerative system, proposed in Chapter 5, is able to switch from the double-tank strategy to the single-tank strategy and vice versa, the capabilities of both systems can be used at the same time. Therefore, the double-tank method can decrease the fuel consumption at least by 19% in the UUDS and 14% in the FTP75 drive cycles.

Table 7-3: Fuel consumption in different cycles

	UDDS	% of improvement	FTP75	% of improvement
Conventional powertrain	9.1 (l/100 km)	0	10.1 (l/100 km)	0
Air hybrid/single-tank	8.57 (l/100 km)	6	8.7 (l/100 km)	14
Air hybrid/double-tank	7.35 (l/100 km)	19	9.5 (l/100 km)	6
Air hybrid/single & double-tank	7.35 (l/100 km)	19	8.7 (l/100 km)	14

7.4 Summary

In this chapter, the drive cycle efficiency of the single-tank and double-tank regenerative braking systems were compared. To create an equivalent basis for this comparison, the power management strategy for each structure was optimized by a dynamic programming optimization method. The results indicate that the double-tank compression strategy can contribute in recovering the vehicle kinetic energy for a high braking torque range (about 19% improvement), whereas the single-tank strategy contributes more for the low torque range (about 14% improvement). Thus, the double-tank air hybrid engine structure that can

implement both the single- and double-tank compression strategies can capture both low and high braking torque ranges.

Chapter 8
Conclusions and Future Work

8.1 Summary of Contributions

In this thesis a new air hybrid engine with higher efficiency and lower complexity was developed. It was shown in Chapter 3 that the storing capacity of a conventional, single-tank regenerative air hybrid system was limited. Thus, a compression strategy based on using two tanks was proposed to increase the energy storing capacity of the system during braking. The double-tank compression strategy increases the volumetric efficiency of the engine during braking, the system capacity in storing air mass, and the range of the braking torque compared with the single-tank compression method. Although the efficiency of regenerative braking system is dependent to the vehicle initial velocity, it was shown that the double-tank strategy could lead to 28% energy recovery, whereas the single-tank system captures only 14% of the vehicle initial kinetic energy in a single braking event The double-tank strategy was tested and compared experimentally with the single-tank regenerative system in Chapter 4. The experimental results confirmed the higher energy storing capacity of the double-tank system.

A switchable cam-based valvetrain was proposed for implementing the air hybrid engine in Chapter 5. Both single-tank and double-tank regenerative systems can be implemented by the proposed configuration. One of the advantages of the proposed system is that the regenerative braking torque can be controlled by the same electronic throttle used in the traction torque control. The feasibility and performance of the proposed cam-based valvetrain were shown through simulation and experiments.

The feasibility of engine braking torque control using the electronic throttle was shown in Chapter 6. Since the engine is a highly non-linear system, the regenerative braking mean value model was derived and an adaptive sliding mode controller was developed for this particular application.

In Chapter 7, drive cycle efficiency of single-tank and double-tank regenerative braking systems were compared. In order to create an equivalent basis for this comparison, the optimized power management strategy for each method was obtained using the dynamic programming. The results showed that the cam-based double-tank air hybrid engine can improve the fuel economy by 19% in UDDS and 14% in FTP75 drive cycles. A higher fuel economy could be expected if the air hybrid engine is run in supercharged mode and as a result, a down-sized engine is used (34% in MVEG-95 drive cycle [24])

8.2 Publications Resulting from This Thesis

Several publications and a patent have resulted from this research as follows:

1. Fazeli A., Zeinali M., Khajepour A., 'Application of Adaptive Sliding Mode Control Regenerative Braking Torque Control', IEEE/ASME Transactions on Mechatronics, DOI 10.1109/TMECH.2011.2129525.
2. Fazeli A., Khajepour A., Devaud C., 'A Novel Compression Strategy for Air Hybrid Engines', Journal of Applied Energy, 2011 doi:10.1016/j.apenergy.2011.03.008.
3. Fazeli A., Khajepour A., Devaud C., Pournazeri M., 'Regenerative Braking Torque Control of Air Hybrid Engines with Cam-Based Valvetrains', Int. Journal of Powertrains, 2010 (Accepted for publication).
4. Fazeli A., Khajepour A., Devaud C. and Pournazeri M., "A Novel Air Hybrid Engine Configuration Utilizing Cam-based Valvetrain", SAE World Congress & Exhibition 2011, paper# 2011-01-0871.
5. Fazeli A., Zeinali M., Khajepour A., Pournazeri M., "Air Hybrid Engine Torque Control Using Adaptive Sliding Mode Control", ASME International Mechanical Engineering Congress and Exposition IMECE2010, November 12-18, 2010, Vancouver, British Columbia, Canada, Paper# IMECE2010-38762.
6. Fazeli A., Khajepour A., Devaud C., Lashgarian N., "A New Air Hybrid Engine Using Throttle Control", SAE World Congress & Exhibition, Detroit, Michigan, USA, 2009, Paper# 2009-01-1319.

7. Khajepour A., Fazeli A., Devaud C. and Azad N., ‘Air compression method and apparatus’ PTC pending patent number: 090218-0028, 2010.

8.3 Suggestions for Future Work

In regards to the future work on air hybrid engines, the following directions are suggested:

1. Complete thermal analysis: Since the speed was low and engine was not fired in the available setup, the temperature increase during compression was not significant. At nominal engine temperature and speed ranges, the temperature rise due to the compression is an important factor and should be investigated.
2. Full implementation of the switchable cam-based valvetrain: The switchable valvetrain was not implemented using fixed valve timings in this thesis. A full implementation is needed to study different engine operational modes and switching between them at the nominal speed range of an engine.
3. Full implementation of the suggested air hybrid engine: Although the proposed double-tank strategy was proven to have higher efficiency and a simpler valvetrain, it needs to be implemented on a real engine.

Appendix A

Compressor Efficiency Definitions

There are several definitions for compressor efficiency which are widely used by compressor manufacturers and scientists. Figure A-1 shows the thermodynamics cycle of a reciprocating compressor.

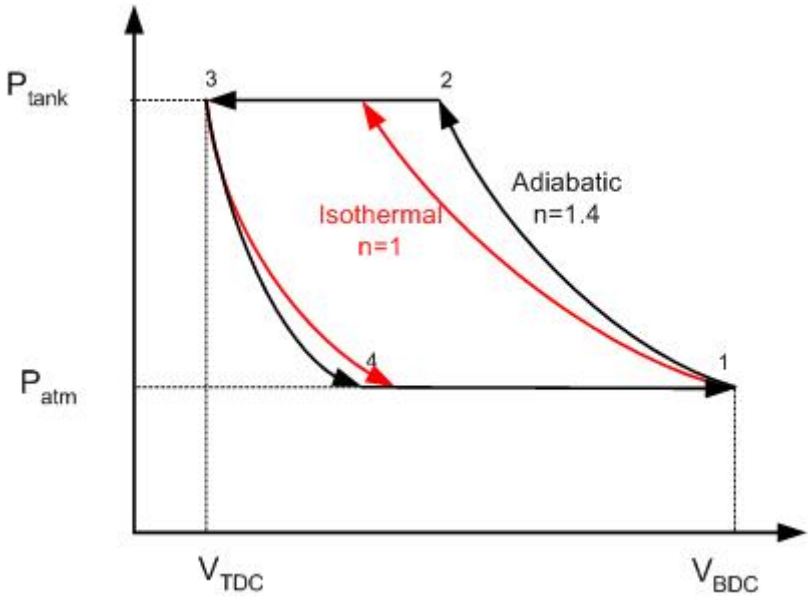

Figure A- 1: Compressor thermodynamic cycle [55]

The following equation describes the compression and expansion process of the cycle shown in Figure A.1.

$$PV^{\gamma} = \text{Constant}, \tag{A.1}$$

where $1 \le \gamma \le 1.4$. $\gamma = 1$ corresponds to isothermal compression process and is only valid when there is a substantial amount of heat transfer from the fluid to the cylinder wall. $\gamma = 1.4$ corresponds to adiabatic compression when no heat transfer occurs. An actual compression process is between isothermal and adiabatic processes. The theoretical work of the mentioned cycles can be found by integrating the pressure w.r.t. to the volume as:

$$W = \oint P(V)dV. \tag{A.2}$$

Theoretical power is also expressed by following relation:

$$\dot{W} = \frac{\omega_{compressor}}{2\pi} W. \tag{A.3}$$

Adiabatic power, $\dot{W}_{ad}$ and $\dot{W}_{iso}$ are the theoretical compressor power if all the expansions and compressions are assumed to be adiabatic or isothermal respectively. Actual power, $\dot{W}_{act}$, is also the measured power from an experimentally measured P-V curve. The experimentally measured power to run the compressor is shaft power, $\dot{W}_{shaft}$, and is expressed as follows:

$$\dot{W}_{shaft} = \dot{W}_{act} + \dot{W}_{friction} \tag{A.4}$$

Based on the mentioned cycle and definitions, the following definitions for efficiency can be derived:

Volumetric Efficiency:

The ratio of the volume actually pumped to the volume swept by the piston is volumetric efficiency and, according to Figure A.1, is defined by the following relation:

$$\eta_{vol} = \frac{V_1 - V_4}{V_1 - V_3} \tag{A.5}$$

The volumetric efficiency of a compressor is always less than one because of trapped gas in the clearance volume, the imperfect nature of the valves and wall friction [56].

Adiabatic Efficiency:

Adiabatic efficiency is the ratio of adiabatic power to the actual power and is defined as follows:

$$\eta_{adiabatic} = \frac{\dot{W}_{ad}}{\dot{W}_{act}} \tag{A.6}$$

Isothermal Efficiency:

Isothermal efficiency is the ratio of isothermal power to the actual power and is defined as follows:

$$\eta_{iso} = \frac{\dot{W}_{iso}}{\dot{W}_{act}} \tag{A.7}$$

Mechanical Efficiency:

Mechanical efficiency is the ratio of actual power to the shaft power and is defined as follows:

$$\eta_{mech} = \frac{\dot{W}_{act}}{\dot{W}_{shaft}} \tag{A.8}$$

Appendix B

Regenerative Braking Thermodynamic Cycle

Figure B.1 shows the ideal thermodynamic cycle of a regenerative braking system. In this section, we show that a cycle in which the charging valve opens exactly when the cylinder pressure equals the tank pressure has the maximum regenerative efficiency.

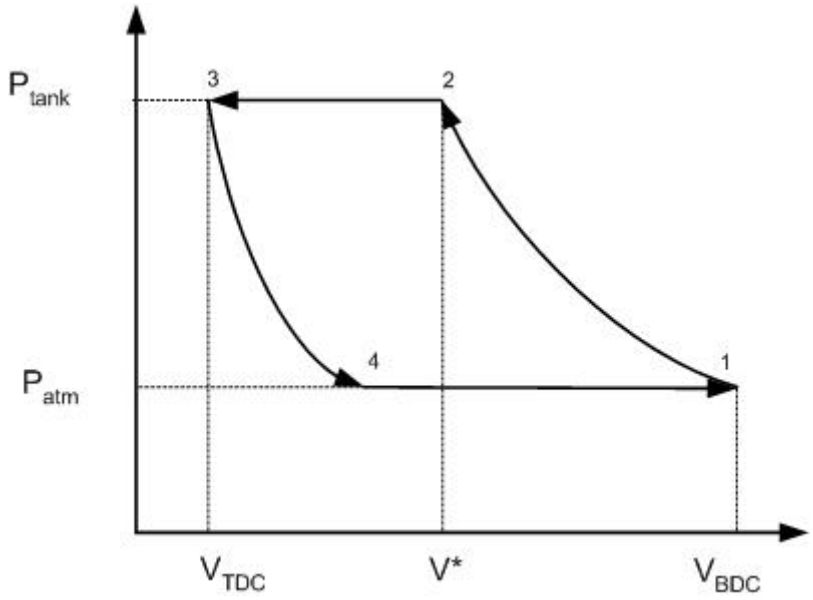

Figure B- 1: Regenerative ideal thermodynamic cycle

Suppose that point ‘1’ is precisely at BDC, ‘3’ is at TDC, ‘4’ is when the cylinder pressure equals atmospheric pressure, and point ‘2’ is variable. The amount of work performed on the gas from ‘1’ to ‘2’ is expressed as follows:

$$W_{1-2} = \frac{P_2 V^* - P_{atm} V_{cyl}}{\gamma - 1}\ , \tag{B.1}$$

where,

$$P_2 = P_{atm}\left(\frac{V_{cyl}}{V^*}\right)^{\gamma}. \tag{B.2}$$

Gas temperature at ‘2’ is:

$$\upsilon_2 = \upsilon_{atm}\left(\frac{V_{cyl}}{V^*}\right)^{\gamma-1} \quad . \tag{B.3}$$

Work between ‘2’ and ‘3’ is expressed by:

$$W_{2-3} = \frac{P_3\left(\frac{V_{cyl}}{C_r} + V_{\text{tank}}\right) - P_2^* V^*}{\gamma - 1} \, , \tag{B.4}$$

where,

$$P_2^* = \frac{V^* P_2 + V_{\text{tank}} P_{\text{tank}}}{V^* + V_{\text{tank}}} , \tag{B.5}$$

and,

$$P_3 = P_2^*\left(\frac{V_{\text{tank}} + V^*}{V_{\text{tank}} + \frac{V_{cyl}}{C_r}}\right)^{\gamma} \quad . \tag{B.6}$$

Temperature at point ‘3’ is:

$$\upsilon_3 = \upsilon_2^*\left(\frac{V_{\text{tank}} + V^*}{V_{\text{tank}} + \frac{V_{cyl}}{C_r}}\right)^{\gamma-1} \quad , \tag{B.7}$$

where, assuming ideal mixing of gases we have:

$$\upsilon_2^* = P_2^*\left(V_{\text{tank}} + V^*\right)\left(\frac{P_2 V^*}{\upsilon_2} + \frac{P_{\text{tank}} V_{\text{tank}}}{\upsilon_{\text{tank}}}\right)^{-1} \quad . \tag{B.8}$$

Work between ‘3’ and ‘4’ is defined by:

$$W_{3-4} = \frac{P_{atm} V_4 - P_3 \frac{V_{cyl}}{C_r}}{\gamma - 1} \, , \tag{B.9}$$

where,

$$V_4 = \frac{V_{cyl}}{C_r}\left(\frac{P_3}{P_{atm}}\right)^{\frac{1}{\gamma}} . \tag{B.10}$$

Work between '4' and '1' is also defined by:

$$W_{4-1} = P_{atm}\left(V_4 - V_1\right). \tag{B.11}$$

The total work of the cycle can be defined by:

$$W_{tot} = W_{1-2} + W_{2-3} + W_{3-4} + W_{1-4} . \tag{B.12}$$

The amount of mass stored in the tank is:

$$m_{induced} = \frac{1}{R}\left(\frac{P_{atm}V_{cyl}}{\upsilon_{atm}} - \frac{P_3\frac{V_{cyl}}{C_r}}{\upsilon_3}\right)M_{air} . \tag{B.13}$$

Now, in order to maximize the cycle efficiency, the following equation should be solved:

$$\frac{dm_{induced}}{dW_{tot}} = 0 . \tag{B.14}$$

Using MAPLE, the solution of the above equation with respect to V^* is found to be:

$$V^* = V_{cyl}\left(\frac{P_{atm}}{P_{\tan k}}\right)^{\frac{1}{\gamma}} . \tag{B.15}$$

The result shows that in order to have maximum efficiency of a regenerative cycle, the charging valve should open when the cylinder pressure equals the tank pressure.

Appendix C

LP tank capacity

In this section, the maximum pressure of the LP tank when both of the tanks are full (Eq.(3-15)) and no more energy can be stored by the double-tank system is derived. We first assume that HP and LP tanks are full. Thus, the HP tank is not charged, as shown in the related thermodynamic cycle (Figure C.1). LP supercharges the engine when the piston is at BDC, and is charged when the piston is at TDC. Although LP pressure varies throughout the cycle, its final pressure equals its initial pressure because both the LP and HP are assumed to be saturated.

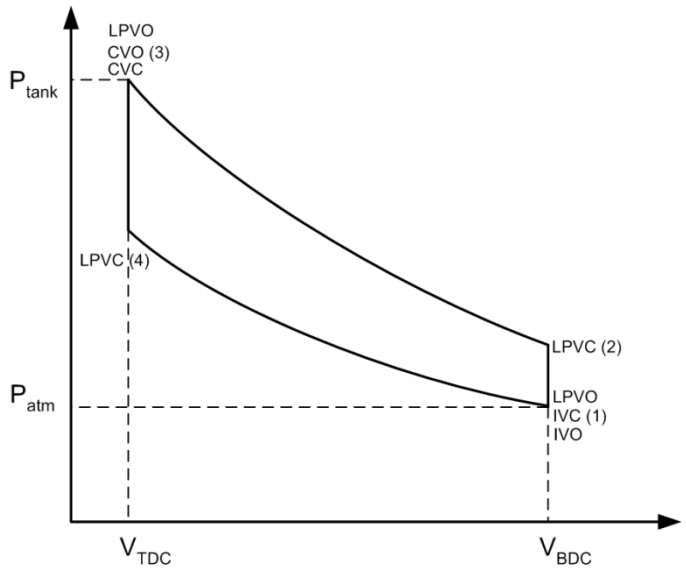

Figure C.1: Double-tank compression thermodynamic cycle when both of the tanks are full

With reference to Figure C.1, cylinder pressure at point ‘2’ where the LP charging valve is closed, considering ideal gas exchange, is:

$$P_2 = \frac{P_{atm}V_{cyl} + P_{LP}V_{LP}}{V_{cyl} + V_{LP}}. \tag{C.1}$$

Since the LP tank should be cooled down, its initial temperature is assumed to be equal to the atmospheric temperature, $\upsilon_2 = \upsilon_{atm}$. Thus, the cylinder pressure and temperature at point '3' assuming no heat transfer from the cylinder are:

$$P_3 = \frac{P_{atm}V_{cyl} + P_{LP}V_{LP}}{V_{cyl} + V_{LP}}\left(C_r\right)^{\gamma}, \tag{C.2}$$

$$\upsilon_3 = \upsilon_{atm}\left(C_r\right)^{\gamma-1}. \tag{C.3}$$

Since the HP tank is already full, there is no flow exchange between the cylinder and the tank. LP valve opens at TDC and the pressure of the LP tank after the ideal flow exchange between the tank and the cylinder is:

$$P_4 = \frac{\frac{P_{atm}V_{cyl} + P_{LP}V_{LP}}{V_{cyl} + V_{LP}}\left(C_r\right)^{\gamma}\frac{V_{cyl}}{C_r} + \frac{P_{atm}V_{cyl} + P_{LP}V_{LP}}{V_{cyl} + V_{LP}}V_{LP}}{V_{lp} + \frac{V_{cyl}}{C_r}}. \tag{C.4}$$

The LP tank temperature after closing the charging valve is:

$$\upsilon_4 = \frac{\left(\frac{\frac{P_{atm}V_{cyl} + P_{LP}V_{LP}}{V_{cyl} + V_{LP}}\left(C_r\right)^{\gamma}\frac{V_{cyl}}{C_r} + \frac{P_{atm}V_{cyl} + P_{LP}V_{LP}}{V_{cyl} + V_{LP}}V_{LP}}{V_{lp} + \frac{V_{cyl}}{C_r}}\right)\left(\frac{V_{cyl}}{C_r} + V_{LP}\right)}{\frac{P_{atm}V_{cyl} + P_{LP}V_{LP}}{V_{cyl} + V_{LP}}\frac{V_{LP}}{\upsilon_{atm}} + \frac{\frac{P_{atm}V_{cyl} + P_{LP}V_{LP}}{V_{cyl} + V_{LP}}\left(C_r\right)^{\gamma}\frac{V_{cyl}}{C_r}}{\upsilon_{atm}\left(C_r\right)^{\gamma-1}}}. \tag{C.5}$$

Since LP and HP tanks are already saturated, the LP tank pressure should be equal to its initial pressure after its temperature reaches the environment temperature (i.e. no change in the LP tank air mass occurs in a cycle). Thus,

$$P_{LP} = \frac{P_4}{\upsilon_4}\upsilon_{atm} = \frac{\dfrac{\dfrac{P_{atm}V_{cyl}+P_{LP}V_{LP}}{V_{cyl}+V_{LP}}\left(C_r\right)^{\gamma}\dfrac{V_{cyl}}{C_r}+\dfrac{P_{atm}V_{cyl}+P_{LP}V_{LP}}{V_{cyl}+V_{LP}}V_{LP}}{V_{lp}+\dfrac{V_{cyl}}{C_r}}}{\left(\dfrac{\dfrac{P_{atm}V_{cyl}+P_{LP}V_{LP}}{V_{cyl}+V_{LP}}\left(C_r\right)^{\gamma}\dfrac{V_{cyl}}{C_r}+\dfrac{P_{atm}V_{cyl}+P_{LP}V_{LP}}{V_{cyl}+V_{LP}}V_{LP}}{V_{lp}+\dfrac{V_{cyl}}{C_r}}\right)\left(\dfrac{V_{cyl}}{C_r}+V_{LP}\right)}{\dfrac{P_{atm}V_{cyl}+P_{LP}V_{LP}}{V_{cyl}+V_{LP}}\dfrac{V_{LP}}{\upsilon_{atm}}+\dfrac{\dfrac{P_{atm}V_{cyl}+P_{LP}V_{LP}}{V_{cyl}+V_{LP}}\left(C_r\right)^{\gamma}\dfrac{V_{cyl}}{C_r}}{\upsilon_{atm}\left(C_r\right)^{\gamma-1}}}}\upsilon_{atm}, \tag{C.6}$$

and,

$$P_{LP} = \frac{\dfrac{1}{V_{LP}+\dfrac{V_{cyl}}{C_r}}}{\dfrac{1}{\dfrac{P_{atm}V_{cyl}+P_{LP}V_{LP}}{V_{cyl}+V_{LP}}\left(\dfrac{V_{LP}}{\upsilon_{atm}}+\dfrac{V_{cyl}}{\upsilon_{atm}}\right)}}\upsilon_{atm} = \frac{P_{atm}V_{cyl}+P_{LP}V_{LP}}{V_{LP}+\dfrac{V_{cyl}}{C_r}}. \tag{C.7}$$

Now if we solve the above equation for P_{LP}, we will have:

$$P_{LP} = C_r P_{atm}. \tag{C.8}$$

Thus, when both of the tanks are full, the pressure in the LP tank is $P_{LP} = C_r P_{atm}$ if the LP tank temperature is kept at the environment temperature.

Appendix D

Multi-tank Compression

It is assumed that there are n_s storage tanks (the last one is the main storage tank) with an initial pressure of P_i. These tanks are filled using the same procedure presented in Section 3.4.2. This means that the charging starts by feeding the cylinder at atmospheric pressure, then the charging valves of each storage tank other than for the last one (the main tank) successively opens and closes (Figure D-1). Then, the piston moves up to TDC and compresses the air adiabatically. The charging valves of all the tanks open and close reversely, one by one, from the main storage to the first storage (Figure D-2).

Suppose $\chi_k = \dfrac{V_k}{V_{cyl} + V_k}$ and $\beta_k = \dfrac{V_k}{\dfrac{V_{cyl}}{C_r} + V_k}$ where V_{cyl} is cylinder volume and V_k is kth storage volume. The cylinder pressure, after feeding the cylinder with kth Storage, P_{cyl}^k, can be calculated using the following relation:

$$P_{cyl}^k = P_{atm}\prod_{i=1}^{k}(1-\chi_i) + \sum_{i=1}^{k}\chi_i P_i \prod_{j=i+1}^{k}(1-\chi_j). \qquad \text{(D.1)}$$

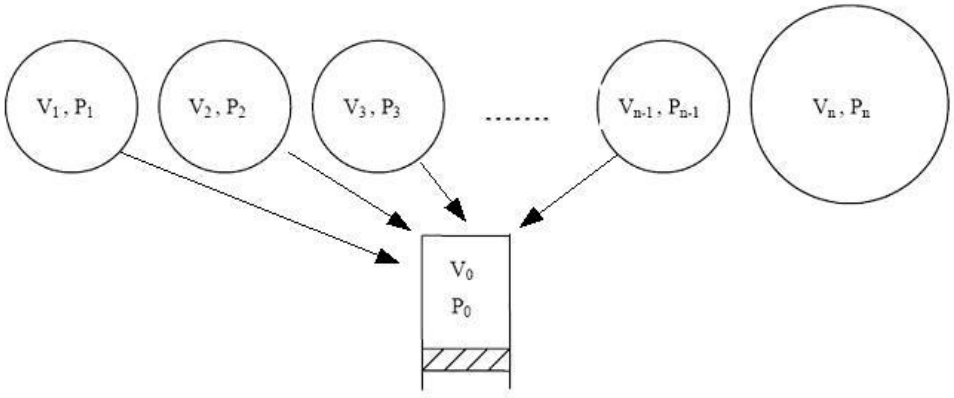

Figure D-1: Charging the cylinder

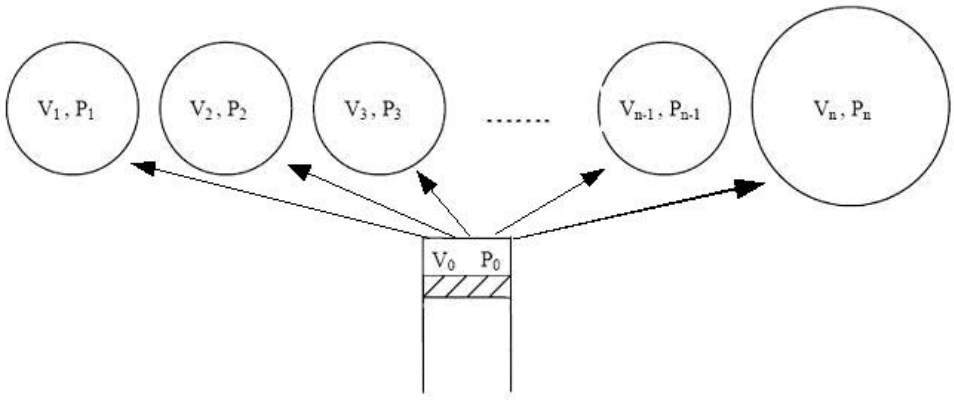

Figure D-2: Charging the storages

The cylinder pressure at the end of feeding the cylinder by $n_s - 1$ storage tanks is:

$$P_{cyl}^{n_s-1} = P_{atm}\prod_{i=1}^{n_s-1}(1-\chi_i) + \sum_{i=1}^{n_s}\chi_i P_i \prod_{j=i+1}^{n_s-1}(1-\chi_j). \tag{D-2}$$

The piston moves up to the TDC. The cylinder pressure after compression is:

$$P_{cyl} = \left[P_{atm}\prod_{i=1}^{n_s-1}(1-\chi_i) + \sum_{i=1}^{n_s}\chi_i P_i \prod_{j=i+1}^{n_s-1}(1-\chi_j)\right] C_r^{\gamma}. \tag{D-3}$$

Now the charging valve of the main storage opens. The pressure, after feeding the main storage can be calculated by:

$$P_{cyl} = (1-\beta_n)\left[P_{atm}\prod_{i=1}^{n_s-1}(1-\chi_i) + \sum_{i=1}^{n}\chi_i P_i \prod_{j=i+1}^{n_s-1}(1-\chi_j)\right] C_r^{\gamma} + \beta_n P_n. \tag{D-4}$$

The charging valves of the other storage tanks open and close. The cylinder pressure after feeding k^{th} storage is:

$$P_{cyl}^{k} = \left[\prod_{i=k}^{n_s}(1-\beta_n)\right]\left[P_{atm}\prod_{i=1}^{n_s-1}(1-\chi_i) + \sum_{i=1}^{n_s}\chi_i P_i \prod_{j=i+1}^{n_s-1}(1-\chi_j)\right] C_r^{\gamma} + \sum_{L=k}^{n_s}\beta_L P_L \prod_{j=k}^{L-1}(1-\beta_j). \tag{D-5}$$

Now the performance of regenerative braking using different numbers of air tanks is compared. Figure D-2 shows the maximum pressure in the main storage tank of a 1400 kg

vehicle decelerates from different initial velocities for different numbers of tanks. The storage specifications are given in Table D-1.

Table D-1: Simulation parameters

Storages initial pressure	1 [bar]
Main Storage Temperature	750 [K]
Small Storages Temperature	298 [K]
Main Storage Volume	30 [L]
Small Storages Volume	2 [L]

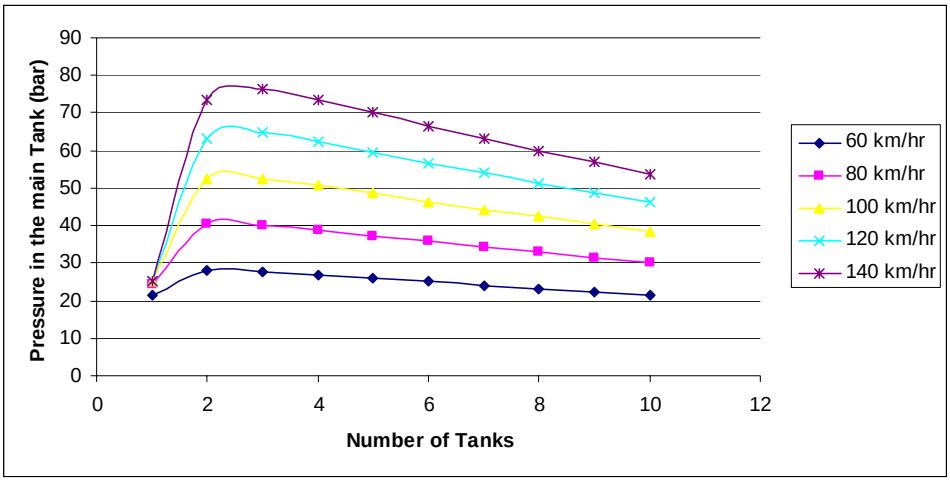

Figure D-2: Maximum pressure in the main tank

As shown in Figure D-2, the maximum pressure is achieved mostly when a two-storage tank system is used. As can be seen, using the two-storage system produces the maximum efficiency regardless of initial speed. Thus, it can be concluded that using two-storage system can improve regenerative braking efficiency and its performance, and that there is no need to consider more than two tanks.

Appendix E
Simulation Parameters

Simulation parameters used in theoretical modeling of Chapter 3 are presented in detail in this section. Table E.1 shows the used parameters.

Table E- 1: Simulation parameters

Vehicle mass	1800/4 kg
Initial velocity	80 km/hr
Final velocity	0 km/hr
Engine displacement	450 cc
Compression ratio	8.5
HP tank volume	10 l
LP tank volume	1 l
Tire radius	0.3 m
Final drive ratio	3.94
Valve discharge coefficient	0.9
Valve diameter	0.04 m
Low pressure tank heat transfer	10 J/K
High pressure tank heat transfer	5 J/K

Appendix F

Voltage to Current Converter Drive

In this section the performance of smooth SMC to use for engine torque control purposes is studied in more details. Figure F.1 shows the performance of smooth SMC with different boundary layer thickness in simulation. As can be seen, performance of a SMC with smoothing function (boundary layer) is highly dependent on the thickness of the boundary layer. So if we change the standard control signal to the following control signal:

$$\theta = A^{-1}\left(g_1^{-1}\left(-g_2 + \dot{T}_d - \lambda e - Ksat(S/\varepsilon)\right)\right), \tag{F.1}$$

Performance of the closed-loop system varies significantly based on the layer thickness, as can be seen in Figure F.1.

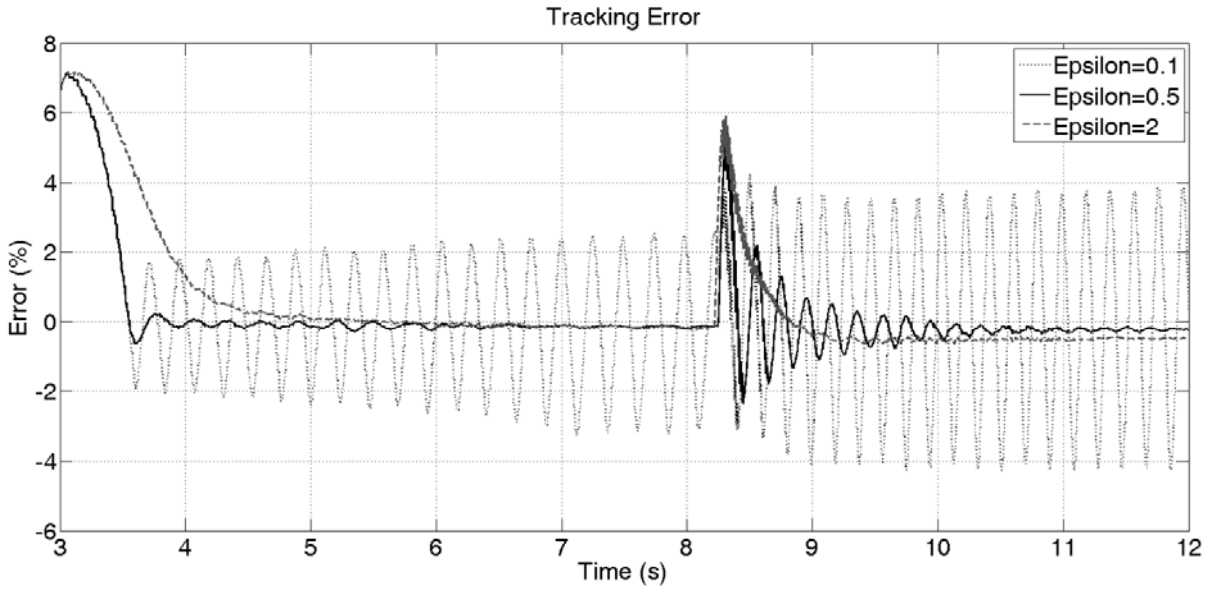

Figure F.1: Smooth SMC for different boundary thickness

If the thickness is small ($\varepsilon = 0.1$), the controller acts similar to the standard SMC and chattering cannot be eliminated. Although choosing a large thickness ($\varepsilon = 2$) eliminates chattering, it deteriorates the controller tracking performance. This is what is called "tracking to within a guaranteed precision rather than perfect tracking"[49]. According to Slotin and Li[49]: "SMC with a smoothing function (boundary layer) needs a tune up so as to achieve a

trade-off between tracking precision and robustness to unmodeled dynamics. It can be shown that the so-called chattering can be removed, as long as high-frequency unmodeled dynamics are not excited". Furthermore, due to the presence of uncertainties, there is no systematic approach to find the boundary layer thickness, and it is completely based on trial and error method. However, application of the recently proposed adaptive sliding model controller eliminates the chattering systematically without deteriorating the robustness of the SMC method.

Using a SMC with boundary layer always introduces a tradeoff between the performance and control discontinuity. Although for a given system, an optimum value for the thickness can be obtained ($\varepsilon = 0.5$ for our system without uncertainties), the closed-loop system might be not robust to the plant uncertainties and external disturbances. For instance Figure F.2 compares the tracking error obtained by the tuned smooth SMC ($\varepsilon = 0.5$) and ASMC. As can be seen, the two controllers perform almost similarly, however by adding an external disturbance such as, $T_{dist} = -0.5 + \sin 3t$ N.m, the performance of the SMC with smoothing function is deteriorated as shown in Figure F.3.

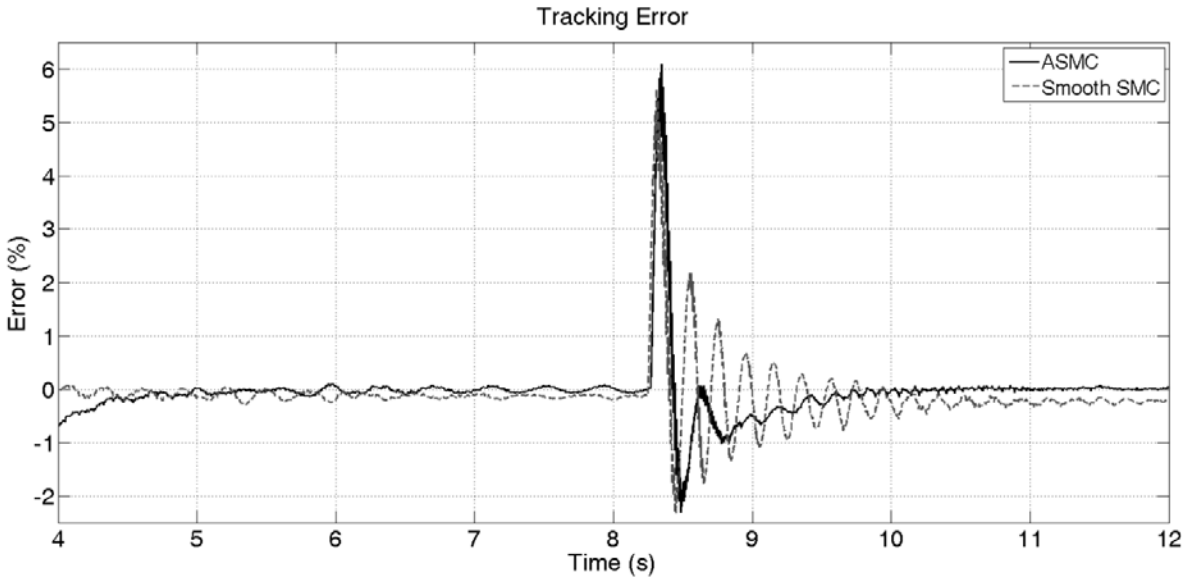

Figure F.2: Tracking error obtained by the tuned smooth SMC ($\varepsilon = 0.5$) and ASMC

The second drawback of the SMC with smoothing function is the time-taking tuning up process. Since the design of the SMC with smoothing function is a tradeoff between the performance and robustness to unmodeled dynamic and external disturbances, so it is a cumbersome task to find the optimum boundary layer thickness. For instance, the ASMC controller is tuned after 4 trials for the experiments, however, it took 30 trials for tuning the smooth SMC.

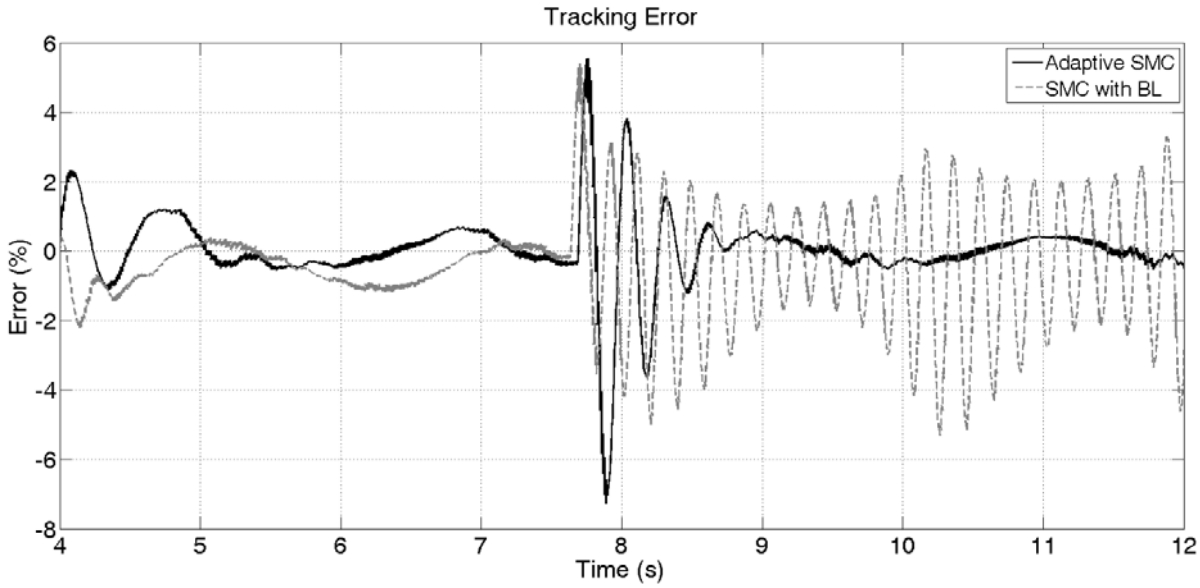

Figure F.3: Tuned Smooth SMC versus Adaptive SMC for a disturbed plant

Appendix G

Voltage to Current Converter Drive

Following voltage-controlled current source circuit is fabricated and used for controlling the proportional valves [57].

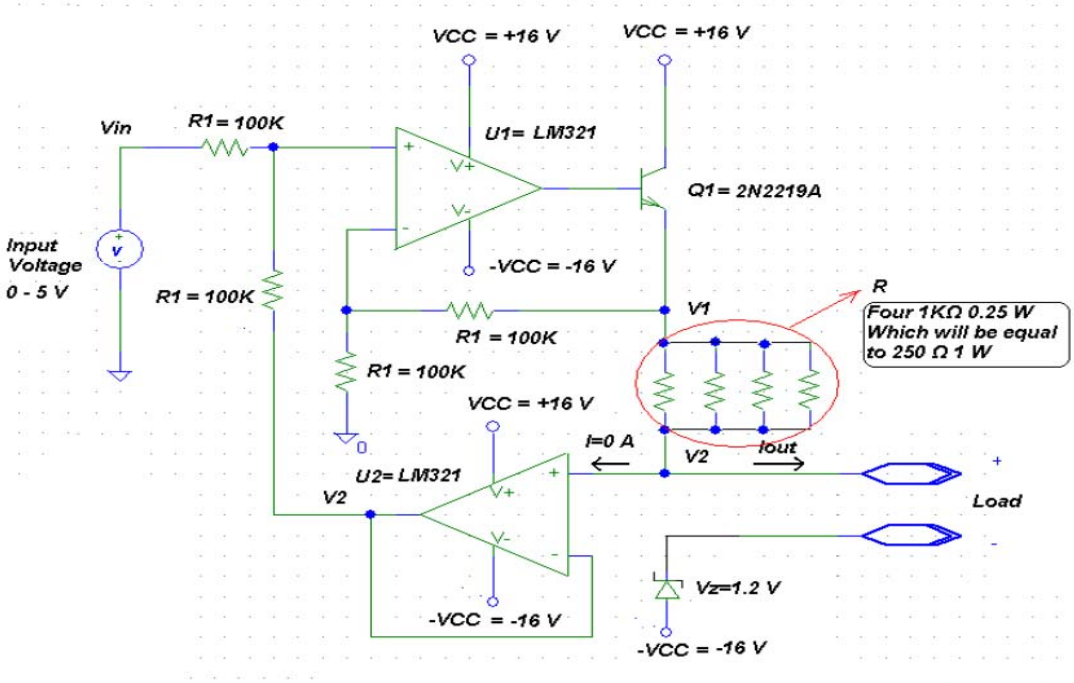

Figure G.1: Voltage to current converter drive

Appendix H
Identifying the Engine Dynamic Model

In order to implement the adaptive SMC experimentally, the parameters of the engine mean value model should be verified (Eq.(H.1)). As discussed in Section 6.2, the mean value model should be obtained from the engine volumetric efficiency maps. However, due to the limitations of the current setup, volumetric efficiency maps cannot be obtained. This is because the engine speed is very low and the manifold pressure does not change by changing the throttle. In addition, the mass flow rate to the engine cannot be measured. Thus, the parameters of the system dynamic equation (H.1) should be verified directly using the experimental data:

$$\dot{T}_{engine} = g_1 A(\theta) + g_2. \qquad \text{H.1}$$

In the above equation, g_1 and g_2 are functions of tank pressure and engine speed. However, in the current setup, engine speed is fixed. Thus, g_1 and g_2 should be verified as function of tank pressure. Table H.1 shows $\dot{T}$ of the single-tank system for various tank pressures and inlet valve signals obtained experimentally (measurements were carried out at higher number of points than what listed in Table H.1).

Table H. 1 Rate of change of engine torque for different tank pressures and valve signals

		Tank Pressure (bar)						
	$\dot{T}[N.m/s]$	1	1.5	2	2.5	3	3.5	4
Control Signal (mA)	280	0	0	0	0	0	0	0
	300	0.009	0.003	0	0	0	0	0
	320	0.019	0.015	0.005	0	0	0	0
	340	0.021	0.02	0.015	0.008	0.005	0	0
	360	0.037	0.032	0.02	0.015	0.007	0.006	0
	380	0.035	0.034	0.033	0.023	0.01	0.006	0
	400	0.035	0.032	0.033	0.023	0.01	0.006	0

$A(\theta)$,which as a function of valve control signal, is shown in Figure H.1.

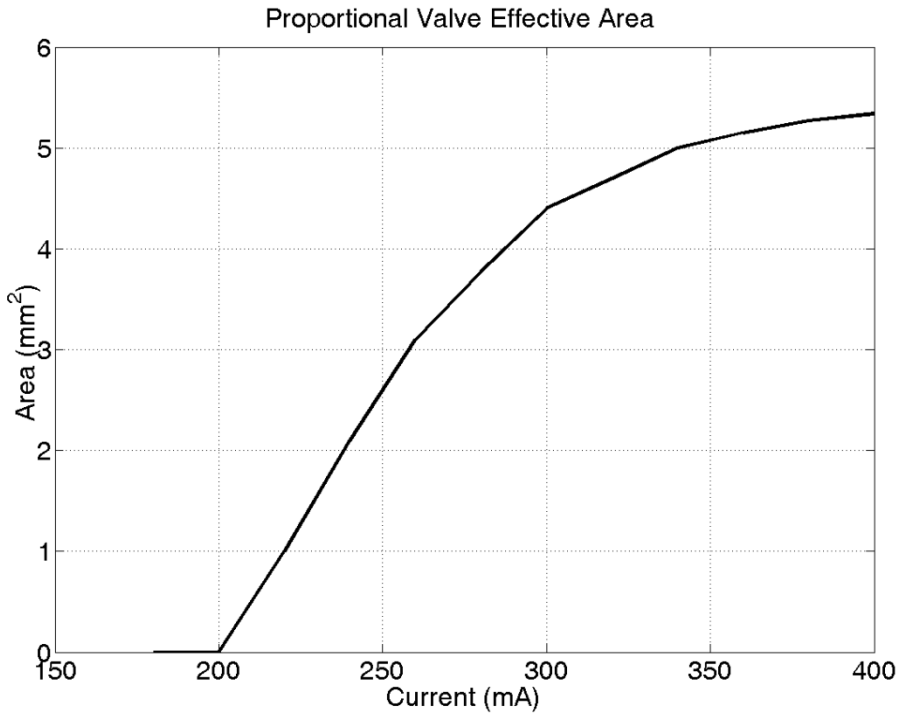

Figure H.1: Proportional valve effective area (suggested by manufacturer)

Assuming the shown profile for $A(\theta)$, now the experimental data could be arranged as follows:

$$\begin{bmatrix} 0 & 0 & 0 & 0 & 0 & 0 & 0 \\ 0.009 & 0.003 & 0 & 0 & 0 & 0 & 0 \\ 0.019 & 0.015 & 0.005 & 0 & 0 & 0 & 0 \\ 0.021 & 0.02 & 0.015 & 0.008 & 0.005 & 0 & 0 \\ 0.037 & 0.032 & 0.02 & 0.015 & 0.007 & 0.006 & 0 \\ 0.035 & 0.034 & 0.033 & 0.023 & 0.01 & 0.006 & 0 \\ 0.035 & 0.032 & 0.033 & 0.023 & 0.01 & 0.006 & 0 \end{bmatrix} =$$

$$\begin{bmatrix} 3.77\times10^{-6} & 1 \\ 4.4\times10^{-6} & 1 \\ 4.7\times10^{-6} & 1 \\ 5\times10^{-6} & 1 \\ 5.15\times10^{-6} & 1 \\ 5.27\times10^{-6} & 1 \\ 5.34\times10^{-6} & 1 \end{bmatrix} \begin{bmatrix} g_1(1) & g_1(1.5) & g_1(2) & g_1(2.5) & g_1(3) & g_1(3.5) & g_1(4) \\ g_2(1) & g_2(1.5) & g_2(2) & g_2(2.5) & g_2(3) & g_2(3.5) & g_2(4) \end{bmatrix}. \quad \text{H.2}$$

The above equation can be rearranged as follows:

$$[\dot{T}] = [A(\theta)][G]. \quad \text{H.3}$$

Now, $[G]$ can be defined using least square method:

$$[G] = (A^T A)^{-1} A^T [\dot{T}]. \quad \text{H.4}$$

Now, the obtained $[G]$ along with the smooth profile for $A(\theta)$ shown in Figure H.1, construct the dynamic equation (H.1).

Appendix I
Accessory assisting Mode

The other option to use the stored pressurized air is to run the off-engine accessories such as power steering, alternator, water pump and air conditioning system. In this case, an auxiliary air motor, which is fed directly by the air tank, is needed to run the accessories. The power required to run the engine accessories varies significantly with the engine speed; however, in this section, an average of 3.9 [kW] is considered for the accessories power consumption. Thus, a 3.9 [kW] air motor with the specification shown in Table I.1 is chosen as the auxiliary air motor.

Table I.1 Air motor specifications [58]

Working pressure	4 [bar]
Power	3.9 [kW]
Air consumption	60 [l/s] (free air)
Second law efficiency	53%

The air motor along with the air tank and a pressure regulator valve are modeled in AMESim software. Figure I.1 shows the air motor supply pressure versus time. As can be seen, the stored air in the tank can run the air motor for about 10 seconds. After that, the tank pressure drops below the air motor's working pressure (Figure I.2). Thus, the overall efficiency of the system in regenerating the initial vehicle's kinetic energy is:

$$\eta_{\text{overall}} = \frac{3.9\frac{kJ}{s}\times 10s}{\frac{1}{2}M_{vehicle}\left(v_1^2 - v_2^2\right)} \cong 12\%. \qquad 8\text{-}1$$

Although the overall efficiency of the accessory assisting mode is a bit higher than the startup mode, the engine accessories can be run independent of the engine only for a short period of time (only about 10 seconds). Thus, the fuel economy obtained by accessory assisting mode is negligible. Furthermore, the engine still has to be on during short stops. Thus, the reduction in fuel consumption that could be gained by avoiding engine idling during short stops cannot be achieved. In addition an extra weight is also added due to the

need for an auxiliary air motor in the powertrain which makes this mode of operation inefficient comparing to startup mode.

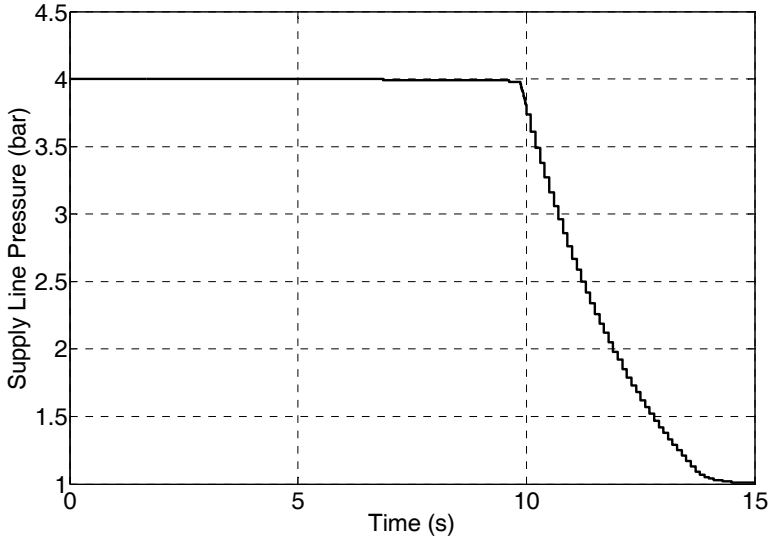

Figure I.1: Air motor supply line pressure

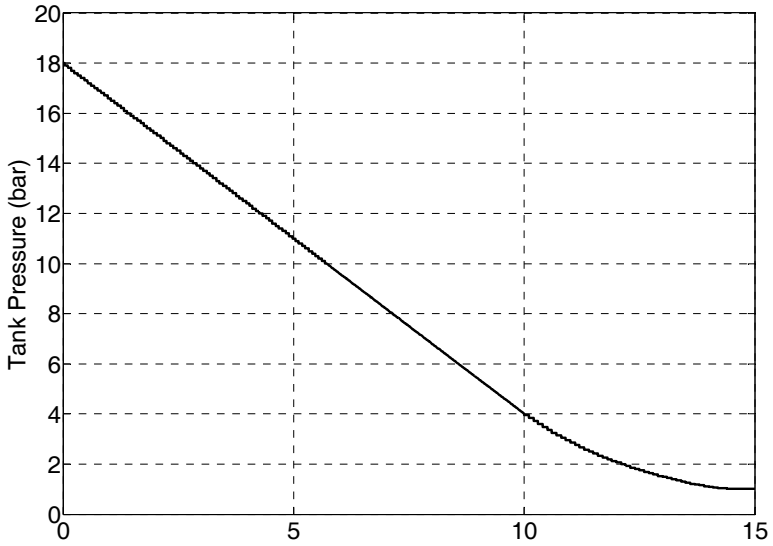

Figure I.2: Tank pressure

References

[1] "Transportation Statistics Annual Report," The Bureau of Transportation Statistics, 2008.

[2] Kluger, J., Harris, M., "Fuel Economy Benefits of Electric and Hydraulic Off Engine Accessories," in *SAE World Congress*, 2007.

[3] Ali, I., Yang, K., Kim, S., "E3 System - A Two speed Accessory Belt Drive System for Reduced Fuel Consumption," in *SAE International Powertrains, Fuels and Lubricants Congress*, 2008.

[4] Donitz, C., Vasile, L.,Onder, C., Guzzella, L., "Realizing a Concept for High Efficiency and Excellent Drivability: The Downsized and Supercharged Hybrid Pneumatic Engine," in *SAE World Congress*, 2009.

[5] Wang, Y., Megli, T., Haghgooie, M., "Modeling and control of electromechanical valve actuator," in *SAE World Congress*, 2002.

[6] Giglio V., Lorio B. and Police G., "Analysis of advantages and of problems of electromechanical valve actuators," in *SAE World Congress*, 2002.

[7] Pournazeri, M., Fazeli, A., Khajepour, A., "A cam-based electro-hydraulic variable valve timing system for pneumatic hybrid engines," in *ASME International Mechanical Engineering Congress and Exposition IMECE09*, 2009.

[8] Tai, C., Tsao, T., "Control of an electromechanical camless valve actuator," in *Proceeding of the American Control Conference*, 2002.

[9] Amiri, M.,Esfahanian, M.,Hariri-Yazdi, M.,Esfahanian, V. , "Minimization of Power Losses in Hybrid Electric Vehicles in View of the Prolonging of Battery Life," *Journal of Power Sources*, vol. 10, no. 2, pp. 372-379, May 2009.

[10] I. Kim, "The Novel State of Charge Estimation Method for Lithium Battery Using Sliding Mode Observer," *Journal of Power Sources*, vol. 163, pp. 584-590, 2006.

[11] Guzzella, L., Sciarretta, A., *Vehicle Propulsion Systems Introduction to Modeling and Optimization*, 2nd ed. New York: Springer, 2007.

[12] Schechter, M., "New Cycle for Automobile Engines," in *SAE World Congress*, Detroit, 1999.

[13] Schechter, M., "Regenerative Compression Braking- A Low Cost Alternative to Electric Hybrids," in *SAE World Congress*, 2000.

[14] Schechter M., "Operating a vehicle with braking energy recovery," 7231998, 2007.

[15] Tai, C.,Tsao, T., Levin, M. B. ,Barta, G., Schechter, M., "Using Camless Valvetrain for Air Hybrid Optimization," in *SAE World Congress*, 2003.

[16] Kang, H.,Tai, C. ,Smith, E. ,Wang, X. ,Tsao, T. ,Stewart, J.,Blumberg, P.N. , "Demonstration of Air-Power-Assist Engine Technology for Clean Combustion and Direct Energy Recovery in Heavy Duty Application," in *SAE Technical Paper # 2008-01-1197*, 2008.

[17] Wang, X., "Modeling and Experiment of Compressed Air," University of California, Los Angeles, A dissertation submitted in partial satisfaction of the requirements for the degree Doctor of Philosophy in Mechanical Engineering 2008.

[18] Andersson, M., Johansson, B., Hultqvist, A., "An Air Hybrid for High Power Absorption and Discharge," in *SAE World Congress*, 2005.

[19] Trajkovic, S.,Tunestal, P., Johansson, B., "Introductory Study of Variable Valve Actuation for Pneumatic Hybridization," in *SAE World Congress*, 2007.

[20] Trajkovic, S.,Tunestal, P., Johansson, B., "Investigation of Different Valve Geometries and Valve Timing Strategies and their Effect on Regenerative Efficiency for a Pneumatic Hybrid with Variable Valve Actuation," in *SAEWorld Congress*, 2008.

[21] Trajkovic, S.,Tunestal, P., Johansson, B. , "Vehicle Driving Cycle Simulation of a Pneumatic Hybrid Bus Based on Experimental Engine Measurements," in *SAE World Congress*, 2010.

[22] Ivanco, A.,Charlet, A.,Chamaillard, Y. ,Higelin, P. , "Energy Management Strategies for Hybrid-Pneumatic Engine Studied on an," in *SAE world congress*, 2009.

[23] Donitz, C., Vasile, I., Onder, C., Guzzella, L., "Modelling and optimizing two- and four-stroke hybrid pneumatic engines," *Journal of Automobile Engineering*, vol. 223, no. 2, 2009.

[24] Onitz, C. , Vasile, I. , Onder, C., Guzzella, L., "Dynamic Programming for Hybrid Pneumatic Vehicles," in *American Control Conference*, Hyatt Regency Riverfront, St. Louis, MO, USA, 2009.

[25] Huang, K. D., Tzeng, S. C., "A new parallel-type hybrid electricvehicle," *Applied Energy*, no. 79, pp. 51-64, 2004.

[26] Huang, K. D., Tzeng, S. C., Chang, W. C., "Energy saving hybrid vehicle using a pneumatic power system," *Jorunal of Applied Energy*, vol. 1, pp. 1-18.

[27] Huang, K. D.,Tzeng, S. C.,Ma, W. P., Chang, W. C. , "Hybrid pneumatic power system which recycles exhaust-gas of an internal combustion engine," *Applied Energy*, vol. 82, pp. 117-132, 2005.

[28] Ehsani, M., Gao, Y., Gat, S., Emadi, A., *Modern Electric Hybrid Electric, and Fuel Cell Vehicles*. Washington, D.C., USA: CRC Press, 2005.

[29] Cengel, Y., Boles, M., *Thermodynamic: An Engineering Approach*, 6th ed.: McGraw-Hill Science, 2006.

[30] Ehrlich, GM., Gitzendanner, R., Puglia, F., Marsh, C., Bragg, B. J., "A Lithium Ion Cell for the EMU Battery," in *SAE Aerospace Power Systems Conference and Exposition*, 1999.

[31] Joseph, P., Fellner, R., Miller, M., Shanmugasundaram, V., "Rechargeable Lithium-Ion Based Batteries and Thermal Management for Airborne High Energy Electric Lasers," in *SAE Power Systems Conference*, 2006.

[32] Ferguson, C. R., *Internal Combustion Engines*.: John Wiley & Sons, 1986.

[33] Heywood, J. B., *Internal Combustion Engines Fundamentals*, McGraw-Hill Science, Ed., 1988.

[34] Oliver, G., "Computer Simulation of Air Injection to Inlet Manifold On Turbocharged Engines," in *FISITA 2006*, 2006.

[35] Lee, C., Zhao, H. , Ma, T. , "Analysis of a Cost Effective Air Hybrid Concept," in *SAE World congress*, 2009.

[36] Lee, C., Zhao, H., Ma, T., "The Perfromance Characteritics of a Production Oriented Air Hybrod Powertrain," in *SAE World Congress*, 2010.

[37] Psanis, C., "Modelling and experomentation on air hybrid engine concept for automotive application," Brunel University, A thesis submitted for the degree of Doctor of Philosophy 2007.

[38] Hosaka, T., Hamazaki, M., "Development of the variable valve timing and lift (Vtec) engine for the Honda Nsx," in *SAE Technical Paper 910008*, 1991.

[39] Gafvert M., Arzen K., Pedersen L. and Bernhardsson B., "Control of GDI engines using torque feedback exemplified by simulations," *Journal of Control Engineering Practice*, vol. 12, 2004.

[40] Carvalho, L., "Exergitic Analysis of Compressed Air for Vehicular Propulsion," in *SAE World Congress*, 2008.

[41] Wagner, J., Dawson, D., Zeyu, L., "Nonlinear Air-to_Fuel Ratio and Engine Speed Control for

Hybrid Vehicles," *IEEE Transactions on Vehicular Technology*, vol. 52, no. 1, 2003.

[42] Souder, J., Hedrick, J. K., "Adaptive Sliding Mode Control of Air-Fuel Ratio in Internal Combustion Engines," *International Journal of Robust and Nonlinear*, vol. (DOI:10.1002/rnc.901)., pp. 525-541, 2004.

[43] Tang, H., Weng, L., Dong, Z., Yan, R., "Adaptive and Learning Control for SI Engine Model with Uncertainties," *IEEE/ASME Transactions on Mechatronics*, vol. 14, no. 1, 2009.

[44] Slotine, J. J. E., Li, W., *Applied Nonlinear Control*.: Prentice-Hall Inc., 1991.

[45] Hendricks, E., "Engine Modeliing for Control Applications: A Critical Survey," *Mechanica*, vol. 32, pp. pp. 387-396, 1997.

[46] Hendricks, E., Sorenson, S.C., "Mean Value Modelling of Spark Ignition Engines," in *SAE International Congress and Exposition*, vol. and Exposition Detroit, Michigan, 1999., Detroit, Michigan, 1999.

[47] De Nicolao, G., Scattolini, R., Siviero, C., "Modelling the volumetric efficiency of IC engines: Parametric, non-parametric and neural techniques," vol. 4, pp. 1405-1415, 1996.

[48] Zeinali, M., Notash, L., "Adaptive Sliding Mode Control with Uncertainty Estimator for Robot Manipulators," *Journal of Mechanism and Machine Theory*, vol. 45, 2010.

[49] Slotine, J. and Li, W., *Applied Nonlinear Control*. New Jersey: Prentice hall, 1991.

[50] Chunji, L., "Global Asymptotic Stability of Generalized Lienard Equation," *Trends in Mathematics Information Center for Mathematical Sciences*, vol. 4, no. 2, pp. 127-131, December 2001.

[51] Kokotovic, P., Marino, R., "On vanishing stability regions in nonlinear systems with high-gain feedback," *IEEE Transactions on Automatic Control*, vol. 31, no. 10, pp. 967-970, October 1986.

[52] Sundström, O.,Ambühl, D., Guzzella, L., "On Implementation of Dynamic Programming for Optimal Control Problems with Final State Constraints," *Oil & Gas Science and Technology*, vol. 65, no. 1, pp. 91-102, 2010.

[53] P´erez, L., Bossio, G., Moitre, D., Garc´ıa, G. , "Optimization of power management in an hybrid electric vehicle using dynamic programming," *Mathematics and Computers in Simulation*, vol. 73, pp. 244–254, 2006 2006.

[54] Brahma, A.,Guezennec, Y.,Rizzoni, G. , "Optiml Energy Managment in Series Hybrid Electric

Vehicles," in *American Control Conference*, Chicago, 2000.

[55] Ueno, K. ,Bye, R. E. , Hunter, K. S., "Compressor Efficiency Definitions," University of Colorado, 2003.

[56] Chlumský, V., *Reciprocating and rotary compressors*. Prague: SNTL, 1965.

[57] Hosseini, M. www.astinco.com. [Online]. http://www.astinco.com/pdf/vccs.pdf

[58] TDI Tech development. [Online]. http://www.tdi-turbotwin.com/t30m.php